HYPEREXCITABLE MOLECULAR LAYER INTERNEURONS DRIVE CEREBELLAR CIRCUIT DYSFUNCTION IN SPINOCEREBELLAR ATAXIA TYPE I

Christopher Robert Douthwaite

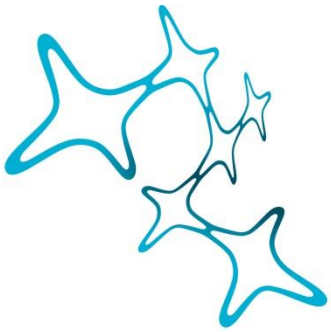

Graduate School of Systemic Neurosciences

LMU Munich

Dissertation der Graduate School of Systemic Neurosciences der Ludwig-Maximilians-Universität München

22nd June, 2023

Supervisor
Prof. Dr. Dr. Sabine Liebscher
Institute of Clinical Neuroimmunology
University hospital of Munich and Biomedical Centre
Ludwig-Maximilians-Universität München

First Reviewer: Prof. Dr. Dr. Sabine Liebscher
Second Reviewer: Prof. Dr. Tobias Rose
External Reviewer: Dr. Francesca Prestori

Date of Submission: 22.06.2023
Date of Defense : 15.01.2024

TABLE OF CONTENTS

LIST OF ABBREVIATIONS

AADC	aromatic l-amino acid decarboxylase
AAV	adeno associated virus
AD	Alzheimer's disease
ALS	Amyotrophic lateral sclerosis
AMPA	α-amino-3-hydroxy-5-methyl-4-isoxazolepropionic acid
BSA	Bovine serum albumin
CIC	Capicua transcriptional repressor
CF	Climbing fiber
CNO	Clozapine-N-oxide
DBS	Deep brain stimulation
DCN	Deep cerebellar nuclei
DREADD	Designer Receptors Exclusively Activated by Designer Drugs
EAAT4	Excitatory amino-acid transporter 4
EA1	Episodic ataxia type 1
EEG	Electroencephalogram
FRET	Fluorescence resonance emission transmission
FOV	Field of view
GABA	γ-Aminobutyric acid
GECI	Genetically encoded calcium indicator
GFP	Green fluorescent protein
GCs	Granule cells
HD	Huntington's disease
IO	Inferior olive
IP3R1	Inositol 1,4,5-triphosphate receptor type 1
LTD	Long-term depression
LTP	Long-term potentiation
MRI	Magnetic resonance imaging
mGLuR	Metabotropic glutamate receptor
MF	Mossy fiber
MLIN	Molecular layer interneuron
NGF	Nerve growth factor
NMDA	N-methyl-D-aspartate
PFA	Paraformaldehyde
PD	Parkinson's disease
PF	Parallel fiber
PN	Purkinje neuron
PV	Parvalbumin
PV INs	Parvalbumin Expressing Interneurons
ROI	Region of interest
rTMS	Repetitive transcranial magnetic stimulation
SARA	Scale for the assessment and rating of ataxia
SCA	Spinocerebellar ataxia
Sca1	Spinocerebellar ataxia type 1
SEM	Standard error mean
SD	Standard deviation
WT	Wild Type

LIST OF FIGURES

ABSTRACT

Spinocerebellar ataxia type 1 (*Sca1*) is an autosomal dominant, neurodegenerative disease, emerging from a CAG repeat expansion mutation in the gene *ATXN1*. Classical patient symptoms include motor incoordination and abnormal gait, which coincide with the hallmark pathology of atrophy across the cerebellum and brainstem, in particular, degeneration of the cerebellar cortex Purkinje neurons (PN). Given that there are currently no disease modifying treatments for patients, it is imperative to understand the pathogenesis of *Sca1*. Research has primarily focussed on how the *ATXN1* mutation leads to PN dysfunction and ultimately degeneration. However, *ATXN1* is ubiquitously expressed, and many cell types other than PNs degenerate, thus are likely also altered in *Sca1* (Seidel et al., 2012). Indeed, recent evidence has shown that in the presymptomatic stage of a *Sca1* mouse model there is already an increase in synaptic connections from surrounding inhibitory neurons onto PNs (Edamakanti et al., 2018). Despite such findings, early alterations in distinct neuronal populations of the cerebellar cortex, and their interactions as a circuit, are poorly understood. To investigate early cellular and circuit dysfunction in distinct neuronal populations of the cerebellar cortex, I investigated a *Sca1* mouse model as symptoms are emerging. Specifically, I utilized *in vivo* two-photon calcium imaging, simultaneously recording the three primary inhibitory neurons of the cerebellar cortex circuit; PNs, molecular layer interneurons (MLINs) and Golgi cells. In order to unravel alterations in either spontaneous activity or response properties to cerebellum-associated behaviours, we recorded neuronal calcium signals in anesthetised mice and during a range of awake conditions. The most prominent deficits emerged in the MLIN population, which were hyperactive during quiet wakefulness and hyperresponsive to sensorimotor input MLIN dysfunction also appeared to drive a breakdown in the capacity of the cerebellar cortex to encode sensorimotor information. The PN dendrites, which receive extensive input from MLINs, also displayed enhanced calcium signals. To establish the pathophysiological relevance of these findings to *Sca1*, I used chemogenetic tools to specifically inhibit MLINs. Acute prevention of MLIN hyperactivity in *Sca1* mice reduced aberrant PN dendrite calcium signals, restored network encoding, and most importantly, improved motor coordination. Thirty-day chronic inhibition of MLINs induced lasting motor improvements and delayed disease progression. The critical role of hyperactive MLIN in triggering symptoms typical of *Sca1*, was further corroborated by mimicking the increased MLIN excitability through chemogenetic stimulation of MLINs in healthy mice. Acute stimulation of MLINs disrupted motor function and could drive pathological features in PN dendrites, whilst chronic MLIN stimulation in young healthy mice induced lasting motor impairments and reduction of PN post-synapses reminiscent of *Sca1* pathology, detectable over four months after treatment end. These findings together show, for the first time, that aberrant MLIN activity

is a clear feature of early *Sca1*, and can drive neuronal circuit dysfunction. Moreover, our experiments revealed that non-cell autonomous mechanisms are sufficient in driving PN pathology. Crucially, we showed that selectively targeting MLINs in the early stages of the disorder alleviates classical motor symptoms in *Sca1* mice, opening up a novel therapeutic avenue.

1. INTRODUCTION

1.1. Spinocerebellar Ataxia

1.1.1. Background of the Spinocerebellar Ataxias

The term “ataxia” comes from the Greek word loosely translating to “without order”. Originally, the term was used in medicine to refer to “irregularity of bodily functions”. Ataxia became a prominent phrase following use by the French neurologist Guillaume-Benjamin Duchenne in 1858, whilst providing early detailed descriptions of neurological movement disorders (Barboi, 2000). Ataxia has since become a common phrase in medicine, both in naming diseases and as a description of symptoms. Following decades of reports into such conditions, by the mid 20th century there was an established group of diseases consisting of spinocerebellar pathology, with a dominant hereditary component, as summarised by Joseph Greenfield (Greenfield, 1954). Building upon the work of Greenfield and others, research led to further classification of such hereditary spinocerebellar ataxias (SCA) based on clinical appearance, onset, and brain regions affected (Rosenberg and Grossman, 1989). In the last 30 years, genetic research has allowed us to pinpoint mutations responsible for subgroups within the SCAs, thus allowing distinct characterisations of patient cohorts and unprecedented insight into molecular pathogenesis. Several SCAs, including SCA type I (*Sca1*), contain a CAG repeat expansion in the affected gene, referred to as polyglutamine SCAs (Paulson et al., 2017). In *Sca1*, an autosomal dominantly inherited expansion of CAG repeats in the gene now known as *ATXN1*, encoding the protein ataxin-1 (Orr et al., 1993). This pioneering work from Harry Orr and Huda Zoghbi paved the way to improving our understanding of *Sca1* and currently provides the foundation for the development of novel therapeutics.

Traditionally, research on neurodegenerative diseases was centred around neuronal atrophy and loss of dedicated vulnerable neuronal populations; however, there is now a growing consensus that understanding such diseases in earlier stages prior to cell death is favourable in the search for medicinal intervention. With studies even focussing on the early developmental period, far prior to symptom onset, in order to understand disease pathogenesis (Braz et al., 2022). Recent evidence in a *Sca1* mouse model showed an increased inhibitory connectivity within the cerebellar cortex, already emerging in the weeks after birth and contributing to an imbalance of excitation and inhibition in the cerebellar cortex (Edamakanti et al., 2018). We therefore hypothesised that alterations to the inhibitory network of the cerebellar cortex circuit contribute to early *Sca1* pathogenesis.

To investigate the extent of dysfunction among inhibitory neurons caused by the *ATXN1* mutation, we harnessed *in vivo* two-photon calcium imaging in a *Sca1* mouse model.

Over this thesis, I will outline our research into three main inhibitory interneurons of the cerebellar cortex, in mice carrying the *ATXN1* mutation. To unravel dysfunction across these distinct neuronal populations, we investigated neuronal activity of all three groups simultaneously in a variety of conditions. We recorded calcium signals in awake animals, in darkness and with visual feedback provided through a virtual reality, during sensorimotor input relevant to the function of cerebellar neurons. Neuronal activity can be altered during the same motor action dependent on the animal being in darkness or light (Helmchen and Büttner, 1995). These recordings were complemented by monitoring the same set of neurons under light anesthesia, which in the past was a standard investigation to probe alterations in neuronal activity in mouse models of neurodegenerative diseases (Busche et al., 2008; Chapman et al., 1999). Light anesthesia particularly reduces neuronal inhibition (Haider et al., 2013) and can thus potentially 'unmask' alterations in intrinsic excitability or neuronal excitation, which are otherwise covered during wakefulness. Due to such distinctions, alterations to neuronal activity in a disease model that occur in one condition, may not be consistent in the other (Greenberg et al., 2008), hence we investigated the same neurons during these distinct states. Additionally, we assessed calcium signals in these conditions at different ages, to investigate how alterations develop over the disease course. Finally, we provided functional insight into our descriptive findings through chemogenetic modulation of neuronal activity.

Whilst traditionally the term "ataxia" commonly refers to the disorder of a patient's movements, here we shine light on the disorder of cerebellar cortex inhibitory neurons in *Sca1*.

1.1.2. Clinical Features & Neuropathology of SCAs

Spinocerebellar ataxias (SCAs) comprise a group of genetically heterogeneous neurodegenerative disorders, with wide-ranging clinical features. The points of convergence in SCA patients are the slow progressing ataxic symptoms, which consist of perturbed balance, and motor incoordination among others. The shared physical symptoms generally coincide with a degeneration of the cerebellum and brainstem, however, cellular mechanisms and pathology vary among distinct subgroups. Originally, these disorders were categorised by the variations in ataxic symptoms, in combination with appearance of extrapyramidal, sensory and cognitive deficits. Moving forward, research identified subgroups with hereditary components, leading to the recognition of autosomal dominant SCAs. This led to the discoveries of distinct genetic loci that are predominantly used to define such SCA subgroups, as is the case for the *Sca1*, the focus of our research.

The prevalence for all autosomal dominant SCAs is reported as high as 5-7 per 100,000 (Dueñas et al., 2006). Symptom onset is commonly in the 3rd or 4th decade, however it can also occur later in life (Dueñas et al., 2006; Matilla-Dueñas et al., 2008). Patients suffer

primarily from a dysfunction and degeneration of the cerebellum, brain stem and spinal cord (**Fig. 1**), which manifests as progressive motor skill and balance impairment, muscle weakness, alongside oculomotor deficits, speaking and swallowing difficulties (dysarthria/dysphagia) (Tejwani and Lim, 2020). At later stages, muscle weakness and breathing difficulties become debilitating, and death usually occurs 10-20 years after symptom onset depending on the subtype (Matilla-Dueñas et al., 2008). The collaboration between Huda Zogbi and Harry Orr led to the characterisation of the *Sca1* gene in the early 1990s, by identifying the CAG repeat mutation on the gene *ATXN1*, leading to the polyglutamine expansion on the protein ataxin-1 (Orr et al., 1993).

The hallmark pathological feature of *Sca1*, is the striking degeneration of the Purkinje neurons (PNs) of the cerebellar cortex. Post-mortem studies of brain tissue show severe cell death, and magnetic resonance imaging (MRI) in living patients revealed a decrease in cerebellum volume, progressively throughout the disease course, even in very early stages of symptom onset (Bürk et al., 1996; Nigri et al., 2022; Seidel et al., 2012). Aggregation of mutated protein, ataxin-1, is found in other regions, such as the brainstem, although it can be challenging to identify in PNs given the degree cell loss by the time of death (Duyckaerts et al., 1999; Skinner et al., 1997). However, studies in *Sca1* mouse models have revealed that localisation of the mutant ataxin-1 to the PN nucleus is essential to ataxia symptoms and atrophy (Klement et al., 1998). Despite some reports of mild granule layer atrophy (Robitaille et al., 1995), the other neurons of the cerebellar cortex are largely spared from cell death across the autosomal dominant SCAs (Koeppen et al., 2005). Thinning of the molecular layer occurs due to shrinkage of PN dendritic branches, there is also reports of lower parallel fiber (PF) density within this layer, again without significant loss of the granule cells (GCs) these axons originate from (Koeppen et al., 2005; Seidel et al., 2012). Clinical imaging studies in patients have shown that alongside atrophy to the cerebellum, there is significant volume loss

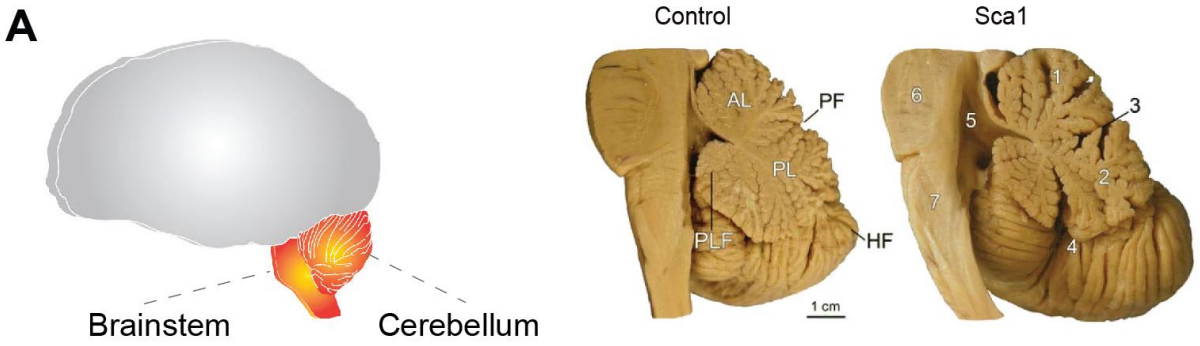

Figure 1: ***Pathology of Sca1 (A)*** *The cerebellum and brainstem are the primary affected regions in Sca1 patients; patient brains post mortem show severe atrophy of both regions. Images on right are taken from Seidel, et al., 2012, numbers indicate "(1) atrophic anterior lobe, (2) atrophic posterior lobe, (3) widened posterior fissure, (4) widened posterolateral fissure, (5) enlarged fourth ventricle, (6) flattened pons, (7) atrophic medulla oblongata" (Seidel et al 2012). Abbreviations used in (A); AL-anterior lobe, HF-horizontal fissure, PF-posterior fissure, PL-posterior lobe, PLF-posterolateral fissure. Reprint from Acta Neuropathologica with permission from Springer Nature (Seidel, et al., 2012).*

to the brainstem (Seidel et al., 2012). It is of note that studies with patients around symptom onset showed the reductions in cerebellar volume actually occur to a lesser extent than reductions to the brainstem regions (Nigri et al., 2022).

It is therefore important to also consider the impact of the *Sca1* mutation in areas away from the cerebellar cortex. It is clear from post mortem analysis that alongside PN loss, atrophy is prominent in the deep cerebellar nuclei and further brainstem regions including the inferior olive and pontine nuclei (Seidel et al., 2012). Furthermore, case studies reveal widespread degeneration throughout the brain encompassing cortical, midbrain, cholinergic and dopaminergic systems (Rüb et al., 2012). There is a strong argument that PNs are simply more vulnerable to degeneration, than cell types around them, rather than the central feature driving *Sca1* symptoms (Hekman and Gomez, 2015). MRI and magnetic resonance scanning (MRS) showed that the most significant changes in patients at the early-moderate stage of the disease occurred in the pons, moreover, these findings could accurately predict the severity of disease progression (Deelchand et al., 2019). The pons is connected to the GCs of the cerebellar cortex through mossy fibers (MFs), indicating that input to the cerebellar cortex may be altered early in *Sca1*. In agreement with this, there is a correlation between brainstem degeneration and disease severity (Guerrini et al., 2004). In addition to the brainstem, position emission tomography has identified dysfunction in frontal regions also correlating with behavioural severity (Wang et al., 2007). The authors propose such dysfunction could be caused by deficits in projections from the cerebellum to these frontal regions (Wang et al., 2007). Indeed, the three peduncles connecting the cerebellum and midbrain are certainly reduced in volume in SCA patients (Seidel et al., 2012). Further indicating, that connections to and from the cerebellum are altered. Corroborating these findings, degeneration of spinocerebellar and corticospinal tracts is prominent in post mortem tissue (Zoghbi & Orr, 1995) and dysfunction in SCA patients prior to severe symptoms onset has been shown through electromyography (EMG)/electroencephalography (EEG) and transmagnetic stimulation (TMS) studies (Rakowicz et al., 2019; Velázquez-Pérez et al., 2017). In addition, electrophysiological characterisation has highlighted polyneuropathy as a common feature among SCA patients with individual subtypes having distinct characteristics (Linnemann et al., 2016; Matilla-Dueňas et al., 2008). *Sca1* often shows prolonged peripheral and central motor conduction times (Schöls et al., 1997), with a more recent report suggesting 82% of peripheral nerves are affected, compared to SCA6 with only 22% (Linnemann et al., 2016). These findings not only highlight the variation between these genetically defined subgroups, but also further indicate that dysfunction extends beyond the cerebellar cortex.

It is clear that our research should avoid focussing entirely on one cell type alone, but should consider circuits and cell-cell connectivity. With this in mind, we aimed to assess

multiple neuronal populations in the cerebellar cortex of *Sca1* in unison, to unravel how mutated *ATXN1* alters distinct groups and network function. In the next section, I outline the neurons we focus our research on, and how they are connected within the cerebellar cortex.

1.2. The Cerebellum

The cerebellum is a part of the hindbrain and located dorsally to the brain stem, it is named from the Latin for “mini brain”, given the relative small size in comparison to the cerebrum in humans. Despite being considerably smaller in appearance and weight than the neocortex, the cerebellum, captivatingly, contains over half the neurons of the entire brain and has a far larger surface area than the cerebrum (Azevedo et al., 2009; Sereno et al., 2020). The cerebellum is traditionally associated with facilitating coordinated motor function, largely due to initial lesion experiments revealing breakdown in coordination and impaired movements, without paralysis or clear disruption to sensory and cognitive function (Glickstein et al., 2009). Research since, has not only confirmed an important role in motor function (Manto et al., 2012), but also in handling sensory information (Baumann et al., 2015), and it has become known that cerebellar output has strong influence in learning, emotional regulation and other forms of higher cognitive function (Jacobi et al., 2021). With this, although indeed dysfunction of the cerebellum causes the classical motor impairments, as is clearly observable in SCA patients, understanding the complexities of this region is likewise highly relevant in a variety of psychiatric disorders (Phillips et al., 2015).

1.2.1. Anatomical Divisions of the Cerebellum in Humans and Mice

Being an older region of the vertebrate brain, the function and cytoarchitecture of the cerebellum is largely conserved across mammals, although varies considerably in size and relative position to the cerebrum (**Fig. 2A**) (Narayanan and Thirumalai, 2019). Research into cerebellar lesions and models of cerebellar disorders in animals have found remarkable consistencies in symptoms with comparative cerebellar conditions in humans (Manto et al., 2012).

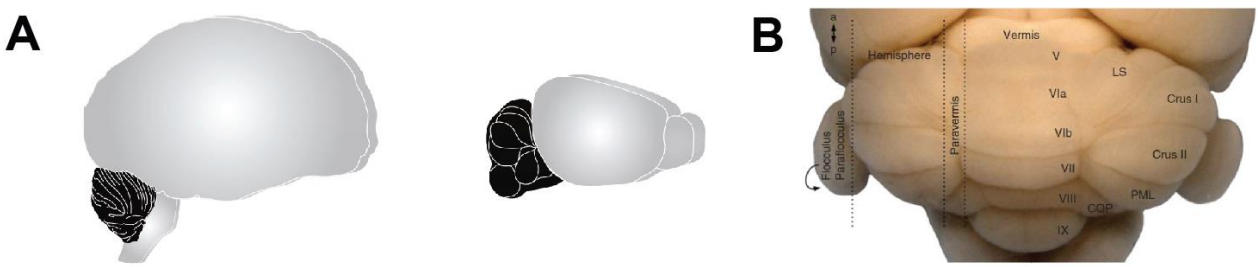

Figure 2: ***The cerebellum in humans and mice*** (A) Graphical representation of the anatomical location of the cerebellum in humans and mice indicated in the black shaded area ***(B)*** *Divisions of the cerebellum, image from White and Sillitoe, 2012. “LS, lobulus simplex; PML, paramedian lobule; COP, copulapyramidis (a, anterior; p, posterior)“ (B) Reprint from WILEY INTERDISCIPLINARY REVIEWS: MECHANISMS OF DISEASE with permission from John Wiley and Sons (White and Sillitoe, 2012).*

The macrostructure is split into a central column of lobules, the vermis, and two hemispheres (**Fig. 2B**), originally delineated in the early 18th century by Johann Christian Reil (1759–1813) and Karl Friedrich Burdach (1776–1847) (Reil, 1807). Three major white matter tracts connect the brainstem and cerebrum to the cerebellum, the superior, middle and inferior peduncles respectively. These consist of various afferent and efferent tracts. Output of the cerebellum stems primarily from deep cerebellar nuclei (DCN) (the dentate, emboliform, fastigial and globose nucleus). Two major excitatory inputs to both these nuclei and the cerebellar cortex, are the climbing fibers (CFs) and MFs. CFs emerge from the inferior olive (IO), whilst MFs project from a number of regions including the pons and other brainstem nuclei, and the spinal cord (**Fig. 3A**). The output of the DCN is modulated by the inhibitory circuit of the cerebellar cortex (Prestori et al., 2019a). The cerebellar cortex circuit receives excitatory input from the aforementioned climbing and MFs, and inhibits the DCN through the PNs, the only output of the cortex (**Fig. 3B**).

Despite that cerebral gyrification is lacking from the rodent brain in comparison to humans, the cerebellum macrostructure and folding is largely consistent across vertebrates, from birds to rodents to humans (Larsell, 1970; Miterko et al., 2018; Semple et al., 2013). In addition, the topographical structure and cytoarchitecture outlined here, is also conserved from humans to mice. Furthermore, cerebellar deficits in mice provide comparable symptoms to symptoms present in humans following cerebellar damage (Manto and Marmolino, 2009). Recent work has provided detailed genetic insight into the comparisons between rodent and humans cerebellar regions. Transcriptome mapping supports a high homogeneity between human Crus I and every region of the mouse cerebellum (Beauchamp et al., 2022). On the other hand, single cell sequencing has also indicated a large difference in genomic expressions in the cerebellum between human and mice (Apsley and Becke, 2022). Whilst it is important to understand further these differences to improve translation of preclinical research, the anatomical, functional and transcriptomic similarities in the cerebellum from mice to humans, indicates this is a valid model to better understand the human cerebellum.

1.2.2. Structural Architecture of the Cerebellar Cortex Circuit

The cerebellar cortex is divided into three layers, the most superficial molecular layer, followed by the PN layer and finally the innermost granule layer (**Fig. 3B**). The MFs provide excitatory drive onto the only glutamatergic cells of the circuit, the densely packed GCs of the granule layer. Within this layer the primary inhibitory cells are the Golgi cells, which are one of so-called “non-traditional large” neurons of the granule layer (Barmack and Yakhnitsa, 2011). This group also comprise of the GABAergic/Glycinergic Lugaro cells and excitatory unipolar brush cells (Flace et al., 2004). Lugaro cells are innervated by serotonergic inputs of MFs,

inhibited by PNs and in turn inhibit MLINs, whilst unipolar brush cells excite GCs alongside the MFs (Kalinichenko and Okhotin 2005; Miyazaki et al., 2021). Further small inhibitory neurons, including globule cells have also been studied in this layer but are less abundant (Hirono et al., 2012). GCs excite PNs and MLINs through PFs, so named as they project superficially and form parallel tracts stretching along the molecular layer, innervating the dendrites of the PNs, which also extend into the molecular layer from their deeper cell bodies (**Fig. 3B**). PNs are also directly excited from CFs, their activity is temporally and spatially modulated through the inhibitory MLINs, residing in the most superficial layer. MLINs are divided morphologically into deeper lying basket cells and superficial stellate cells, primarily inhibiting the PN somata and dendrites respectively (Kim and Augustine, 2021). Physiologically they are difficult to differentiate, therefore are commonly grouped together in research (Kim and Augustine, 2021; Sultan and Bower, 1998). PNs are the sole output of the cerebellar cortex. Their unusually large somata lie in between the granule and molecular layers, they each display extensive tree-like dendritic branches extending into the molecular layer, whilst their inhibitory axon projects deep to the DCN, modulating the overall output of the cerebellum (**Fig. 3B**). Also predominantly residing in this PN layer, are the Candelabrum cells, another GABAergic interneuron targeting MLINs, whilst receiving excitation from MFs and GCs and inhibition from PNs (Osorno et al., 2022). For the purpose of this research we focus on the three primary inhibitory cells of the cerebellar cortex; MLINs, PNs and Golgi cells.

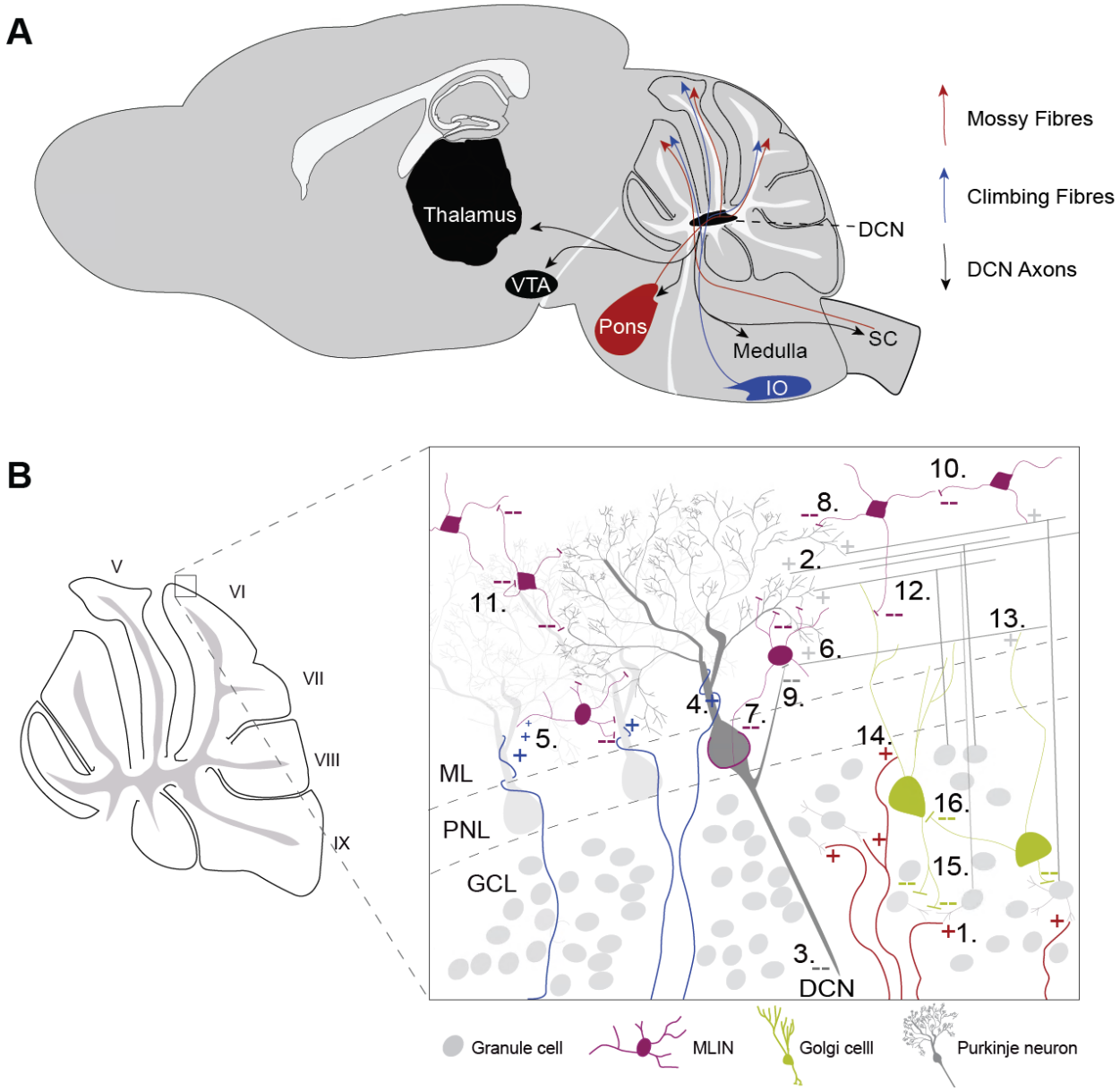

Figure 3: ***Connectivity of the cerebellum and cerebellar cortex circuit. (A)*** *Primary inputs to the cerebellum are climbing and mossy fibers. Climbing fibers originating from the inferior olive (IO) within the medulla oblongata (medulla) region of the brainstem project directly to PNs of the cerebellar cortex in each of the lobules. Mossy fibers originating from multiple areas including the pons and spinal cord (SC) synapse with the deep cerebellar nuclei (DCN) as well as projecting directly to the granule cell layer of the cerebellar cortex of all lobules. The DCN are the sole output of the entire cerebellum and project back to the spinal cord and brain stem, as well as targeting ventral tegmental area (VTA) and several cortical regions via thalamic nuclei.* ***(B)*** *The cerebellar cortex of each lobule is divided into 3 layers, molecular layer (ML), Purkinje neuron layer (PNL) and the granule cell layer (GCL). Mossy fibers excite granule cells (1), which are the primary excitatory neuron of the cerebellar cortex. Granule cell axons project into the molecular layer forming parallel fibers exciting PNs (2), which in turn provide the sole output of the cerebellar cortex, an inhibitory drive onto the DCN (3). PNs each receive excitation from a singular climbing fiber (4), glutamate spillover from this input can lead to MLIN excitation (5). Parallel fibers also excite MLINs (6), inhibitory interneurons targeting Purkinje neurons, both at the somata (7) and the dendritic branch (8), PNs in turn provide feedback inhibition onto MLINs (9). MLINs also provide inhibitory connections to each other (10), autaptic inhibition (11), and have direct connections to Golgi cells (12). Dendrites of Golgi cells descend from the molecular layer to their somata lying in the granule cell layer. They also receive excitatory drive from the parallel fibers (13) and mossy fibers (14). Golgi cells provide the main inhibitory drive of the granule cell layer, inhibiting granule cells (15), and provide inhibition onto one another (16). DCN - deep cerebellar nuclei, VTA - ventral tegmental area, IO - inferior olive, SC - spinal cord, ML - molecular layer, PNL – Purkinje neuron layer, GL – granule cell layer. V-IX in (B) correspond to lobule numbers. + indicates excitatory input (descending size indicates spillover), -- indicates inhibitory, colour of each indicates type of neuron input emerges from.*

1.2.3. Physiology & Function of Distinct Neuronal Populations of the Cerebellar Cortex Circuit

Molecular layer interneurons

Basket and stellate cells comprise the MLINs, so named from their distinctive morphological structures, stellates with star like formation and basket cell axons forming specialised basket shaped web around the PN somata, which are referred to as pinceau (Brown et al., 2019; Eccles et al., 1966). MLINs are parvalbumin positive GABAergic neurons, which provide the primary inhibitory tone onto PNs, along with reportedly some inhibition of Golgi cells (D'Angelo, 2008). The most superficial stellate cells, the soma of which reside in the outer two thirds of the molecular layer have sagittal projecting dendrites and axons, primarily targeting PN dendrites (Rizza et al., 2021). Lying deeper towards the PN layer, basket cells form direct pericellular nets surrounding the PN axon initial segment, ideally positioned to modulate PN output (Prestori et al., 2019a). These pinceau provide GABAergic inhibition, but notably, activation of basket cells also creates an instant ephaptic inhibition preceding the chemical interaction (Blot and Barbour, 2014). The inhibitory drive onto PNs, produced through convergence of approximately 5-10 MLINs per PN, is the result of complex electrochemical MLIN-MLIN coupling, autaptic inhibition and feedback inhibition from PN contacts directly onto MLIN soma (Kim and Augustine, 2021). Both Stellate and Basket cells display fast spiking action potential firing properties, reaching up to 300 Hz (Bao et al., 2010). *In vivo* recordings reveal that MLINs display irregular intrinsically modulated firing frequencies can range between 1-35 Hz, supporting findings in slices (Bao et al., 2011; Häusser and Clark 1997; Jörntell and Ekerot, 2002; Kim and Augustine 2021). MLINs are interconnected electrically and chemically to each other on a sagittal plane, with gap junctions likely to allow synchronous activity (Kim et al., 2014; Mann-Metzer & Yarom, 2000). The organisation of local MLIN clusters together modulate the spatial and temporal output of PNs primarily through lateral and feedforward inhibition, driven by PFs from the GCs innervating both PNs and MLINS (Kim and Augustine, 2021). There is also glutamatergic excitation of MLINs from CFs, via glutamate spillover (Kim and Augustine, 2021). Through the dendritic and somatic modification of PN activity, MLINs regulate the pacemaker output and narrow the window for suprathreshold summation following GC excitation (Buzsáki, 1984; Prestori et al., 2019a). In addition, MLINs have direct functional connections to Golgi cells (Dumoulin et al., 2001). However, the extent of this inhibition is controversial, simultaneous electrophysiological recordings of MLINs and Golgi cells have indicated there is no synaptic input, and optogenetic stimulation of MLINs with simultaneous Golgi cell and PN recordings also showed inhibition of PNs but not Golgi cells (Hull and Regehr, 2012). Therefore, the functional relevance of the direct MLIN-Golgi cell connections is yet to be established (Prestori et al., 2019a).

MLINs are highly driven by sensory stimulation and motor action (Kim and Augustine, 2021). For example, calcium imaging studies using genetically encoded calcium indicators expressed in MLINs, show high correlation of neuronal activity with locomotion and orofacial movements such as licking and bruxing (Astorga et al., 2017; Gaffield and Christie 2017; Ozden et al., 2012). Furthermore, optogenetic stimulation of MLIN drives eyelid closure, which shows a direct functional influence of MLIN activity on behaviour (Heiney et al., 2014). Similarly, optogenetic inhibition of MLINs, through the light activated proton pump, Archaerhodopsin 3.0, has also been shown to impair locomotion (Jelitai et al., 2016). Aside from these traditionally associated cerebellar functions, MLINs are also implicated in the facilitation of learning (Wulff et al., 2009). A mouse model in which PNs lack the $GABA_A$ receptor, showed an impaired ability to modify the amplitude and timing of the optokinetic reflex over multiple training sessions (Wulff et al., 2009). The stark reduction in vestibulo-ocular learning was particularly interesting given that the initial impairment was significant but relatively mild, which suggests the strongest consequence of the disrupted MLIN-PN inhibition, is disrupted learning (Wulff et al., 2009). Electrophysiological and calcium recordings PN dendrites later showed that MLINs inhibit CF driven calcium signals in the PN dendrite without altering somatic activity (Rowan et al., 2018). When PFs and CFs were stimulated simultaneously, MLIN inhibition of CF related activity in the PN dendrite was shown to facilitate long-term potentiation (LTP) of PF–PN dendrite postsynaptic potentials. Whereas, lack of MLIN inhibition, supported long-term depression (LTD) of PF potentials, thus showing that MLIN activity has a range of influence on PN dendrite plasticity (Rowan et al 2018). Rowan and colleagues also revealed the behavioural relevance of the MLIN influence in plasticity, with simultaneous optogenetic activation of CFs and MLINs leading to a reduced vestibulo-ocular reflex, whilst stimulation of CFs alone increased the reflex (Rowan et al., 2018). Therefore showing that MLIN influence on functional PN plasticity could be the mechanism by which MLINs facilitate motor learning. Furthermore, these data show that MLIN can drive differential alterations of activity in distinct PN compartments. Through chemogenetic manipulation, Badura and colleagues performed a fascinating functional segmentation of cerebellar regions (Badura et al., 2018). They found that inhibition of MLINs in lobule VI blocked reversal learning, whilst VII activity was required for novelty seeking behaviour and the Crus I/II MLINs were involved in social preference decision making (Badura et al., 2018). In addition two-photon imaging in lobule VI also revealed that MLIN calcium responses encode preference information during associative learning (Ma et al., 2020). These studies provide strong evidence that MLIN activity is intertwined with a range of higher cognitive functions in rodents. The impact of cerebellar cortex function on such behaviours has also been studied in humans, using non-invasive techniques.

Although not specific to MLINs, manipulation of cerebellar cortex excitability has been shown to influence motor learning and higher cognitive function in humans (Pauly et al., 2021). TMS protocols applied to the cerebellum have been documented to alter (increasing or decreasing depending on the protocol) motor evoked potentials in downstream motor cortex, which is suggested to be due to modulation of PN output (Pauly et al., 2021). Anodal transcranial direct current stimulation (tDCS) of the posteromedial cerebellum in humans improved results in a cognitive sequencing learning task, remaining up to one week post stimulation (Ma et al., 2023). Furthermore, tDCS can also improve mental state recognition, tested through the ability of subjects to match a description of an emotion to the corresponding image of a human face (Clausi et al., 2022). Whilst changes to excitability in this region with such broad stimulation methods are poorly understood, this indeed underscores the importance of the output of the cerebellar cortex circuit to a wide range of behaviours in humans, supporting the findings in rodents. As discussed research in mice shows that MLINs are essential in governing the output of the cerebellar cortex through spatiotemporal regulation of PN excitability. This is overall in line with growing evidence that MLINs and the cerebellum per se are highly integrated in higher social and cognitive function, and potentially compromised in psychiatric disorders, (Mapelli et al., 2022; Stoodley et al., 2016), alongside the well-documented role in sensorimotor processing (Chu et al., 2012; Jörntell et al., 2010; Ma et al., 2020). Understanding the interactions between the MLINs and their primary target PNs, is crucial to mapping how the cerebellar cortex circuit breaks down leading to altered behaviour in *Sca1*; we therefore also examine the sole output cell of the network, the Purkinje neurons.

Purkinje Neurons

PNs are one of the most recognisable neurons of the brain, characterised by their large soma, tree-like dendritic branches and with the prominent axon, projecting to the DCN (Attwell and Mehta, 2021). They are parvalbumin positive GABAergic neurons, and the only output of the cerebellar cortex. PN are each stimulated by a singular CF, depolarizing the entire membrane through voltage gated calcium channels. Remarkably, the dendritic branches receive only individual or few synaptic contacts from over 100,000 different PFs in humans and rodents (Hirano, 2018; Ito et al., 1982). Their inhibition of the DCN are the result of complex computations of the densely packed cell–cell interactions within the cerebellar cortex. This manifests in two activity forms, simple spiking, which is intrinsically generated pacemaker activity, heavily influenced by GC input via PFs, or complex spikes, driven largely by CF input (Beckinghausen and Sillitoe, 2019; Streng et al., 2018). Simple spiking is the dominant output, resting around 40-50Hz in mice, however firing frequencies can increase up to above 200Hz for example during locomotion, an effect that is largely modulated through the MF - GC - PF pathway (**Fig. 2**) (Arancillo et al., 2015; de Solages et al., 2008; Thach, 1967). Complex spiking

occurs at a low frequency of 0.5-1Hz (Arancillo et al., 2015; Streng et al., 2018) and are suggested to encompass dendritic calcium spikes, contributing to LTD at the PF-PN synapse, they occur in the form of a single fast spike followed by two-four slow spikes (Schmolesky et al., 2002).

As the centrepiece of the cerebellar cortex, the PN output exhibits a major influence of the initiation and maintenance of motor behaviour. Studies in multiple species have revealed that the PN firing rate is coordinated with onset, intensity and timing of locomotion, thereby varying widely across cycles of movement (Armstrong and Edgley, 1988; Chang et al., 2020; Llinás, 2011; Sauerbrei et al., 2015; Tsutsumi et al., 2020). The IO drives large synchronous generation of complex spikes across PNs during locomotion (Welsh, 2002) and simple spiking is reported to coordinate with step cycles in cats (Apps and Lidierth, 1989). Complex spiking drives a cessation of simple spiking, the functional relevance of these two distinct types, and their intricate relationship with one another is gradually being unravelled by research predominantly in rodent models (Burroughs et al., 2017; Horn et al., 2010). The balance of excitation-inhibition at the PN dendrite orchestrates the output of the cerebellar cortex. GCs drive depolarisation in the PN dendrites, which, modulated through MLINs, drives simple spiking output facilitating locomotor function (Jelitai et al., 2016).

Training mice in sensorimotor tasks can reveal how PN firing facilitates information processing. In a study by Tsutsumi and colleagues, mice were trained to lick within a 500ms time frame in order to receive a reward, only if they received both air puff and auditory tone in unison (Tsutsumi et al., 2020). The authors used optogenetic manipulation of PNs in combination with silicon probe mediated electrophysiological recordings. They revealed that the coordination of coherent complex spike activity provides the temporal accuracy to the specific motor response following the sensory stimuli, whilst simple spikes modify the latency and initiation (Tsutsumi et al., 2020). In rats, multi-electrode recordings unravelled further the functional clustering of PNs across step cycles, revealing a dependency of PN firing on the phase of step, supporting earlier findings that PN firing is rhythmically altered with step cycle (Armstrong & Edgley, 1984; Powell et al., 2015; Orlovsky, 1972). Studies have shown that locomotion speed can either negatively or positively drive PN firing (Sauerbrei et al., 2015). Research using high density silicon probes recordings to study locomotion in vermis lobules IV, V, Via of mice, identified the majority of neurons they recorded from (a combination of PNs, Golgi and MFs) to indeed be modulated by stepping cycle (Muzzu et al., 2018). They found that around 45% of neurons indeed increased their firing with locomotion speed, whilst others were negatively correlated with it. Interestingly, of these positively modulated cells the firing properties represented upcoming speeds, activity driving motor activity, as opposed to sensory

response (Muzzu et al., 2018). This details a role in locomotion, particularly execution of motor output.

Miniaturised head-mounted one-photon imaging was utilized to monitor vermis PNs in lobule V of mice navigating a 3D environment (Lyu et al., 2023). This showed a counter balance activity between MLINs and PNs, with calcium transients of the latter decreasing whilst moving either up or down the environment on a population level, in time with augmented responses of the MLINs (Lyu et al., 2023). Non-specific inhibition of all neurons within the superficial cortex of lobule V, using chemogenetic tools, prevented running uphill in the mice. The authors suggest that activation of MLINs in time with PN inhibition is therefore essential for adjusting locomotion to a non-horizontal environment (Lyu et al., 2023). Evidence using more specific inhibition of MLIN is required to verify the exact mechanism underlying the functional deficits, however, this study already reveals how specific motor skills can breakdown following compromised cerebellar cortex circuit function within one lobule alone.

PN activity has been shown to associate with numerous behaviours, including whisking (Chen et al., 2016), visual and ocular motor responses (Norris et al., 2004), fine motor control (Heiney et al., 2014; Hewitt et al., 2015) and a variety of learning tasks (Jirenhed et al., 2007; Lisberger et al., 1994; Nguyen-Vu et al., 2013; Ojakangas and Ebner, 1992). The extensive range of functional roles possibly shows why damage to these cells causes widespread symptoms in diseases such as SCA. Lyu and colleagues here take advantage of studying multiple cells simultaneously to reveal novel insights into cerebellar cortex functionality. Similarly, in our own research, we wanted to not only explore the relationship between PNs and MLINs, but also consider the third major inhibitory neuron of the cerebellar cortex circuit, the Golgi cells.

Golgi cells

The primary inhibitory neurons of the GC layer, Golgi cells, have a close connection to central figures in the history of neuroscience, identified by and ultimately named after Camillo Golgi with his pioneering stains (Golgi, 1883), and later detailed morphologically by Ramón y Cajal (Garcia-Lopez et al., 2010; Sotelo, 2008). Golgi cells are primarily both GABAergic and Glycinergic, although sub populations use either GABA (~20% of Golgi cells) or Glycine (~5%) alone (Prestori et al., 2019a). Structurally, their sagittal arrangement of axon terminals form approximately three to five inhibitory synapses per GC in their surrounding area, whilst they receive excitation from MF inputs within the GC layer and have dendrites that reach into the molecular layer, receiving input from both MLINs and PFs (D'Angelo, 2008; Duguid et al., 2015). Furthermore, Golgi cells are electrically and chemically coupled to one another (Prestori et al., 2019a). The electrical gap junctions connecting Golgi apical dendrites, characteristically lying in the molecular layer, have been shown allow low frequency synchrony (Dugué et al.,

2009). Yet, these junctions also facilitate the rapid de-synchrony, occurring with local MF activation (Vervaeke et al., 2010).

Golgi cells are positioned to gate the excitatory drive of the 100 billion GCs within the cerebellar cortex, thereby modulating the MF input to the cerebellar cortex (Eccles et al., 1967). Physiologically described by Eccles in the 1960s, they also display pacemaker activity (Eccles et al., 1967). Their firing properties identified with single unit recordings *in vivo* show intrinsically generated rhythmic activity, which is maintained across species (Edgley and Lidierth, 1987; Miles et al., 1980), in rodents occurring at roughly 2-30Hz (Holtzman et al., 2006; Vos et al., 1999a). Golgi firing displays partial synchrony arranged over the parasagittal axis in line with local PF tracts (D'Angelo, 2008; Vos et al., 1999b).

Golgi cell pacemaker activity is modulated through MF inputs following sensory stimulation or motor behaviour occurring in two distinct forms. Frequency of Golgi cell pacemaker firing may be adjusted, as with locomotion (Edgley and Lidierth, 1987). The second form is a burst spiking activity over around 10 ms, in the pattern of 1-3 sequential spikes (Galliano et al., 2010). This can be elicited by facial sensory stimulation (Holtzman et al., 2006), following which an extended pause in activity occurs (Voz et al., 1999a; Galliano et al., 2010). It is suggested, that the three spikes reflect; (1) trigeminal MF input, (2) pons MFs from cortical sensory motor processing and finally, (3) stimulation from PFs respectively (Galliano et al., 2010). Two primary forms of Golgi cell activity that then inhibits GCs, can be grouped as feedforward (MF - Golgi cell - GC) or feedback inhibition (MF - GC - Golgi cell - GC), thereby modulating the sensorimotor responses of the GCs (Dugoid et al., 2015).

Golgi cell modulation of GC layer activity encompasses the regulation of plasticity at the MF – GC synapse (Mapelli and D'Angelo 2007; Sgritta et al 2017). Golgi cells also provide lateral inhibition that organises nearby GC activity into tight groups (referred to as "centre-surround organisation"), thereby controlling depolarization in GCs, limiting NMDA receptor opening and therefore LTP (D'Angelo et al., 2013). Higher inhibitory tones generally induce LTD, whilst weaker would allow increased calcium influx and therefore encourage LTP in GCs, slowing and increasing responsiveness to MFs respectively (D'Angelo, 2008; Lisman, 2003; Nieus et al., 2006). Even sparse MF input directly onto Golgi cells can alter their pacemaker activity with high precision, leading to a feedforward inhibition of GCs (Kanichay and Silver, 2008). Together, Golgi activity creates a precise reorganisation of MF information (D'Angelo et al., 2013; Sudhakar et al., 2017). *In vitro* and *in vivo* recordings, along with computational models, are gradually unravelling the complexities of how this fascinating input circuit is balanced to facilitate cerebellar associated behaviours.

Various sensory stimulation (tactile and air puff) and motor activity influences Golgi cell activity, directly or indirectly through MF pathways (Holtzman et al., 2006; Prsa et al., 2009). Indeed impairing the cerebellar network through targeting Golgi cells causes a range of symptoms. Ablation of Golgi cells, for example, can cause severe motor impairments (Watanabe et al., 1998). More specifically, a knock-out mouse model disrupting Golgi-GC inhibition produces severe deficits not only in coordination but also motor learning (Meng et al., 2019). These findings indicate multifaceted functional roles for Golgi cells. In support of this, simultaneous *in vivo* recordings in monkeys of MF and Golgi cells reveal that the activity in the latter does not simply reflect the behaviour driven MF discharge (Prsa et al., 2009). Therefore arguing against the notion that Golgi cells simply provide "gain control" for GC activity, indicating more complex roles. Indeed, a recent study using *in vivo* two-photon calcium imaging, identified a collective slow behaviourally-associated (locomotion and whisking) alteration in Golgi cell responses across the network, in both the vermis and Crus I/II (Gurnani and Silver, 2021). However, observing population responses under the shorter time-span of 1 second consisting of more heterogeneous Golgi activity encoded accurate behaviourally relevant information (Gurnani and Silver, 2021). These data provide elegant descriptive evidence that supports earlier observations that Golgi cells not only provide a general gain control, but are essential to encoding of sensorimotor processing within the cerebellar cortex. This is achieved by precise spatiotemporal modulation of MF inputs to the GC layer (D'Angelo and De Zeeuw, 2009; Kanichay and Silver, 2008).

Overall, given these crucial roles in various behaviours relevant to *Sca1* symptoms and in the complex organisation of the input to the cerebellar cortex circuit, we therefore also included Golgi cells in our analysis to understand circuit alterations in *Sca1*.

1.3. Spinocerebellar Ataxia Type 1 (*Sca1*).

1.3.1. Genetic Background of *Sca1*.

After establishing a sub group of autosomal dominant SCAs, the causative gene for *Sca1* was identified on chromosome 6 in the HLA region in the 70s, a crucial step forward in the field (Jackson et al., 1977; Orr, 2012; Yakura et al., 1974). Similar to work with trinucleotide repeat expansion based-diseases such as Huntington's disease (HD), Orr and colleagues identified an unstable CAG repeat encoding a polyglutamine tract (polyQ tract) through cloning of the *Sca1* gene (Orr et al., 1993). In addition, they showed that an increased length of these CAG repeats associated with greater severity and younger age of onset (Orr et al., 1993). Identification and further study of the *Sca1* gene revealed that it encoded the protein ataxin-1, the gene became known as *ATXN1* (Banfi et al., 1994). This research led to establishing a variety of mouse models, propelling the understanding of the disorder forward. Importantly, it

became clear that classical SCA features such as ataxic gait and motor deficits occurred prior to cell death. Therefore, such symptoms are driven by neuronal dysfunction, rather than atrophy (Orr & Zoghbi, 2001).

The ataxin-1 protein is ubiquitously expressed across the brain, with a healthy *ATXN1* gene containing 6-42 CAG repeats (**Fig. 4A**) (Zoghbi & Orr, 1995). Repeat numbers exceeding 21 are however interrupted by one to three CAT trinucleotides. In *Sca1*, there will be a minimum of 39 uninterrupted CAG repeats (Olmos et al., 2022). In the healthy condition, ataxin-1 can be shuttled between cytoplasm and nucleus, mutant ataxin-1 on the other hand, can be transported to the nucleus, but cannot then move back (Irwin et al., 2005). The ataxin-1 protein has been shown to be able to bind to chromatin, transcription factors and RNA, thus being involved in repression in transcription via the Notch signalling pathway, and RNA splicing (Didonna et al., 2020; Kohiyama and Lagalwar, 2015; Seidel et al., 2012; Tong et al., 2011; Zoghbi and Orr, 2009). Studies have shown that the *ATXN1* mutation is a gain-of-function mutation, and indeed, the expanded CAG tract in *ATXN1* is required for pathogenesis (Burright et al., 1995; Zoghbi and Orr, 2009). When a loss of function *ATXN1* mutation was investigated in mice, no classical disease symptoms were observed (Matilla et al., 1998). For the purpose of this study, we utilised the knock-in mouse line, *Sca1*$^{154Q/2Q}$, based on the expression of an expanded repeat of 154 CAGs in the *Sca1* locus, inserted through homologous recombination (Watase et al., 2002). These mice display symptoms closely mirroring the human disorder, beginning with loss of motor skills, then displaying ataxic gait muscle wasting, cognitive impairment and ultimately, premature death (**Fig. 4A**). Importantly, the mutated *ATXN1* is present in all cells as it is in the human disorder, as opposed to just PNs, which is common in several models (Burright et al., 1995). Knock-in models with shorter CAG repeats have also been utilised but do not induce the severity of muscle wasting and ultimately a decreased lifespan that is reminiscent of the human disease. With this longer tract, Watase and colleagues found, consistent with earlier models, the selective neuronal atrophy occurs only in the late stage of the disorder, far after symptom onset (Watase et al., 2002). This suggests that neuronal dysfunction, as opposed to neuron loss, is the driver of symptoms. Which leads to the question, how does neuronal dysfunction manifest in *Sca1*? As is a common feature of neurodegenerative disorders, there is an accumulation of protein aggregates, in this case suggested to be due to the mutant ataxin-1 protein-protein and protein-DNA interactions (Chen et al., 2022). Earlier work investigated the relationship between such intracellular aggregates and symptom onset in mouse models of *Sca1* (Orr, 2001).

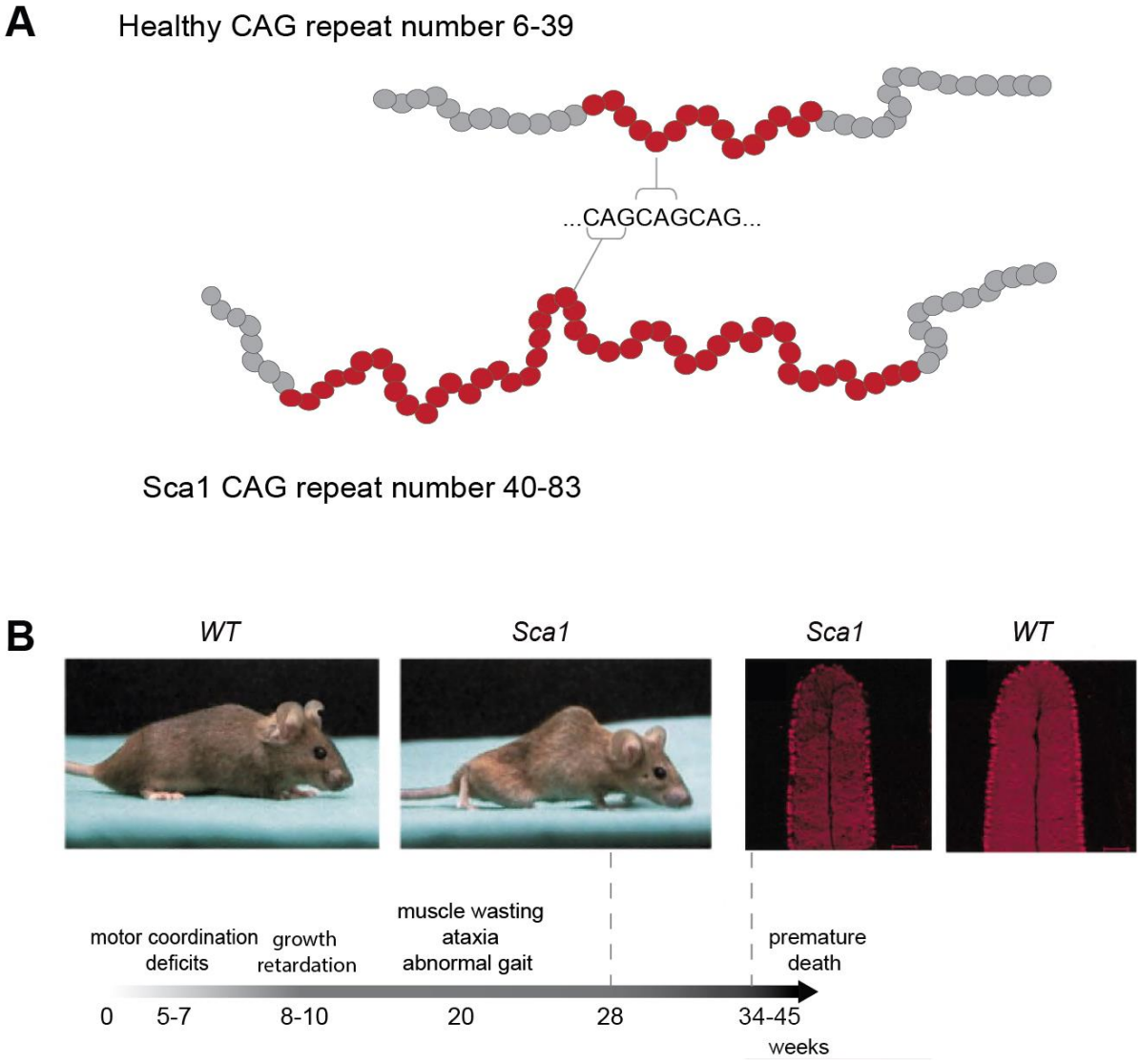

Figure 4: ***Timeline of Sca1 disease progression. (A)*** *CAG repeat expansions in the gene ATXN1 cause a polyglutamine repeat expansion in the ataxin-1 protein. (**B**) Sca1$^{154Q/2Q}$ knock-in mice (referred to as Sca1 mice throughout). Images show 28-week-old Sca1 mouse with wild type littermate and PN degeneration occurring in Sca1 compared to WT at 34 weeks. Dashed line indicates age (weeks) of images in relation to timeline of key behavioural deficits and visible symptoms. WT –wild type littermate. Scale bar in (B): 100 µm. Adapted from Neuron with permission from Elsevier (Watase et al., 2002).*

1.3.2. Protein Aggregation in *Sca1*

The specific nature of how the *ATXN1* gene mutation leads to pathogenesis is unclear. However much research has focused on the emergence of nuclear inclusions and protein aggregates, a hallmark feature of several polyglutamine and neurodegenerative disorders (Orr, 2001; Ross and Poirier, 2004). Misfolded polyglutamine aggregates forming nuclear inclusions in neurons were initially described in HD patients (Roizin, 1979), followed by the confirmation in patients of *Sca1* & SCA type 3 (*Sca3*) (Paulson et al., 1997; Skinner et al., 1997).

The ataxin-1 protein is present in both the cytoplasm and nucleus, given it readily binds with a number of proteins regulating transcription, it is suggested that the primary function lies

within transcriptional modification (Kohiyama and Lagalwar, 2015; Menon et al., 2013; Servadio et al., 1995). In the process of translocation to the nucleus from the cytoplasm, ataxin-1 is phosphorylated and then associates with 14-3-3 (Jafar-Nejad et al., 2011; Lai et al., 2011), a family of ubiquitously expressed multifunctional eukaryotic proteins that make up around 1% of soluble brain protein (Cornell and Toyo-Oka, 2017). The ataxin-1/14-3-3 complex must dissociate before entry to the nucleus (Lai et al., 2011). The cytoplasmic stabilisation of mutant ataxin-1 protein via phosphorylation and 14-3-3 interaction leads to nuclear localisation and ultimately aggregate formation (Irwin et al., 2005; Kohiyama and Lagalwar, 2015). Therefore, understanding the mechanisms of nuclear translocation has been a major focus of research. Phosphorylation of ataxin-1 occurs at the serine 776 (Ser-776) site, and evidence points towards a role for this phosphorylation in directing protein complex formation, not only with 14-3-3, but also the transcriptional repressor Capicua (CIC) and other complexes handling transcription (de Chiara et al., 2009; Menon et al., 2012). Chen and colleges revealed in a fly model, that the specific formation of Ser-776/ataxin-1 and 14-3-3 complex drives *Sca1* nuclear inclusions (Chen et al., 2003). Formation of this new complex is crucial to slowing cytoplasmic degradation of mutant ataxin-1 and therefore leads to nuclear translocation and protein accumulation (Chen et al., 2003). Further corroborating these findings, the generation of a *Sca1* mouse model with alanine at position 776 rather than serine, led to dramatic slowing of nuclear inclusions and only minor disease state, with PN atrophy largely prevented (Emamian et al., 2003). This suggests that a combination of polyglutamine expansion and protein-protein interaction within the nucleus initiated through phosphorylation specifically at a serine site in the cytoplasm may drive pathology (Emamian et al., 2003). Building upon these findings, recent work has further implicated these protein interactions in the facilitation of *Sca1* pathogenesis. The mutant ataxin-1-CIC complex is indeed required for gain of function toxicity, whereas preventing this interaction inhibits toxicity and *Sca1* pathology (Rousseaux, Tschumperlin, Lu et al., 2019). Furthermore, Chopra and colleagues showed that mutant ataxin-1-CIC interaction can generate neuronal dysfunction in a region specific manner via altered ion channel expression, consequently driving PN spiking abnormalities and degeneration (Chopra et al., 2020). These findings are in agreement with earlier work which showed exercise could alleviate *Sca1* symptoms also through reduction of CIC levels (Fryer et al., 2011). It is important to note however, success in mouse models through targeting 14-3-3 or CIC appears to address specifically dysfunctional PN phenotypes, without alleviating brainstem related pathology (Fryer et al., 2011; Jafar-Nejad et al., 2011; Rousseaux, Tschumperlin, Lu et al., 2019). It is therefore unclear if these interactions can lead to genuine therapeutic interventions in patients.

The exact nature of the relationship between protein-protein interaction, aggregation and human *Sca1* pathology remains elusive. Whilst strong evidence detailed above outlines

the necessity for protein-protein interaction in driving disease state, nuclear inclusion aggregation per se does not appear to cause *Sca1* dysfunction and degeneration (Orr and Zoghbi, 2001). The contrary to these findings was initially suspected, given large insoluble ubiquitin positive intranuclear inclusions were identified in PNs of the cerebellum, the pons and other neurons throughout the brains of *Sca1* patients (Duyckaerts, et al., 1999; Skinner, et al., 1997). Also in cell culture experiments such aggregates do raise the susceptibility to cell death, along with inducing oxidative stress and derailing protein synthesis in induced pluripotent stem cells (IPSCs) (Hackam et al.,1998; Laidou et al., 2020). However, in 1998, Klement and colleagues studied a transgenic mouse model expressing mutant ataxin-1 in the nuclei of PNs, but with a deletion in the self-associated region of ataxin-1 (Burright et al., 1997), which prevented the formation of ataxin-1 aggregates (Klement et al., 1998). Crucially, these mice presented ataxia and PN pathology despite the lack of nuclear aggregates. Conversely, disrupting nuclear localisation of the mutant protein did indeed prevent disease course, indicating nuclear localisation but not aggregation underlies pathogenesis (Klement et al., 1998). In line with this, a mouse model preventing expression of ubiquitin E3 ligase of Ube3A, which is required for degradation of ataxin-1 via ubiquitin-dependent proteasome complex, again prevented nuclear inclusion formation but increases the severity of *Sca1* like pathology (Cummings et al., 1999). Additionally, in a knock in mouse model, in which, ataxin-1 is not overexpressed, PNs remain highly vulnerable despite inclusions only occurring in the very late stages of disease progression, long after symptom onset (Watase et al., 2002). In support of these findings, research on post-mortem tissue has indicated that cells with inclusions are in a better condition, suggesting a protective role (Nagaoka et al., 2003). More recent evidence has supported this, suggesting these insoluble polyQ aggregates provide some neuroprotective qualities, and it is in fact the soluble form that is cytotoxic (Todd and Lim, 2013). Indeed Takahashi and colleagues in 2008 showed that neuronally differentiated cells survived longer with inclusion bodies than with soluble polyQ oligomers (Takahashi et al., 2008), this has been shown in a HD model (Arrasate et al., 2004), however is currently lacking in *Sca1*. Overall, such mounting evidence points towards that these protein aggregates in the form of nuclear inclusions are not causal in *Sca1* dysfunction and degeneration (Orr H., 2001; Takahashi, et al., 2008).

Protein aggregation has been a major focus of research in neurological disorders, with no therapeutic benefit translating to the clinic. There are still potential therapies in clinical trials, and prospects for aiding early diagnosis (Soto and Pritzkow, 2018; Takalo et al., 2013; Takeuchi and Nagai, 2017), however, focus is moving to alternate targets for intervention. Identifying dysfunction early in neurodegenerative disorders has become another important area of research.

1.3.3. Altered Calcium Dynamics and Neuronal Excitability in *Sca1*

The development of neuronal dysfunction is a critical aspect to understand in *Sca1*, as it was shown to occur prior to neuronal atrophy, and independent of protein aggregation (Dell'Orco et al., 2015; Orr, 2012; Orr & Zoghbi, 2001). It is common that such dysfunction manifests in the form of altered action potential firing properties and intriguingly, across several neurodegenerative diseases, there is now evidence to suggesting that neurodegeneration could be delayed or even prevented by targeting early dysfunctional neuronal activity (Braz et al., 2022; Palop et al., 2006; Tobin and Singer, 2000). So how does an expanded ataxin-1 protein affect the physiological properties of neurons and at what point do such abnormalities emerge?

Mouse models are crucial to answer such questions. One element to understand is how mutant *ATXN1* alters gene expression, potentially highlighting the origin of downstream pathophysiology. Pathogenic transcriptional reduction has been identified in multiple *Sca1* models of varying severity, which has allowed for a pinpointing of genes relevant to symptom development (Crespo-Barreto et al., 2010; Ingram, et al., 2016; Serra et al., 2004). Studying alterations in gene and protein expression, with particular focus on those highly expressed in PNs, has consistently shone a spotlight on the regulation of glutamate and calcium signalling (Serra et al., 2004). Disruption of PN calcium homeostasis and calcium mediated physiological processes can drive dysfunction and cell death (Prestori et al., 2019b). Examples of such early alterations in *Sca1* were identified in the *Sca1* B05 mouse model, which expresses 82 CAG repeat (82Q) mutant ataxin-1 (Pcp2-ATXN1[82Q]), under the PCP promoter (therefore solely in PNs). The mice then present *Sca1* like symptoms and pathology (Burright et al., 1995). A decrease in expression of several genes related to glutamate and calcium handling was identified in these mice around the age of symptom onset (~ 5 weeks old/p35), as well as in the later stages of the disorder. These findings were further supported by immunostaining in *Sca1* human tissue, revealing downregulation of excitatory amino acid transporter 4 (EAAT4) and inositol 1,4,5-triphosphate receptor (IP3R1) as early as postnatal day (P) 10, and the dendritic protein Homer-3 (Lin et al., 2000; Serra et al., 2004). In support of this, proteomic studies of the knock-in mouse model *Sca1*$^{154Q/2Q}$, with universal expression of mutant *ATXN1*, revealed widespread alterations to the PN synaptic proteome (Ruegsegger et al., 2016). Proteins essential to regulation of glutamate signalling and intracellular calcium cascades were again disrupted, once more including the dendritic protein Homer-3, which couples IP3R1 with metabotropic glutamate receptor 1 (mGluR1) (Shiraishi et al., 2004). Importantly, restoring

Homer-3 expression could alleviate symptoms and prolong survival of the mice (Ruegsegger et al., 2016).

IP3R1 is the predominant isoform in neurons of such calcium transporters, expressed on the endoplasmic reticulum. Mice deficient of IP3R1 across the cerebellum and brainstem show perturbed PN complex spikes firing, coinciding with dystonic movements (Hisatsune et al., 2013). Additionally, computational modelling of the biochemical calcium balance and membrane excitability in PNs, indicates a central role for IP3R1 in regulation of PN excitability, through functional coupling with calcium-activated channels such as BK channels and expression of dendritic AMPA receptors (Brown et al., 2014). Adapting this model to *Sca1*, based on mouse and clinical studies, suggests that with the lower abundance of IP3R1 expressed in *Sca1*, the transporter is hypersensitive, contributing to PN dysfunction (Brown et al., 2014).

The glutamate transporter EAAT4, reduces extracellular glutamate spillover (largely following CF innervation of PN dendrites), given its distribution localising with mGluR1 receptors on PN dendrites (Lin et al., 2000). Deficiency of EAAT4 can disrupt pacemaker activity through enhanced mGluR1 activation, induce ataxic phenotypes and trigger glutamate medicated neuronal apoptosis of PN (Perkins et al., 2018). Inhibition of EAAT4 is indeed linked to facilitation of LTD of PF-PN dendrite synapses downstream of mGluR1 activation (Brasnjo and Otis, 2001; Serra et al., 2004). This was further corroborated with RNA sequencing data, examining gene expression in the B05 mice and Pcp2-ATXN1[30Q]D776 mice, which model progressive PN pathology with ataxia, and ataxia independent of such pathology, respectively (Ingram et al., 2016). "Weighted Gene Coexpression Network Analysis" revealed distinct networks of co-expressed genes from the *Sca1* transcriptome, two of which were significantly disease-associated (Ingram et al., 2016). The expression profile of one module in particular that mirrored the development of pathology in PNs, implicated genes crucial to synaptic LTD and signalling pathways downstream of glutamate receptor activation (Ingram et al., 2016, Tejwani and Lim, 2020). Thus supporting earlier findings which implicated of dysfunctional signalling pathways intertwined with mGluR and LTD (Ingram et al., 2016). These data clearly outline a number of mechanisms by which calcium homeostasis is altered in *Sca1* models, which can drive changes in neuronal activity. Pathophysiology driven by aberrant calcium handling is a common feature across SCAs (Prestori et al., 2019b), it is therefore important to understand how pathophysiology manifests across the cerebellar cortex circuit in *Sca1.*

Neuronal plasticity and excitability at the dendritic spine is typically altered early in neurodegenerative disorders, contributing to symptomatic states (Tobin and Singer, 2000). Furthermore, several types of ataxias with similar profiles to *Sca1*, manifest specifically from mutations leading dysfunction to, or altered expression of, ion channels (Dell'Orco et al., 2015).

This includes calcium channels in episodic ataxia 2 and SCA type 6 (Ophoff et al., 1996; Saegusa et al., 2007) and potassium channels in SCA types 13, 19 and 22 (Duarri et al., 2015; Waters et al., 2006; Yalan and Kaczmarek, 2016). Implicating alterations in membrane excitability in driving SCA symptoms.

In the B05 model, both in slices and in vivo, PN simple spike firing was already reduced at the presymptomatic stage (2-4 weeks), the severity of this decline correlated with increased expansion of mutant ataxin-1 in PNs (Hourez et al., 2011). Furthermore, the complex spike duration and pause between complex spikes were both significantly increased in *Sca1* (Hourez et al., 2011). Early loss of the PN pacemaker activity has been confirmed in further studies, by 5 weeks of age in other *Sca1* mouse models, in addition to hyperexcitable PN dendrites (Bushart et al., 2018; Dell'Orco et al., 2015). Fascinatingly, the PN firing seems to restore at a later stage, (~15 weeks of age), in time with shrinkage of PN dendritic spines, a classical pathological feature of *Sca1*. The authors suggest that the dendritic shrinkage is therefore a compensatory mechanism to restore PN pacemaker firing, potentially through increasing the relative density of potassium channels with reduced expression in the model. This mechanism was confirmed through showing restoration of the density of calcium activated potassium channel, BK, and subthreshold-activated potassium channels, underlies the firing recovery (Dell'Orco et al., 2015). Furthermore, raising PN BK channel expression in the B05 mice also alleviated motor symptoms (Dell'Orco et al., 2015). In support of these findings, pharmacologically stimulating calcium activated potassium and subthreshold potassium channels was also shown to improve spike firing, and stimulating of the latter alone reduced PN dendritic hyperpolarization (Bushart et al., 2018). Exploring the relationship between BK channels and *Sca1* further, PN dendrites display increased calcium spikes (Chopra et al., 2018), potentially due to increased cytosolic calcium that can occur when BK channel numbers are reduced (Trombetta-Lima et al., 2020). The dendritic hyperexcitability can be recovered by increasing BK expression, in combination with pharmacologically stimulating other potassium channels (Baclofen), again improving motor performance and reducing dendritic shrinking (Chopra et al., 2018) and stimulating BK channels alone restores PN firing (Srinivasen et al., 2022). These data provide compelling evidence that reduction in BK channels provides a novel therapeutic target and further intertwines *Sca1* pathophysiology with calcium homeostasis. Alongside and tightly linked to calcium handling, many of the studies investigating alterations in *Sca1* gene expression discussed above also implicated glutamatergic signalling, downstream of mGluR1 activation.

1.3.4. Metabotropic Glutamate Receptor Signalling in *Sca1*

Aberrant calcium handling is closely tied to pathological adaptations downstream of metabotropic glutamate receptor (mGluRs) activation in *Sca1* (Shuvaev et al., 2017). PF to PN synapse communication occurs primarily through α-amino-3-hydroxy-5-methyl-4-isoxazolepropionic acid (AMPA) (fast excitation) and mGluR1 (slower excitation) (Batchelor and Garthwaite, 1997; Serra et al., 2004). Signalling downstream of mGluR1 modulates intracellular calcium stores via the phospholipase C (PLC)-IP3, protein kinase C (PKC) and short transient receptor potential channel 3 (TRPC3) pathways (Hartmann et al., 2011; Serra et al., 2004). Dysfunctional signalling cascades that regulate calcium can drive neuronal dysfunction and have been investigated in *Sca1* animal models (Lin et al., 2000; Power et al., 2016; Serra et al., 2004; Wu and Kapfhammer, 2022). A mouse model of moderate ataxia (*Sca1* 82Q Tre/Tre;tTA/tTA), displayed enhanced PF-mGluR1 activity at PN dendrites (Power et al., 2016). In the healthy cerebellar cortex circuit PF driven mGluR1 activation can lead to local calcium signals around the PN dendrite synapse (Canepari and Ogden, 2006). Power and colleagues showed that in the ataxic mice, there was an increase in the localised PF driven calcium signals in the PN dendrites, implicating amplified mGluR1 activation (Power et al, 2016). Importantly, motor symptoms of *Sca1* mice, are alleviated following mGluR1 inhibition (Power et al., 2016). Thus associating dysfunction of mGluR1-calcium pathways in PN dendrites in early or mild ataxic symptoms.

Conversely, there is also evidence that stimulation of mGluR1 can alleviate late stage symptoms in knock-in *Sca1*$^{154Q/2Q}$ mice (Notartomaso et al., 2013). In addition slow mGluR calcium responses in PN dendrites, following PF stimulation, have also been reported at 5 weeks in a lentivirus *Sca1* model, 82Q expanded repeat (Shuvaev et al., 2017) and motor impairment could again be temporarily improved through baclofen administration to stimulate mGluR1 (Shuvaev et al., 2017). The γ-Aminobutyric acid receptor-b (GABAb) agonist, baclofen, used at a low concentration (lower than the reported threshold dose for GABAb stimulation, 1um), is closely tied to mGluR1 stimulation without mediating classical GABAb pathways (Tabata & Kano, 2006). The vastly contrasting reports in these studies could be in partial due to the differences in ages and models. Moreover, baclofen is also not a “clean” drug, with most likely many off target affects, whereas Power and colleagues used a less tested but reportedly more specific inhibitor of mGluR1 (Power et al., 2016). It is also of note that all studies were completed in slices, whilst these recordings provide strong insight into *Sca1* circuit dysfunction, there is evidence to suggest that recordings from slices can be variable based on slice preparation and may alter again from *in vivo* recordings (Opitz et al., 2017). These studies indeed show it is highly likely that mGluR signalling is disrupted in *Sca1*, investigation into mGluR1 dysfunction *in vivo* will provide important clarity. Alongside this,

calcium dynamics within PN and their dendrites *in vivo* is required, to further unravel glutamatergic dysfunction, but also investigate GABAergic mechanisms. Indeed, GABAergic inputs onto PNs are far less studied, but have recently reported to be increased in the early weeks after birth in Sca1 mice (Edamakanti et al., 2018). The functional impact of the increased inhibition, remains elusive. Furthermore, many of the mouse models discussed here rely on selective PN expression of mutant ataxin-1. This produces an unrealistic methodological bias, as the mutant ataxin-1 in human patients is ubiquitously expressed. To understand circuit balance in the cerebellum knock-in models such as developed by Watase and colleagues (Watase et al., 2002), present a useful insight by providing a representative universal expression seen in patient populations.

We hope to gain a novel insight into *Sca1* pathophysiology and calcium dynamics, not just in PNs, but also across the cerebellar cortex circuit by also investigating MLINs and Golgi cells in the knock-in *Sca1*$^{154Q/2Q}$ model, by means of *in vivo* two-photon calcium imaging.

1.4. Calcium Imaging in the Cerebellum *in vivo*

Imaging calcium signals with genetically encoded calcium indicators (GECIs) of high spatial and temporal resolution *in vivo* allows recording of neuronal activity at single cell and population level together over time (Holtmaat et al., 2009; Russel et al., 2011). Modern indicators with rapid kinetics such as GCaMP7 or GCaMP8, allow for accurate detection of individual action potentials when imaged through two-photon microscopy (Dana et al., 2019). Furthermore, given that intracellular calcium pathways are essential to neuron health and function, identifying perturbed calcium signals in disease models can be important to understanding pathogenesis in neurological disorders (Liebscher and Meyer-Luehmann, 2012). The GCaMP family of indicators are single fluorophore GECIs. They consist of the enhanced green fluorescent protein (eGFP), calmodulin (calcium binding protein), and calmodulin-binding peptide M13 (Grienberger and Konnerth, 2012; Nakai et al., 2001). Binding with free calcium ions leads to a conformational change in the structure resulting in an enhanced fluoresce emitted (Grienberger and Konnerth 2012; Tian et al., 2009). The other major class of GECIs, are Förster or fluorescence resonance energy transfer (FRET) based indicators, known also as ratiometric indicators, containing two fluorophores. In the absence of calcium, there is emittance of the first fluorophore, the “donor” fluorophore. Upon binding to free calcium there is a conformational change in the structure, leading to energy transfer from donor to “acceptor” fluorophore, resulting in a shift in the ratio from donor to acceptor fluorophore fluorescence intensity (Thestrup et al., 2014). The ratio of fluorescence intensity is therefore dependent on calcium concentration, independent of highly heterogeneous GECI expression volume and concentration (Thestruo et al., 2014). Importantly for studies of disease

models, this allow recordings from FRET GECIs to give a more accurate measure of cytosolic basal calcium levels (Thestrup et al., 2014; Rose et al., 2014), alterations in calcium handling can be indicative of neurodegenerative diseases, in particular *Sca1* as discussed above (see **1.3.3.**).

Calcium imaging can be performed in anesthetised, or awake and behaving mice. Freely moving animals can be imaged using one-photon imaging utilising miniaturised 1-photon microscopes, mounted on the head of the mouse (Resendez et al., 2016). Alternatively, as is used in our research, one may use two-photon imaging in head fixed mice, running on treadmills (**Fig. 5A**). Two-photon imaging provides the higher spatial resolution and is advantageous to visually identify individual neurons, compartments of neurons and distinct neuronal populations based on morphology. Imaging in the cerebellum however does present several challenges. The inhibitory neurons of the cerebellum have fast baseline-firing rates that are too fast to resolve individual action potentials given the temporal resolution of our GECIs (Dana et al., 2019). However, the rapid spiking leads to scaling of fluorescence signal, which was shown by simultaneous patch-clamping and calcium imaging of PNs, and revealed that distinct transients emerge with breaks in the simple spike train (Ramirez & Stell, 2016). PNs display a particularly fast pacemaker firing, Ramirez and Stell showed that although this is too fast for GECIs to record individual action potentials, longer trains do indeed increase the amplitude of the recorded calcium signal (Ramirez & Stell, 2016). Quantifying the area under the curve of these calcium transients, as a measure of neuronal activity, reflects the accumulation of calcium resulting from these spike trains, with a larger area reflecting higher frequency trains of simple spike firing. As both MLINs and Golgis also display fast spiking properties, we thus opt to utilise this to quantify activity of all cell types. Notably, it has also been established through simultaneous calcium imaging and electrophysiological recordings that calcium signals in PN dendrites reflect complex spiking in healthy mice (Wagner et al., 2021). Therefore, by investigating calcium signal in both of these compartments, one can gather insight into distinct forms of PN activity.

2. OBJECTIVES

My research aimed to identify alterations in the activity of distinct inhibitory neurons of the cerebellar cortex in a *Sca1* mouse model. I initially studied these neurons under multiple conditions and distinct stages of the disease course, then investigated the functional implications of our initial descriptive data. The research can thus be broken down into answering the following points of investigation:

Is neuronal activity of inhibitory neurons in the cerebellar cortex circuit affected in Sca1 mice?

Are these changes dependent upon age and disease stage?

Can such alterations be manipulated, to restore circuit function and alleviate Sca1 disease features?

In the following sections **3.1.-3.16.** I will outline all the methods and materials used throughout this thesis. I then detail the results initially of our descriptive recordings in sections **4.1.1.-4.1.6.**, then the series of experiments exploring functional manipulation of this circuit in sections **4.2.1.-4.2.6.** These results are accepted for publication in: Pilotto, **Douthwaite** et al., "Early molecular layer interneuron hyperactivity triggers Purkinje neuron degeneration in SCA1." *Neuron* / 17 May 2023. The discussion of this project then follows in section **5.**

3. MATERIALS & METHODS

Partial text included here is accepted for publication in: Pilotto, **Douthwaite** et al., "Early molecular layer interneuron hyperactivity triggers Purkinje neuron degeneration in SCA1." *Neuron* / 17 May 2023.

Experiments conducted for this research were completed in collaboration between labs at Ludwig-Maximillians University of Munich (LMU) and University of Bern (UniBE). Materials and methods related to work completed at University of Bern will be indicated by "UniBE" throughout.

3.1. Mice Strains

The *Atxn1*$^{154Q/2Q}$ knock-in mice (B6.129S-Atxn1tm1Hzo/J) (*Sca1*, Watase et al., 2002), and the *PV-IRES-cre* mice (B6;129P2-Pvalbtm1(cre)Arbr/J) were obtained from Jackson Laboratory. To establish an *Sca1::PV-cre* mouse line, Atxn1$^{154Q/2Q}$ males were crossed with *PV-cre* homozygous females. Animals of both genders were equally used in the study. Mice were kept at a 12/12-hour light/dark cycle with ad libitum access to food and water and were group housed. Animal care, housing and procedures were approved by the government of upper Bavaria (LMU) and in accordance with the Swiss Veterinary Law guidelines (UniBE).

3.2. Pharmacological Treatments

Clozapine-N-oxide (CNO) (Tocris, Cat. No. # 4936), was administered via intraperitoneal (i.p.) injection using the dosage 3 mg/kg, 45 minutes preceding either behavioural or imaging experiments (during acute MLIN modulation protocols). For chronic modulation experiments, CNO was administered at a concentration 40 µg/ml (Urban et al., 2016), through drinking water with 1% sucrose.

3.3. Adeno-Associated Virus Mediated Gene Delivery

All adeno-associated viruses (AAVs) were purchased from Addgene: AAV2/8-hSyn-DIO-hM4D(Gi)–mCherry (# 44362) viral titer 1×10^{13} vg/ml, AAV2/8-hSyn-DIO-hM3D(Gq)–mCherry (# 44361) viral titer 4×10^{12} vg/mL, AAV2/8-hSyn-mCherry (# 114472) viral titer 1×10^{13} vg/ml, AAV2/8-hSyn-DIO-mCherry (# 50459) viral titer 1×10^{13} vg/ml, AAV2/1-hSyn-jGCaMP7s-WPRE (# 104487) viral titer 1×10^{13} vg/ml and AAV2/1-hSyn1-Twitch2B-WPRE.SV40 (# 100040) viral titer 1×10^{13} vg/ml.

3.4. Cranial Window Implantation and Virus Injection for Single Fluorophore GECI Experiments

Mice of both sexes were implanted with a cranial window at P42 ± 6.70 (mean ± SD, P60 cohort) for imaging of early symptomatic mice, and at P174 ± 2.91 for imaging of late symptomatic mice (P200 cohort). The mice received stereotaxic injections of AAV2/1-hSyn-jGCaMP7s-WPRE, diluted 1:10 in saline, Addgene viral prep # 104487-AAV1; RRID: Addgene_104487-AAV1 into lobule V (5Cb) & VI (6Cb) of the cerebellar vermis. Mice were administered orally with Metacam (10 mg/kg) and Metamizol (200 mg/kg) 30 minutes prior to surgery and were then anesthetized with Fentanyl (0.05 mg/kg), Midazolam (5.0 mg/kg), and Metedomidin (0.5 mg/kg), delivered i.p. A circular craniotomy of 3 mm diameter was centred at 1.5 mm lateral from the midline and -6.5 mm posterior to bregma overlying lobule V & VI and injections were made at two sites at -6.5mm anterior/posterior (AP) and 0.5 mm lateral and -6.8 mm AP and 1mm lateral from the midline (**Fig. 5B**), with 200nl AAV injected at a depth of both 500µm and 150µm from the cortical surface at each site, using a flow rate of 50nl/min. A 3 mm round glass coverslip (Warner Instruments) was placed over the craniotomy and sealed flush to the surrounding skull using UV-curable dental acrylic (Venus Diamond Flow, Heraeus Kulzer GmbH). To allow head fixation during two-photon imaging, a custom metal head bar was then attached onto the skull using dental acrylic (Paladur, Heraeus Kulzer GmbH). At the end of the procedure the anesthesia was antagonized through application of Atipamezol (2.5 mg/kg), Flumazenil (0.5 mg/kg) und Naloxon (1.2 mg/kg, all i.p.) and Metacam (10 mg/kg) was then administered orally at 12, 24, 48 and 72 hours post-op.

3.5. Two-Photon Imaging in Awake and Anesthetized Mice

Early symptomatic mice were imaged at P63 ± 3.85 (mean ± SD), and late symptomatic mice at P204 ± 3.60. In order to habituate the mice to the imaging setup and air-supported treadmill, each was given a minimum of three training sessions of 20 minutes each across the 7 days prior to first imaging time point. This allowed them to become comfortable running head restricted on the air-supported treadmill and engaging with the virtual reality environment. *In vivo* two-photon imaging was performed using a two-photon microscope (Hyperscope, Scientifica, equipped with an 8 kHz resonant scanner) at a frame rate of 30 Hz and a resolution of 512 × 512 pixels. Light source was a Ti:Sapphire laser with a DeepSee pre-chirp unit (Spectra Physics MaiTai eHP). GCaMP7s was excited at 910 nm, with a laser power around 30-70 mW and emitted photons detected by a GaAsP PMT with a bandpass filter in front (525/50 nm). Using a 16x water-immersion objective (Nikon), stacks consisting of 15,000 frames (equivalent to ~8 min) were acquired covering a field of view (FOV) of 453 x 453µm to simultaneously image molecular layer interneurons, Purkinje neurons and Golgi cells. Two-

three FOVs at this resolution were imaged per mouse, each under three distinct conditions, (1) in a virtual reality environment depicting a linear track with patterned walls consisting of lines and dots of contrasting colour, providing visual feedback for locomotion (fb), (2) in darkness (dark), and (3) under light isoflurane anesthesia (iso).

Mice were anesthetized with isoflurane initially at a volume of 2-2.5 Vol % in pure O_2 at a flow rate of 0.5 l/min. This was gradually reduced to 1.0-1.5 Vol % over a minimum of 30 minutes induction period in order to establish a respiratory rate of between 110-130 breaths per minute, which was then maintained throughout the recording. A physiological monitoring system (Harvard Apparatus) was used to ensure body temperature was stable at 37 degrees. During awake recordings, several behavioural parameters were recorded synchronized with the imaging data acquisition. The speed of the mouse on the ball was tracked by an optical mouse sensor (Logitech G500s Laser Gaming Mouse) placed in front of the styrofoam ball. Pupil position and width as well as whisking events were detected in video recordings acquired with an infrared camera (The Imaging Source, DMK 22BUC03, USB 2.0 monochrome industrial camera), positioned to the front right of the mouse to visualize the right eye and whiskers on this side. Information of pupil position and pupil width were derived online using custom-build software (National Instruments). Pupil width was computed post hoc using a custom-written script (Math Works). Whisking was tracked by superimposing a detection window over snout area of the mice. Brief puffs of pressurized air were applied through a thin tube positioned at the right side of the mouse's body.

3.6. Two-Photon Imaging - Image Processing and Data Analysis

Image analyses were performed in Matlab (R2021a, Math Works) using custom-written routines (Liebscher et al., 2016). In brief, full frame images were corrected for potential x and y brain displacement, and regions of interests (ROIs) were semi-automatically selected based on the maximum and mean projection of all frames. Fluorescence intensity of all pixels within a selected ROI were averaged in each frame, and the resulting time series (traces) low pass filtered at 10 Hz and smoothed over 3 frames. Potential neuropil signal contamination was addressed with the following equation (FROI_comp, neuropil-compensated fluorescence of the ROI; FROI, initial fluorescence signal of the ROI; Fneuropil, signal from the neuropil (modified after (Chen et al., 2013; Liebscher et al., 2016; Scekic-Zahirovic et al., 2021)).

$$FROI\_comp = FROI - 0.8 \times Fneuropil$$

In case the median of Fneuropil was higher than the median of FROI, we opted for a neuropil compensation factor of 0.7. To estimate the noise and to compute the baseline of

each trace (F0), we subtracted the 8th percentile in a sliding window of 30 frames. The standard deviation of this trace divided by its median and after subtracting 1, yields the noise of each trace. F0 corresponds to the median of all values lower than the 70% percentile of the noise band. All further analyses are performed on (FROI_comp/F0)-1 traces, reflecting the ΔF/F. The activity of dedicated neurons is given as area under the curve (AUC) of the ΔF/F per time unit. To minimize contributions of noise fluctuations to this metric, we only considered values exceeding 2x the noise. Running responsiveness was assessed by randomly circularly shifting the ΔF/F trace with respect to the speed vector 1000 times and computing the ratio of the median ΔF/F during locomotion and during quiet wakefulness and comparing it to the actual activity ratio of a given ROI. Neurons for which the actual 'locomotion/quiet wakefulness' activity ratio exceeded the 95 percentile of the shuffled data were considered running responsive. Spontaneous activity reflects the AUC during quiet wakefulness. Only experiments with a minimum quiet wakefulness epoch of 4000 frames, corresponding to 2.7 min, were considered in this analysis. Air puff responses were assessed in experiments with at least 2 air puffs, which were not followed by a running response in a window of 3 seconds following the puff application to avoid crosstalk between modalities. Due to these varying sets of criteria, the effective number of neurons differs across analyses.

3.7. Population Activity Dimensionality and Manifold Analysis

To reduce the dimensionality, we applied principal component analysis (PCA) to the 0-centered and z-scored F/F traces of all neurons or of selected cell-types in each FOV in the feedback imaging sessions (Kato et al., 2015; Lanore et al., 2021). To assess the correlation between the population response pattern and the conjunct recorded behaviour, a linear regression was performed for the principal components and the different behavioural parameters, i.e. locomotion, pupil width, whisking and air puff and all measured behaviour combined, to separate active from quiescent states.

To further explore the structure of the behaviourally-associated population response patterns, we conducted a PCA-based manifold analysis by projecting high dimensional population response pattern trajectories into 3 dimensional PCA space. The manifold subspace clearly segregated into two distinct clusters, corresponding to quiet wakefulness and active state (dominated by locomotion). The centre of mass for the respective subspaces was computed as the mean of the coordinates within each subspace. The Euclidean distance within a given subspace corresponds to the average length of each dot to the centre of mass. The Euclidean distance between two subspaces reflects the distance between the centre of mass of each subspace. To compare the Euclidean distances between *WT* and *Sca1*, only experiments with at least 30% of the time spent stationary and a minimum of 20% of the time

spent running were included. Of note, as the number of ROIs in a given FOV varied significantly within the acute chemogenetic stimulation data set, we bootstrapped by subsampling 70 pseudorandomly selected ROIs in each FOV for each of the 100 iterations and computed the mean values of the derived centre of mass.

3.8. Ratiometric Calcium Imaging

A circular 3mm in diameter craniotomy was performed, centred at 1.5 mm lateral from the midline and -6.5 mm posterior to bregma on mice aged P42 (± 7.27). Overall surgical procedure is as described above (see **3.4.**). Stereotaxic injections of AAV2/1-hSyn-Twitch-2B-WPRE (containing the two fluorescent proteins mCerulean3 and cpVenusCD as a FRET pair) at two sites of -6.5mm anterior/posterior (AP) and 0.5 mm lateral and -6.8 AP and 1mm lateral from the midline, with 200nl AAV injected at a depth of both 500µm and 150µm from the cortical surface at each site (50nl/min, diluted 1:3 in saline). The following recovery time and habituation for imaging experiments was consistent as initially described above. Twitch-2B was excited at 860 nm, with a laser power around 30-70 mW, emitted photons were detected via two PMTs (passing through bandpass filters: 460/80nm (CFP) and 560/80 nm (YFP) using identical voltage settings (800 for the blue channel, 830 for the yellow channel) for all animals. Stacks consisted of 15,000 frames and were acquired with a FOV of 453 x 453µm to simultaneously image molecular layer interneurons, Purkinje neurons and Golgi cells. Imaging condition used was isoflurane anesthesia, as described above (see **3.5.**). Imaging experiments were conducted at ages P73 (± 8.20). Imaging data was processed and analysed in a similar fashion as the GCaMP7s recordings (see **3.5.** & **3.6.**), including motion correction and semimanual segmentation to identify regions of interest. The calcium trace here corresponds to the ratio between the yellow channel and the cyan channel (Y/C ratio).

3.9. Calcium Imaging with Acute CNO Administration

All surgical procedures were performed as described above (see **3.4.**) now conducted in *WT::PV* mice and *Sca1::PV* mice at p73 (± 4.46). A circular craniotomy of 3 mm diameter, centred at 1.5 mm lateral from the midline and -6.5 mm posterior to bregma was drilled. Injections of AAV2/1-hSyn-GCaMP7s-WPRE were then made at two sites of -6.5mm anterior/posterior (AP) and 0.5 mm lateral and -6.8 mm AP and 1mm lateral from the midline, with 200nl AAV injected at a depth of both 500µm and 150µm from the cortical surface at each site (50nl/min, diluted 1:10 in saline). Injections of AAV2/8-hSyn-DIO-hM4Gi-WPRE were also made, bilaterally at -6.8 AP, +/-1mm from the midline, 150µm from the cortical surface at each site, and again bilaterally at AP -8.25mm, DV 2.5, ML +/-1mm. The latter two injections at AP -8.25mm were made at a 57° angle to a 0.3-0.4 mm depth from touching the dura surface

(50nl/min, diluted 1:3 in saline), in order to target the posterior lobule VIII. Mice were then imaged at p110 (± 5.26) (habituation protocol as described above) and then the same neurons were again imaged at p114 (± 4.47) 45 minutes following an i.p. injection of CNO (3mk/kg). Mice were imaged as described above (see **3.5.**), using the same imaging equipment, however we only assessed neuronal activity during feedback as well as under isoflurane anesthesia (isoflurane 1.0-1.5 Vol % at a flow rate of 0.5 l/min to establish respiratory rates between 110-130 breaths per minute, induction process and physiological monitoring, as described in initial two-photon imaging experiments, see **3.5.**). For control acute CNO experiments without injection of DREADDs, *Sca1* mice at age P80 underwent the exact same surgical procedures with viral injections AAV2/1-hSyn-GCaMP7s-WPRE and AAV2/8-hSyn-mCherry. The mice were then imaged at P120 and P121 for baseline and CNO experiments respectively following procedures and conditions as the DREADDs mice.

3.10. Surgical Procedure for Acute CNO Treatment Experiments (UniBe)

To induce analgesia, animals were injected i.p. with 0.1 mg/kg Buprenorphine 20 minutes prior to the surgical procedure. Anesthesia was induced using an induction chamber with 5% isoflurane, animals were then placed onto the stereotaxic frame and anesthesia was maintained at 1.5-2% isoflurane throughout the surgical procedure. Body temperature was maintained using a heating pad, and a lubricating eye cream was applied to avoid dehydration of the corneas. The head of the animal was fixed with ear bars. Under a dissecting microscope (Olympus, Tokyo, Japan) a medial skin incision was performed to expose the skull, the incision was extended in order to expose bregma and lambda to align the skull. In order to expose the occipital part of the cerebellum, muscles were cut over the medial line and muscles fibers were gently opened to access the injection site. A drill was used to make two holes in the occipital bone. For DREADDs-mediated circuit modulation experiments, the following coordinates were used to inject AAV2/8-hSyn-DIO-hM4D(Gi)–mCherry, AAV2/8-hSyn-DIO-hM3D(Gq)–mCherry and AAV2/8- hSyn-DIO-mCherry: AP -8.25mm, DV -2.5mm, ML +/- 1mm, angle 57 °, depth 0.3-0.4 mm from the dura. Methods courtesy of Federico Pilotto & Smita Saxena, Inselspital University Hospital, Bern, Switzerland.

3.11. Accelerating Rotarod

In order to be consistent with circadian rhythms, the rotarod test was always completed between 1 pm and 6 pm. Habituation to the experimenter and environment began with handling in the weeks leading up to the experiments, mice were then trained on the rotating rod at fixed speed of 5 rpm for three consecutive days prior to the first rotarod experiment. The protocol consisted of 4 trials per day, in which the rotating rod accelerated from 5 to 40 rpm within 300s,

followed by 300s rest in between trials. Mice were handled and given habituation sessions in the middle of 10 day breaks between trials for chronic experiments. Experimenters were blinded for treatment condition throughout the study. Rotarod experiments for chronic CNO administration studies were completed between LMU and UniBe. The protocol was consistent across both labs, data was merged and presented together.

3.12. Chronic CNO Treatment

To investigate the effects of chronic MLIN inhibition, we either injected AAV2/8-hSyn-DIO-hM4Gi-WPRE (inhibitory DREADD(Gi)) or AAV2/8-hSyn-DIO-mCherry, diluted 1:6 in saline into the cerebellar vermis at the age of P40-45. For induction of anesthesia and application of analgesics, the surgery protocol was as described for imaging experiments (in **3.6.)**. Two small holes (approximately 300µm diameter) were drilled on either side of the midline to allow injection via micropipette at the following coordinates AP -8.25mm, DV 2.5, ML +/-1mm. Injections were made at a 57° angle to a 0.3-0.4 depth from touching the dura surface (rate 50nl/min). CNO (40µg/ml) was administered through the drinking water with 1% sucrose, to mask the CNO taste, over a 30-day period (P60-P90). Mice were given 1% sucrose water 3 days prior to start of treatment to get used to the taste, every 3 days throughout the treatment CNO solution was prepared fresh, mice were weighed and assessed for any physical impairments. Rotarod (as described above/5-40 RPM, 300 seconds) was performed prior to treatment start, with 4 trials (300 second intervals) over 3 days (beginning at p53-56), then 4 trials on 2 consecutive days at P70, P80 and P90, then every two weeks after the treatment ended until P150. Handling of mice (minimum twice per week) and habituation around rotarod (minimum once per week) was performed regularly throughout. The Protocols were identical at both LMU and UniBE, the data was then merged for results.

For chronic stimulation of MLINs in healthy mice, *WT::PV* mice were injected (as described above for chronic CNO inhibition experiments) with either AAV2/8-hSyn-DIO-hM3Dq-WPRE (DREADD(Gq) or AAV2/8-hSyn-DIO-mCherry at P30-33. Chronic CNO treatment (as described for chronic inhibition experiments) was applied from P40-P70. Rotarod (see **3.11.**) was performed at p50 (4 trials on 3 consecutive days), P60, P70, P75 and P90 (4 trials, 2 consecutive days). To assess the impact of chronic chemogenetic stimulation on PN health, mice injected with AAV2/8-hSyn-DIO-hM3Dq-WPRE (DREADD(Gq)) were kept after the discontinuation of CNO and euthanized at P200 for immunohistological analysis. Surgery, CNO treatment and behavioural experiments were here entirely performed at LMU, brains were then sent to UniBE for the immunohistological analysis.

3.13. Hindlimb Clasping and Survival

To assess the *Sca1* clasping phenotype, mice were lifted from the base of the tail and suspended in the air for 20 seconds. In the case that both hindlimbs were steadily extended outwards, away from the abdomen, the mouse would be assigned the score of ‘‘0’’. If only a singular hindlimb was withdrawn towards the abdomen, consistently over time suspended, the mouse would be assigned a score of ‘‘1’’. If the hindlimbs were retracted together nearing the abdomen, the score assigned would be ‘‘2’’. Finally, if both hindlimbs were clasped and interlocked together at the abdomen, the mouse would be given a score of ‘‘3’’. The clasping phenotype for chronic DREADD(Gi) experiments was measured independently at the LMU and UniBE, data was merged and presented together. For survival measurement after chronic CNO treatment, animals’ disease progression was monitored at least once a week, at the LMU at least every 4 days, 10% reduction in body weight was used as humane endpoint for euthanasia in both colonies from LMU and UniBE, that are presented in this study.

3.14. Immunohistochemistry

For LMU experiments animals were transcardially perfused with 1x PBS 0.05% Heparin, followed by 4% PFA; the cerebellum was isolated and kept overnight at 4°C in the same fixative solution, followed by 30% sucrose in PBS for cryoprotection until samples were used. After embedding in Tissue Tek O.C.T compound (Bio system, #4583), sagittal cerebellar sections (50 µm) were sliced on a cryostat (Leica CM1850). Amplification of mCherry signal in combination with NeuroTrace staining was then completed on free floating sections at room temperature unless stated otherwise. Sections were washed three times (x3) in 1% PBS with 0.5% TritonX-100 (Sigma-Aldrich, #9036-19-5) (PBST). Then left in a blocking buffer solution of 0.05% bovine serum albumin (BSA, Sigma, #A9418-10G), 7% Horse Serum (Thermo Fisher Scientific, #16050130), PBST, for 1 hour. The sections were then incubated overnight at 4 degrees with the primary antibody goat-anti-mCherry (1:500, Origene, #AB0081-200) in fresh blocking buffer solution. The following day, following a 3x 15 min PBST wash, the sections were incubated for 2 hours with blocking buffer solution also containing the secondary antibody donkey-anti-goat IgG (H+L) Cross-Adsorbed Secondary Antibody, Alexa Fluor™ 594 (Invitrogen, Thermo Fisher Scientific, #A-11058) and NeuroTrace 435/455 blue fluorescent Nissl stain (Invitrogen, Thermo Fisher Scientific, #N21479). Then washed for 15 minutes in PBST. Sections were then mounted on slides with Polyvinyl alcohol mounting medium with DABCO®, antifading immersion oil (Sigma-Aldrich, #10981).

For UniBE experiments animals were transcardially perfused with 4% paraformaldehyde (PFA) in 1X PBS; Tissue processing is as stated above. Antibodies used

for immunofluorescence were: mouse anti-Parvalbumin (1:1000, Swant, # 235), goat anti-Parvalbumin (1:1000, Swant, # PVG213), mouse anti-Calbindin (1:1000, Abcam, # ab82812), rabbit anti-Calbindin (1:1000, Abcam, # ab108404), rabbit anti-pCaMKII-α, (1:200, Santa cruz, sc-12886), rabbit anti-CaMKII-α, 1:500 (LSB1178, Lifespan Bio), goat anti-mCherry (1:1000, Origene, # AB0081-200), rabbit anti-mCherry (1:1000, Abcam, # ab183628), rabbit anti-Homer-3 (1:500, Origine, # TA308627), rabbit anti-Homer-3 (1:1000, SYSY, # 160303) mouse. Sections were kept for 2h in PBS solution containing 0.05% Triton X-100 and 10% normal donkey serum (NDS, Jackson immunoresearch, #017-000-121), after the antibodies were applied in PBS, 3% NDS, 0.05% Triton X-100, and incubated overnight at 4°C. Sections were then briefly washed with PBS and incubated for 120 min at room temperature (RT), with appropriate combinations of secondary antibodies from Invitrogen.

3.15. Confocal Microscopy and Image Analysis

Confocal images were acquired using a Leica Malpighi TCS SP8 confocal microscope to confirm expression of viral injections in target sites (either 5x air objective, or 20x, 40x oil objective) For quantification of mCherry expression following chemogenetic experiments, field of views used were 350x350 µm (40x oil objective, resolution of 1024x1024, z stack of 8 µm with 2 µm steps). Within lobule VIII, 3-4 FOVs were analysed in two sections per mouse. Six mice in total were used, three with DREADDS (Gi) and three from mCherry control injections. Percentage of NeuroTrace positive neurons that co-expressed mCherry were counted for MLINs and PNs.

For UniBE experiments, confocal images were acquired using an Olympus Fluoview 1000-BX61 (Olympus, Tokyo) microscope (20X, 40X air objective or 60X immersion oil objective). For the analysis of intensities, data were acquired using identical confocal settings, with signals at the brightest cells being non-saturated. For parvalbumin, P-CaMKII, CaMKII, Calbindin signal intensity values were calculated over a maximal intensity projection of several consecutive Z-stack spaced 0.5 µm. Cells were manually ROI and average intensity was measured with Fiji. For parvalbumin neurons with values of intensity below 50 arbitrary units (a.u.) were considered as low expressing, between 50 and 100 a.u. as medium expressing and above 100 a.u. as high expressing. Intensity values were plotted using GraphPad Prism 9. For Homer-3 synapses analysis 3 Z-stacks spaced 0.5 µm were used. Puncta were reconstructed in 3D using Imaris software within a ROI of 35.4 µm2 and the number of synapses was plotted using GraphPad Prism 9.

3.16. Statistical Analysis

Analysis was done using GraphPad Prism and Matlab (R2021a, Mathworks). Statistical significances throughout the paper were evaluated by two-tailed, unpaired Student's *t* test, Two-way ANOVA or Kolmogorov-Smirnov (KS) tests to assess differences in distributions. Post ANOVA Sidak or Tukey test was used to evaluate statistical significance throughout the paper as indicated in the respective figure legend. Values are expressed as mean ± standard error of the mean (SEM). A p-value <0.05 was considered as statistically significant (**p* <0.05, ***p*<0.01, ****p*<0.001).

4. RESULTS

Results from this work were accepted for publication in: Pilotto, **Douthwaite** et al., "Early molecular layer interneuron hyperactivity triggers Purkinje neuron degeneration in SCA1." *Neuron* / 17 May 2023.

4.1. Alterations in Neuronal Calcium Signals in the Cerebellar Cortex of *Sca1* mice

4.1.1. Neuronal Activity is Altered in the Cerebellar Cortex of Early Symptomatic *Sca1* Mice

To assess functional deficits in distinct neuron types of the cerebellar cortex circuit during the early symptomatic phase in *Sca1* mice, we performed *in vivo* two-photon calcium imaging in behaving mice running on a spherical treadmill (**Fig. 5A**). Through expression of the genetically encoded calcium indicator (GECI) GCaMP7s in the three main inhibitory neuronal subtypes in the cerebellar cortex, we were able to record calcium signals from these distinct neurons in unison. Molecular layer interneurons (MLIN), Purkinje neurons (PNs) and morphologically putative Golgi cells (Golgi) **(Fig 5A-D)**, could be tracked whilst mice engaged with a virtual environment (VR), facilitated by the speed of treadmill locomotion being fed back to the visual flow of the VR (feedback, fb), or running in darkness (**Fig. 5A, 5D**).

.

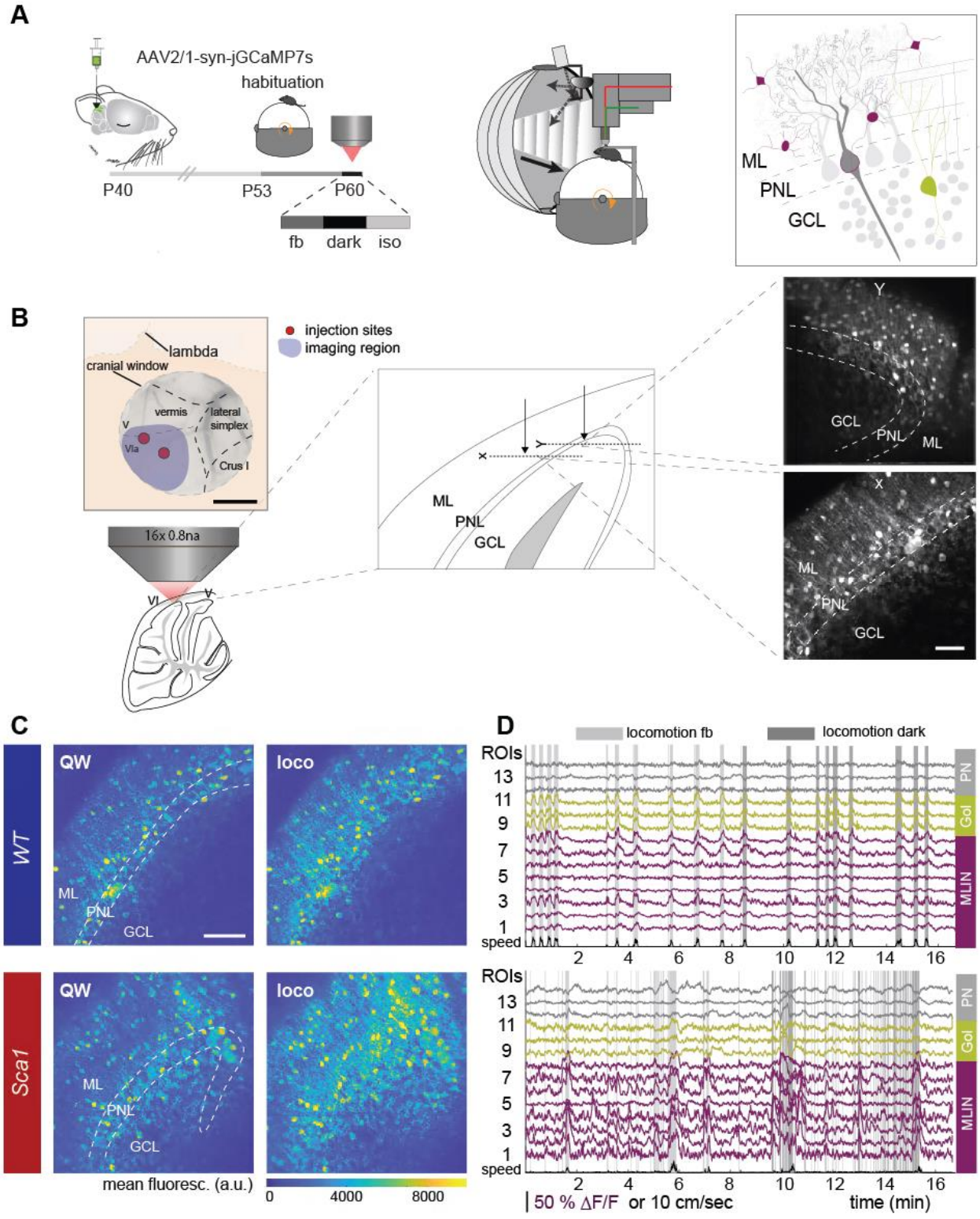

Figure 5: ***Simultaneous monitoring of diverse neuronal subtypes in cerebellar cortex of behaving mice***. ***(A)*** *Left: Experimental design. Mice were injected with AAV2/1-syn-jGCaMP7s into cerebellar cortex of lobule V and VI and imaged 20 days later (fb – feedback, dark – darkness, iso – isoflurane anesthesia). Centre: Scheme of imaging setup, air supported treadmill surrounded by toroidal screen, environment is projected onto the screen via curved mirrors and movement on the treadmill is detected via mouse sensor on the front of the ball. Right: Three distinct cell types in the cerebellar cortex were recorded across the molecular layer (ML), Purkinje neuron layer (PNL) and Granule cell layer (GCL).* ***(B)*** *From left to right: Scheme of the cerebellar window, depicting the location of AAV – injection and in vivo imaging) and scheme showing the two-photon microscope objective focussing on lobule VI. Enlarged sagittal plane of imaging site on lobule VI, depicting cerebellar cortex layers (ML – molecular layer, PNL – Purkinje neuron layer, GCL – granule cell layer.* *Figure legend continued on next page.*

(C) *Average projection of an episode of quiet wakefulness (QW, left) and locomotion (loco, right) of the same field of view (FOV) in a WT and a Sca1 mouse (cerebellar layers are indicated by dashed lines, see (B).* ***(D)*** *Exemplary calcium traces of selected molecular layer interneurons (MLIN, magenta), Golgi cells (GoI, yellow) and Purkinje neurons (PN, gray) in a fb session and in darkness in a WT (upper panel) and a Sca1 mouse (lower panel). Locomotion epochs are delineated by areas shaded in gray. Scale bars (B) 1 mm in cranial window scheme, 50 µm in example FOV (**C**) 50 µm. Figure adapted from Pilotto, Douthwaite et al., "Early molecular layer interneuron hyperactivity triggers Purkinje neuron degeneration in SCA1." Neuron. In Press.*

Monitoring neuronal activity in awake behaving mice revealed differential alterations in baseline fluorescence (indicative of changes in resting cytoplasmic calcium concentration), neuronal activity levels and response properties, across the three neuronal populations in *Sca1* animals (**Fig. 6**). Action potential rates of the neuron groups we monitor here exceed the temporal resolution that can be achieved using GECIs, however, the fluorescence signals scale with overall neuronal firing (Chen et al., 2013; Dana et al., 2019). Therefore, we computed the area under curve (AUC) of the ΔF/F trace as a measure of neuronal activity. We defined periods of our recordings where mice were not engaging in recorded behaviours (stationary on treadmill and no air puff stimulation), as the behavioural state quiet wakefulness (QW).

During QW, our recordings revealed not only a significantly lower baseline fluorescence in MLINs of *Sca1* mice (**Fig. 6A**), but these neurons were also more active in both the feedback and dark sessions (**Fig. 6B**). Conversely, there were no observed alterations in the baseline fluorescence and a slight decrease in spontaneous neuronal activity levels (measured as AUC/min) during QW in Golgi cells (**Fig. 6C-D**). The PNs of *Sca1* mice showed no change to their wild type (*WT*) littermates in either parameter (**Fig. 6E-F)** at this early phase of the disease in P60 old mice. When investigating locomotion related neuronal activity, we found a strong increase in the locomotion-associated neuronal activity specifically in the MLIN group of *Sca1* mice **(Fig. 6G, 6J**), and overall an increase in the proportion of MLINs displaying locomotion-associated responses (**Fig. 6K**). In contrast to the hyperresponsiveness found in MLIN, we identified Golgi cells in *Sca1* to be less strongly driven by locomotion than in *WT* mice (**Fig. 6H, 6L**), and no change in the fraction of running responsive neurons (**Fig. 6M**). We could not detect any alteration in the response to locomotion in PNs at this early stage of the disease **(Fig. 6I, 6N-O)**. It is however worth noting, that across our experiments the number of Golgi cells and PNs we recorded from were considerably lower than those of MLIN. Thus, it is possible that there are indeed alterations to these populations that we fail to detect with our method.

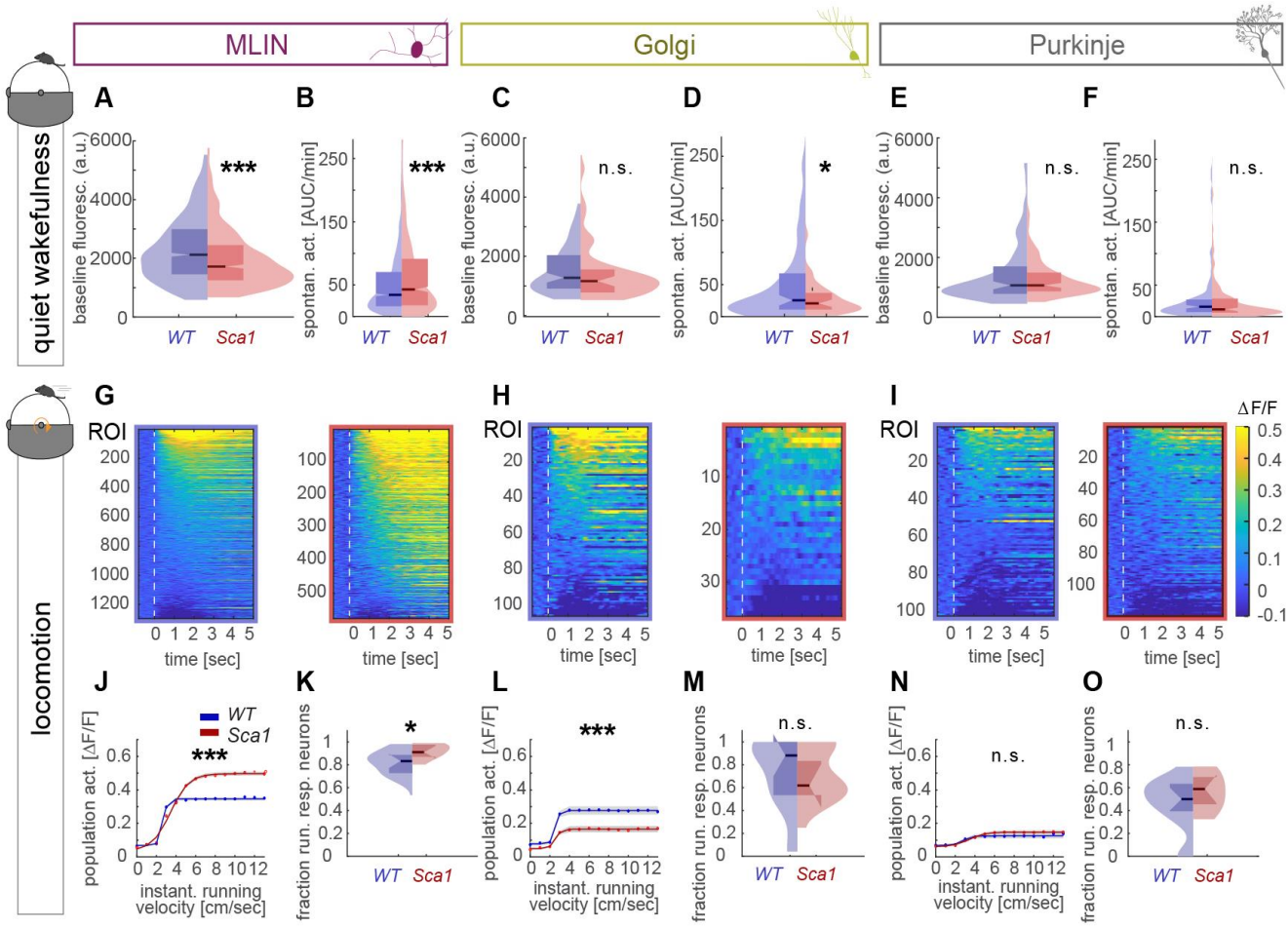

Figure 6: ***Altered calcium signals during quiet wakefulness and locomotion in awake Sca1 mice. (A)*** *Quantification of baseline fluorescence in MLIN ($p < 10^{-11}$).* ***(B)*** *Quantification of spontaneously occurring neuronal activity (area under the curve (AUC)/min) during quiet wakefulness in MLIN (p = 0.0005, WT 1386 MLIN, Sca1 714 MLIN).* ***(C)*** *Same as in (A) for Golgi cells, baseline fluorescence (p = 0.17),* ***(D)*** *Same as in (B) for Golgi cells; neuronal activity (p = 0.048, WT 114 Gol, Sca1 48 Gol).* ***(E)*** *PN baseline fluorescence (p = 0.21) and* ***(F)*** *spontaneous neuronal activity (p = 0.21, WT 112 PN, Sca1 132 PN, all KS test (**A-F**).* ***(G)*** *Heat map depicting the average neuronal activity in response to running onset for all MLIN in WT (left, blue frame) and Sca1 mice (right, red frame).* ***(H)*** *Same as in* ***(G)*** *for Golgi cells and* ***(I)*** *Purkinje neurons.* ***(J)*** *Average population activity as function of instantaneous running velocity in MLIN (genotype effect: $F_{(1,2092)} = 71.89$, $p < 0.001$, 2-way repeated measures ANOVA, superimposed by sigmoidal fit),* ***(K)*** *fraction running responsive MLIN per FOV (p = 0.034, Wilcoxon rank sum test, WT: 16 FOV (8 mice), Sca1: 9 FOV (6 mice)),* ***(L)*** *as in (J) for Golgi cells (genotype effect: $F_{(1,163)} = 12.18$, $p < 0.001$, 2-way repeated measures ANOVA),* ***(M)*** *as in (k) for Golgi cells (p = 0.62, WT 16 FOV (8 mice)), Sca1 6 FOV (4 mice)),* ***(N)*** *as in (J) for PN (genotype effect: $F_{(1,250)} = 0.17$, p = 0.68, 2-way repeated measures ANOVA),* ***(O)*** *as in (K) for PN (p = 0.59, WT 14 FOV (8 mice), Sca1 9 FOV (6 mice)). Data in J, L and N are mean ± SEM. * p < 0.05, *** p < 0.001. Figure adapted from Pilotto, Douthwaite et al., "Early molecular layer interneuron hyperactivity triggers Purkinje neuron degeneration in SCA1." Neuron. In Press.*

To probe sensorimotor integration we assessed the calcium signal responses associated to an applied air puff, which elicits sensory-driven as well as arousal and startle-response-associated signals in the cerebellar cortex (Gurnani and Silver, 2021). We thus quantified neuronal activity in response to an air puff, applied to the side of the mouse's body (when no locomotion occurred within a window of 3 seconds after the air puff to avoid contamination of the neuronal signal) in all three cell types (**Fig. 7**). In comparison to *WT* mice, we observed a significant increase in the *Sca1* MLIN neuronal activity following air puff stimulation (**Fig. 7A, 7D**), a decreased response in mutant Golgi cells (**Fig. 7B, 7E**) and an increase in mutant PNs (**Fig. 7C, 7F**).

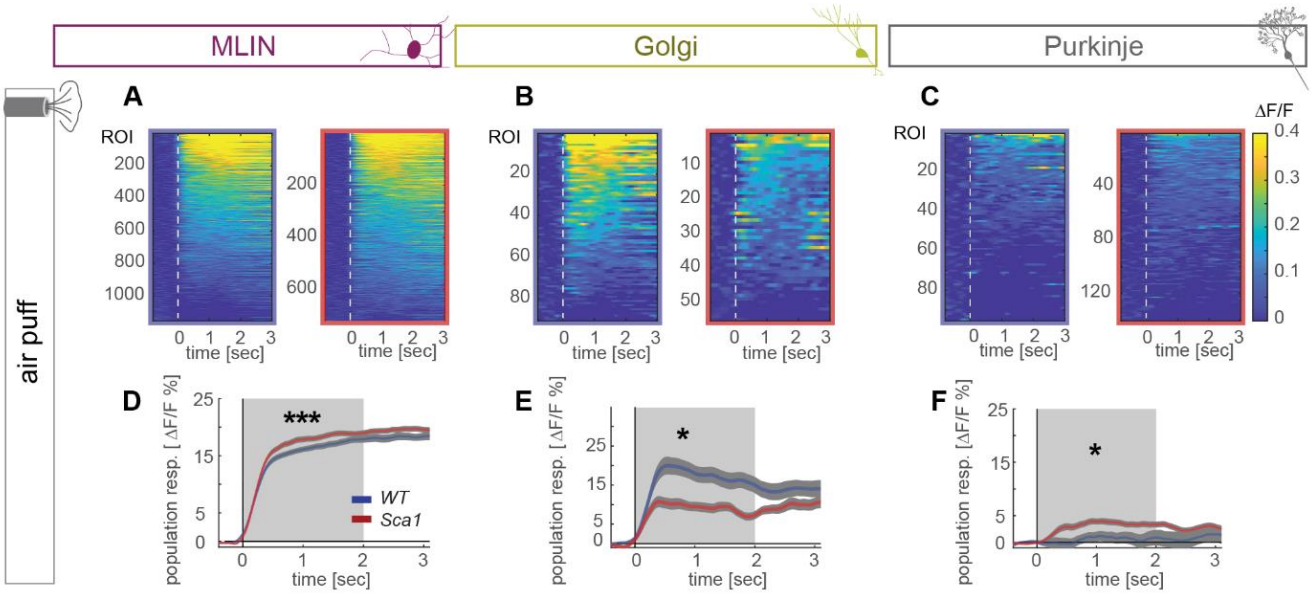

Figure 7: ***Air puff driven responses are altered in Sca1 mice.*** ***(A)*** *Heat maps depicting responses of all MLIN aligned to the application of an air puffs in WT (left, blue frame, 1152 MLIN) and Sca1 (red frame, 719 MLIN) mice,* ***(B)*** *the same in Golgi cells (WT 90 Gol, Sca1 55 Gol),* ***(C)*** *and in PN (WT 95 PN, Sca1 140 PN).* ***(D)*** *Population response to air puff in MLIN normalised to the average neuronal activity within 1 second prior to air puff ($p < 0.001$, Wilcoxon rank sum test of average 0 – 2 sec after air puff, gray area).* ***(H)*** *Air puff population response in Golgi cells ($p = 0.03$) and* ***(I)*** *Purkinje cells ($p = 0.04$). Data in D, E, F are mean ± SEM. * $p < 0.05$, *** $p < 0.001$. Figure adapted from Pilotto, Douthwaite et al., "Early molecular layer interneuron hyperactivity triggers Purkinje neuron degeneration in SCA1." Neuron. In Press.*

To further investigate impairments of sensorimotor integration, we compared neuronal activity levels elicited during sessions with visual input (feedback) to those without any visual input (darkness, **Fig. 8**). We observed an overall strong positive linear correlation between the neuronal activity during feedback and during darkness. However, we found MLIN in *Sca1* mice displayed a leftward shift in the ratio of fb/dark activity (**Fig. 8A**). Conversely, we found Golgi cells to be less active in *Sca1* mice during both fb and darkness settings (**Fig. 8B**), while PNs were slightly more active in *Sca1* mice (**Fig. 8C**) during feedback.

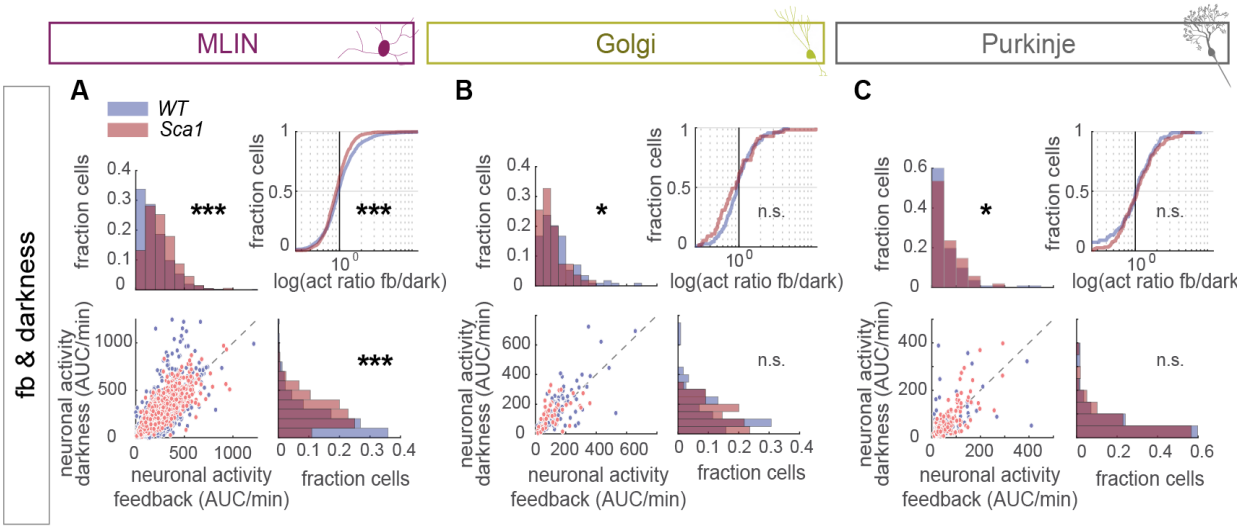

Figure 8*: **Sca1 mice neuronal responses properties are differentially altered between light and dark environments. (A)** Neuronal activity (AUC) of the same MLINs across the entire recording session with visual feedback provided by virtual reality (feedback) and in darkness, displayed with a scatter plot and histograms along with a cumulative distribution of the ratio between the AUC during the distinct conditions for each MLIN in WT and Sca1 mice (fb: p < 0.001, dark: p < 0.001, ratio fb/dark: p < 0.001, all KS tests, WT: 1386 MLIN, 16 FOV, 8 mice; Sca1: 804 MLIN, 10 FOV, 6 mice). **(B)** Same as in (A) for Golgi cells (fb: p = 0.028, dark: p = 0.13, ratio fb/dark: p = 0.22, all KS tests, WT: 114 Golgi, 16 FOV, 8 mice; Sca1: 55 Golgi, 7 FOV, 4 mice). **(C)** Same as in (A) for PN (fb: p = 0.029, dark: p = 0.94, ratio fb/dark: p = 0.65, all KS tests, WT: 112 PN, 14 FOV, 8 mice; Sca1: 157 PN, 10 FOV, 6 mice). Figure adapted from Pilotto, Douthwaite et al., "Early molecular layer interneuron hyperactivity triggers Purkinje neuron degeneration in SCA1." Neuron. In Press.*

Together, these data show that the neuronal dysfunction in *Sca1* mice is based on a combination of altered spontaneous activity and differentially impaired responsiveness to sensorimotor signals. Importantly, the cell type showing the strongest change in *Sca1* mice are MLIN, which in contrast to other neuronal types display increased activity levels, arguing for MLIN being hyperexcitable already in early symptomatic *Sca1* mice

4.1.2. Neuronal Coding Space is Strongly Reduced in *Sca1* Mice

To further unravel how cerebellar network function is compromised in early symptomatic *Sca1* mice, we next addressed how behavioural states are represented by the network consisting of the three main inhibitory cell types in *WT* and *Sca1* mice and how distinct these network representations are. Earlier work has reported that neuronal populations in the cerebellar cortex encode a variety of sensorimotor signals in a multidimensional manner

(Cayco-Gajic and Silver, 2019; Gurnani and Silver, 2021; Lanore et al., 2021). We thus utilized a principal component analysis (PCA)-based method to explore the dimensionality of the population dynamics in behaving mice. To this end, we assembled an input matrix, which consisted of 0-centered, z scored ΔF/F traces of all cells identified in a given field of view (FOV) and we aligned this matrix with the recordings of running speed, whisking activity, pupil width and applied air puffs (**Fig. 9A**). Analyses of the variance explained of the population activity revealed a multidimensional nature (**Fig. 9B**). The first component alone could explain about ~50% of the variance of the population activity in both *WT* and *Sca1* (**Fig. 9C,** *WT* 51.9 ± 8.6%; *Sca1* 54.63 ± 11.6%). We next sought to unravel the main drivers of PC1. PC1 was dominated by locomotion and whisking. However, in *Sca1* mice, the variance of PC1 explained by locomotion, air puff and whisking, was reduced compared to *WT* (**Fig. 9D**). Cell-type specific regression analyses of the PC1 also identified a significant reduction of the aforementioned behavioural parameters for MLIN only, in regards to Golgi cells primarily the contribution of the air puff representation that was altered (**Fig. 9D**). In PNs, there was no significant difference in the encoding of behavioural parameters (**Fig. 9D**).

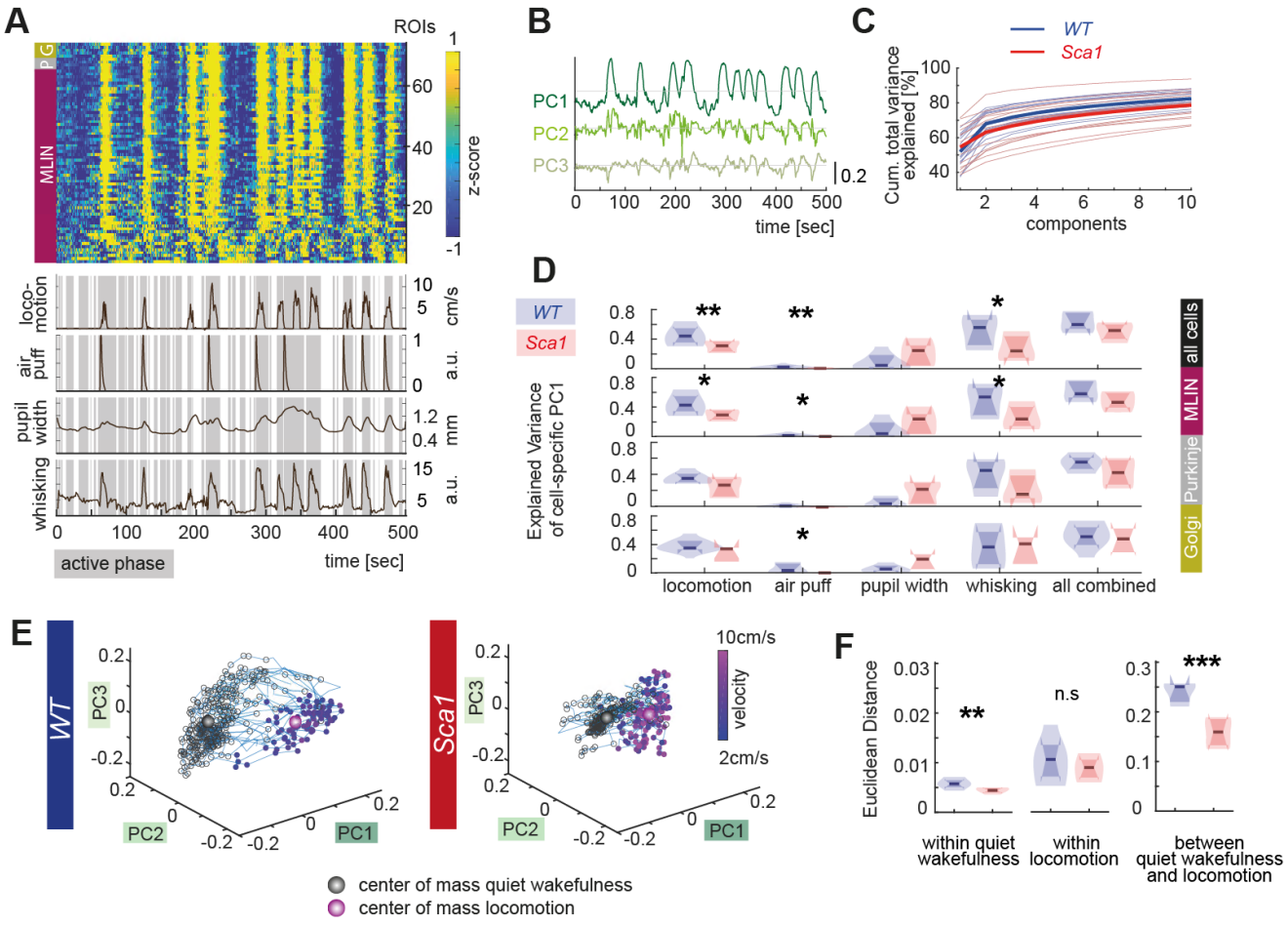

Figure 9: ***Coding space of behavioural parameters is compromised in cerebellar cortex of Sca1 mice. (A)*** *Example of an input matrix consisting of 0-centered and z-scored ΔF/F traces used for dimensionality reduction aligned with behavioural parameters (lower traces) derived from all cells in one field of view (FOV) of a feedback session of a WT mouse. Cell types are indicated by coloured boxes on the left side (magenta – MLIN, molecular layer interneurons, gray – P, purkinje neurons, yellow – G, Golgi cells). Figure legend continued on next page.*

*(**B)** Exemplary PC1, PC2 and PC3 time series derived from the input matrix shown in (A). **(C)** Variance explained of the neuronal activity as a function of the number of principal components in WT (blue, thin lines represent individual FOV, thick line corresponds to the mean) and Sca1 mice (red). PC1 alone explains about ~50% of the variance in both WT and Sca1 (WT 51.9 ± 8.6%, 16 FOV, 8 mice; Sca1 54.63 ± 11.6%, 14 FOV, 7 mice; two-way ANOVA Test, $F_{(1,28)} = 2.07$, $p = 0.16$ for genotype effect). **(D)** Variance of PC1, derived either from all cells observed in a FOV (all cells) or from individual cell types only, explained by the respective behavioural parameters in WT and Sca1. PC1 derived from all cell types combined: the variance explained by locomotion ($p = 0.009$), air puff ($p = 0.0098$), pupil width ($p = 0.14$), whisking ($p = 0.04$), and all behaviour combined ($p = 0.068$); PC1 derived from MLIN only: locomotion ($p = 0.013$), air puff ($p = 0.015$), pupil width ($p = 0.25$), whisking ($p = 0.048$), and all behaviour combined ($p = 0.068$); PC1 from PN: locomotion ($p = 0.053$), air puff $p = 0.085$), pupil width ($p = 0.068$), whisking ($p = 0.095$) and all behaviour combined ($p = 0.11$), and PC1 from for Golgi cells only: locomotion ($p = 0.069$), air puff ($p = 0.018$), pupil width ($p = 0.19$), whisking ($p = 0.53$) and all behaviour combined ($p = 0.37$), all Wilcoxon rank sum tests. **(E)** Representative manifold of quiet wakefulness and active states (as a function of locomotion speed, colour coded) for WT and Sca1 mice. **(F)** Euclidean distance in PC space is shown within and across brain states (within quiet wakefulness, $p = 0.009$, within locomotion $p = 0.36$, between subspaces $P < 0.001$, all Wilcoxon rank sum test; WT: 12 FOV, 8 mice, Sca1: 10 FOV, 5 mice). * $p < 0.05$, ** $p < 0.01$, *** $p < 0.001$. Figure adapted from Pilotto, Douthwaite et al., "Early molecular layer interneuron hyperactivity triggers Purkinje neuron degeneration in SCA1." Neuron. In Press.*

As we identified multi-dimensional neuronal activity profiles based on at least 10 components, we next probed how the geometry of these neuronal representations might be changed in *Sca1* mice. To gain insight into brain state-dependent geometry, we computed the manifolds by projecting the multi-dimensional neuronal population activity to low dimensional space, consisting of the first three components (Gobbo et al., 2022; Lanore et al., 2021, Vyas et al., 2020). In *WT* mice two distinct structures were visible, clearly separating quiet wakefulness from locomotion (**Fig. 9E**), which corroborates previous reports (Lanore et al., 2021). Notably, we found that the PC space representing quiet wakefulness was significantly reduced in *Sca1* mice (**Fig. 9F**) while, overall, the two subspaces were less segregated, as quantified by the reduced Euclidean distance between the two manifolds in *Sca1* mice (**Fig. 9F**). Together these data highlight a compromised encoding capacity of the cerebellar cortex circuit already in early symptomatic *Sca1* mice, an effect that appears primarily driven by MLIN dysfunction.

4.1.3. Neuronal Activity in *Sca1* Mice is Altered Under Anesthesia

Our findings in awake and active mice were further corroborated by recordings of the same neurons conducted under light isoflurane anesthesia (**Fig. 10**). Alterations in the degree of neuronal activity correlation can be an indication of an unstable neural network (Rosenbaum et al., 2014). To assess neuronal activity correlation in *Sca1* mice, we computed the degree of correlation of neuronal activity within our cell populations and between neuronal groups (**Fig. 10E-J**). We found a significant decrease of activity correlation within the MLIN population in *Sca1* mice (**Fig. 10E**), whilst Golgi and PNs displayed no alterations (**Fig. 10F-G**). When comparing the correlation between groups, there was again no change in the correlation between PNs and MLINs (**Fig. 10H)**, and PNs with Golgi (**Fig. 10I)**, however there was indeed

a shift to a higher correlation levels between MLINs and Golgi cells (**Fig. 10J**). Pointing towards primary alterations occurring in MLIN firing properties.

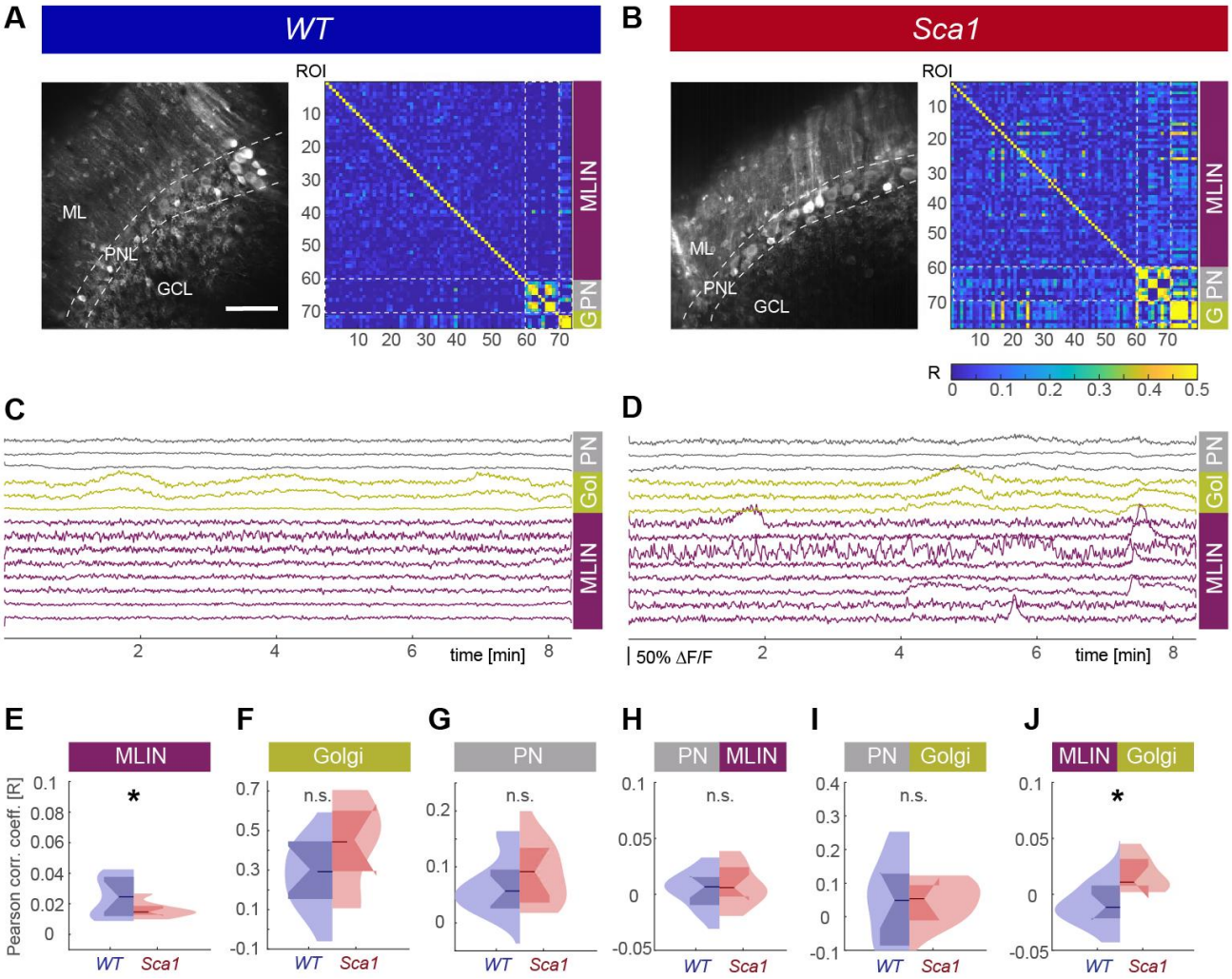

Figure 10: ***Degree of correlation of neuronal activity within and between distinct neuronal subtypes under anesthesia.*** ***(A)*** *Average projection of a recording in a WT mouse together with the corresponding correlogram (for average projection: ML – molecular layer, PNL – Purkinje neuron layer, GCL – granule cell layer. For correlogram: ROI – region of interest, MLIN - molecular layer interneuron, PN - Purkinje neuron, G - Golgi cell, R – Pearson correlation coefficient).* ***(B)*** *Same as in (A) for a Sca1 mouse.* ***(C)*** *Representative example traces of all three main cell types in a WT and* ***(D)*** *Sca1 mouse.* ***(E)*** *Median pairwise correlation of MLIN in individual field of views (FOV) (p = 0.039, WT 16 FOV, Sca1 13 FOV).* ***(F)*** *Average pairwise correlation of Golgi cells (p = 0.13, WT 15 FOV, Sca1 7 FOV),* ***(G)*** *Purkinje neurons (p = 0.24, WT 16 FOV, Sca1 13 FOV),* ***(H)*** *PN und MLIN (p = 0.55, WT 16 FOV, Sca1 13 FOV),* ***(I)*** *Purkinje neurons and Golgi cells (p = 0.66, WT 16 FOV, Sca1 7 FOV) and* ***(J)*** *MLIN and Golgi cells (p = 0.032, WT 16 FOV, Sca1 7 FOV, all two-tailed, unpaired Students t-test). Scale bar:* ***(A)*** *100 µm. Figure adapted from Pilotto, Douthwaite et al., "Early molecular layer interneuron hyperactivity triggers Purkinje neuron degeneration in SCA1." Neuron. In Press.*

Supporting our findings in awake mice, we observed a clear decrease in the baseline fluorescence of MLIN in *Sca1* mice (**Fig. 11A**). Such a drop likely reflects a reduction in resting cytoplasmic calcium levels, while baseline fluorescence was neither altered in Golgi cells (**Fig. 11B**) nor PNs (**Fig. 11C**). In line once more with awake recordings, we identified a rise in spontaneous neuronal activity of MLIN (**Fig. 11D)**, but a decrease in Golgi cell activity (**Fig.**

11E) and no change in spontaneous activity in PNs in this early symptomatic cohort (**Fig. 11F**). However, we acknowledge that as stated above this method lacks the resolution to detect fine changes in the rapid intrinsic firing rates of the PNs, with pacemaker firing of 40-60 Hz (Arancillo et al., 2015). Despite this shortcoming, we were able to resolve larger fluctuations in the PN fluorescence traces, likely caused by pauses in simple spike firing (Ramirez and Stell, 2016). Thus, a reflection of major alterations in PN firing rate. Such fluctuations in our experiments, however, were not significantly different between the *Sca1* mice and their *WT* littermates at P60.

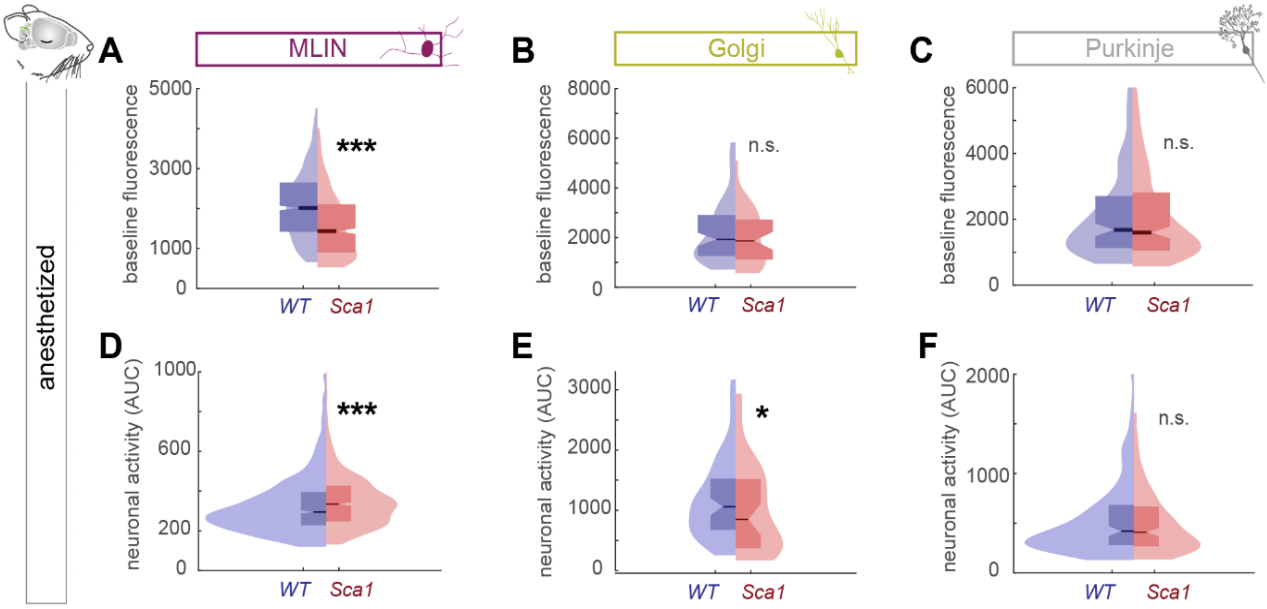

Figure 11: ***Calcium signals of diverse neuronal subtypes of the cerebellar cortex under anesthesia in early symptomatic Sca1 mice. (A)*** *Baseline fluorescence of MLIN in both Sca1 mice and their WT littermates ($p < 10^{-23}$),* ***(B)*** *same as in (A) for Golgi cells ($p = 0.29$) and* ***(C)*** *same as in (A) for Purkinje neurons ($p = 0.66$, all KS tests).* ***(D)*** *Average neuronal activity (area under the curve (AUC) across the entire recording) of MLIN in Sca1 mice and their WT littermates ($p<10^{-7}$, WT 1022, Sca1 702 MLIN),* ***(E)*** *format as in (D) average activity of Golgi cells ($p = 0.028$, WT 90, Sca1 46 Golgi cells) and* ***(F)*** *as in (D) for PN ($p = 0.67$, WT 155, Sca1 219 PN, all KS test). * $p < 0.05$, *** $p < 0.001$. Figure adapted from Pilotto, Douthwaite et al., "Early molecular layer interneuron hyperactivity triggers Purkinje neuron degeneration in SCA1." Neuron. In Press.*

4.1.4. Cytoplasmic Calcium Levels are Altered in *Sca1* Mice

Single fluorophore genetically encoded calcium indicators such as GCaMP only allow for an approximation of calcium levels. We therefore also performed *in vivo* two-photon imaging experiments in early symptomatic mice utilising a genetically encoded ratiometric calcium indicator Twitch2B (Thestrup et al., 2014) (**Fig. 12**). Ratiometric imaging allows for a more accurate measurement of actual calcium concentrations, independent of indicator expression levels. We again targeted the distinct neuronal subgroups recorded in earlier experiments for both *WT* and *Sca1* mice and assessed baseline fluorescence under light isoflurane anesthesia at the age of P60. The analysis here confirmed the reduced resting calcium concentration in the cytoplasm of MLIN (**Fig. 12D**) and identified previously unseen reduced levels in Golgi cells (**Fig. 12E**). However, we failed to detect alterations in PNs at this

early symptomatic stage (**Fig. 12F**). We also assessed neuronal activity levels and once more found significantly increased activity in MLIN in *Sca1* (**Fig. 12G**), however no change in Golgi cell activity (**Fig. 12H**) and a slight, yet significant, increase in PNs (**Fig. 12I**). As discussed above, due to the high baseline firing rates (pacemaker activity) of PNs in combination with the slow kinetics of genetically encoded calcium indicators, we very likely mainly detected larger fluctuations (pauses in firing) in neuronal activity levels (see **1.4**.). Consequently, a decrease in pacemaker activity, as described for PNs in *Sca1* mice (Dell'Orco et al., 2015), could potentially even appear as greater fluctuations in the fluorescent signal.

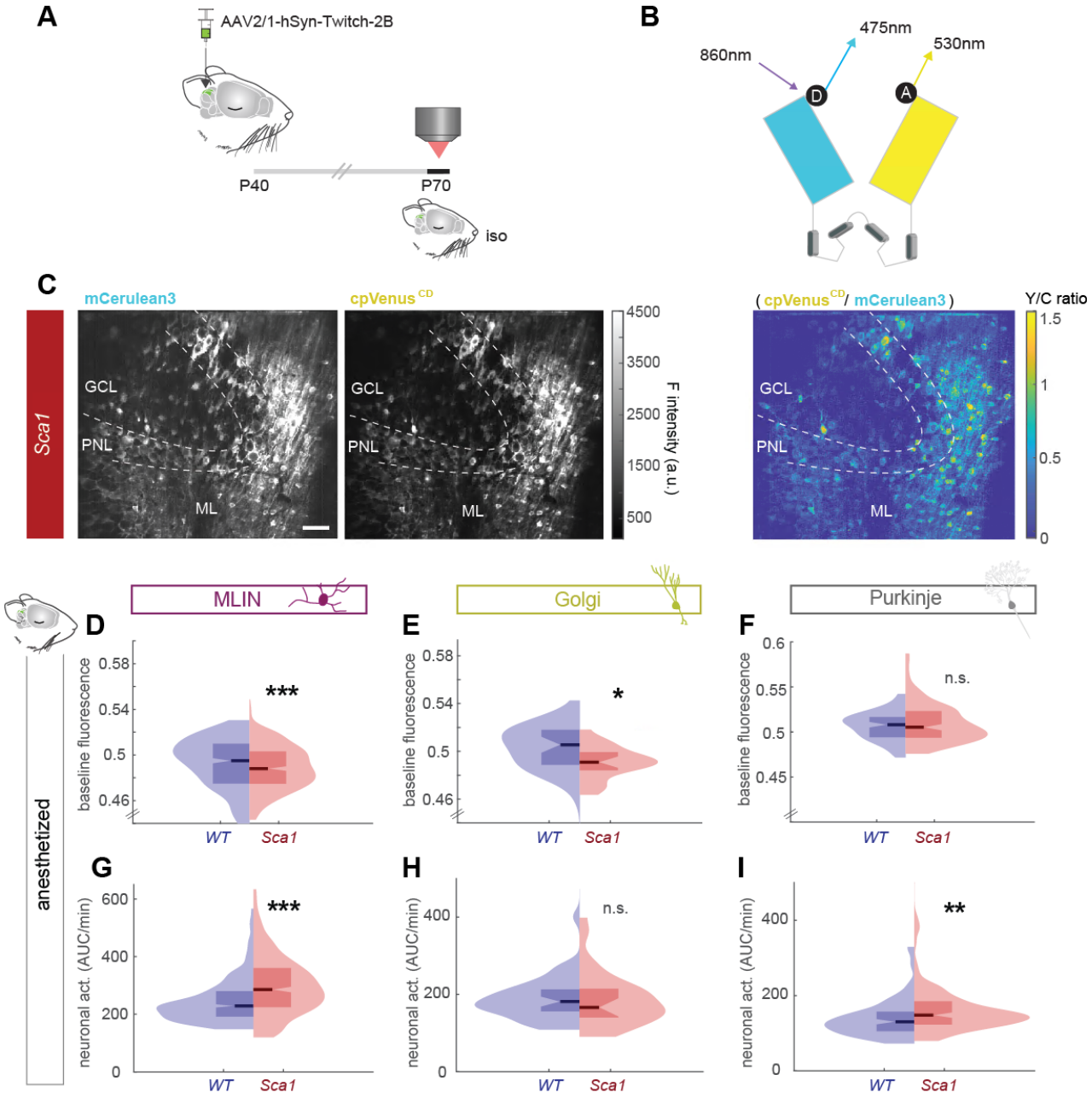

Figure 12: ***Measuring cytoplasmic calcium levels in anesthetized mice using a ratiometric calcium indicator. (A)*** *Timeline of experiments. The genetically encoded ratiometric calcium indicator Twitch2B was expressed and baseline cytoplasmic fluorescence assessed under light isoflurane anesthesia in early symptomatic mice at the age of P70.Figure legend continued on next page.*

(B) *Donor (D, mCerulean3) and acceptor (A, cpVenus) fluorophores were excited at 860nm.* ***(C)*** *Average projection of the blue and yellow channel and the corresponding ratiometric image (Y/C ratio) are shown for one example field of view in a Sca1 mouse. Cerebellar layers are indicated by dashed lines (ML – molecular layer, PNL – Purkinje neuron layer, GCL – granule cell layer).* ***(D)*** *Baseline fluorescence in MLIN ($p < 0.001$),* ***(E)*** *of Golgi cells ($p = 0.011$) and* ***(F)*** *PN ($p = 0.17$).* ***(G)*** *Neuronal activity (assessed as area under the curve (AUC)/min) of MLIN ($p < 10^{-18}$, WT: 535 MLIN, Sca1: 445 MLIN),* ***(H)*** *of Golgi cells ($p = 0.57$, WT: 45 GoI, Sca1: 24 GoI) and (**I**) Purkinje neurons ($p = 0.0011$, WT: 117 PN, Sca1: 161 PN, all tests are KS tests). Data in (D-I) are from WT: 9 FOV, 3 mice, Sca1: 5 FOV, 3 mice. * $p < 0.05$, ** $p < 0.01$, *** $p < 0.001$. Scale bar:* ***(C)*** *50 µm. Figure adapted from Pilotto, Douthwaite et al., "Early molecular layer interneuron hyperactivity triggers Purkinje neuron degeneration in SCA1." Neuron. In Press.*

4.1.5. MLIN Dysfunction is Conserved in Late Symptomatic Mice in Both Awake and Anesthetized Conditions

Given that we found strong evidence for neuronal dysfunction across the cerebellar cortex in the early stage of *Sca1*, we sought to investigate how this would develop over the course of ageing into later disease stages. To this end, we again utilised the calcium indicator GCaMP7s, applying our *in vivo* two-photon imaging paradigm in P200 *Sca1* mice and their *WT* littermates (**Fig. 13**).

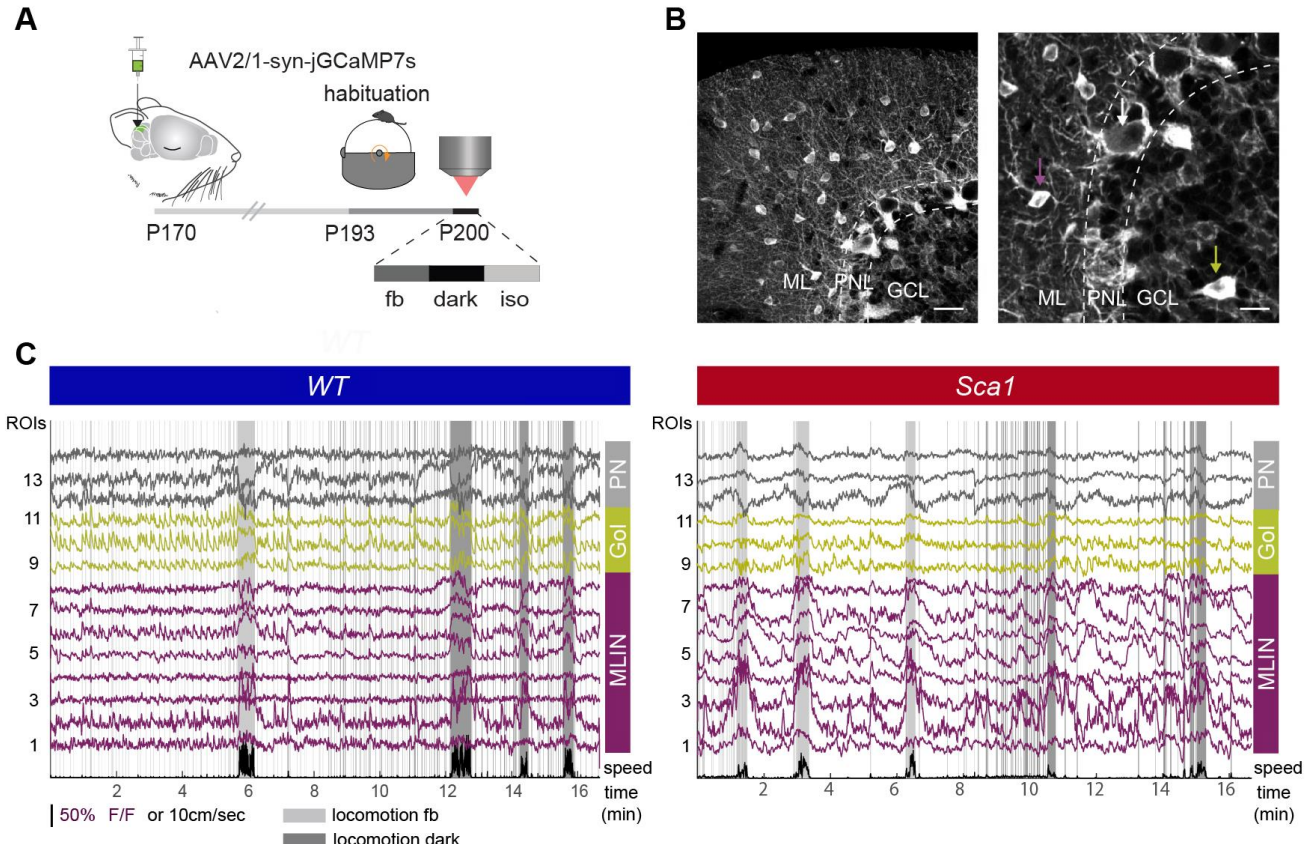

Figure 13: ***In vivo two-photon calcium imaging in late symptomatic Sca1 mice. (A)*** *Experimental design. Mice were injected with AAV2/1-syn-jGCaMP7s into cerebellar cortex of lobule V and VI and imaged 30 days later (fb – feedback, dark – darkness, iso – isoflurane anesthesia).* ***(B)*** *Left: Scheme of the cerebellar window, depicting the location of AAV – injection and in vivo imaging, matching the experiments in younger cohorts. Centre, right: example confocal images of AAV2/1-syn-jGCaMP7s expression in distinct cell types in the cerebellar cortex.* ***(C)*** *Representative calcium traces of molecular layer interneurons (MLIN, magenta), Golgi cells (GoI, yellow) and Purkinje neurons (PN, gray) acquired in a P200 old WT (left) and (B) a Sca1 (right) behaving mouse. Locomotion (lower trace, black) with visual feedback (fb) and during darkness (dark) is indicated by gray areas. Figure legend continued on next page.*

Scale bar: (B) left; 20µm, right; 10µm. Arrows in right image indicate expression of GCaMP7 in MLIN (magenta), PN (white) and putative Golgi (yellow). Figure adapted from Pilotto, Douthwaite et al., "Early molecular layer interneuron hyperactivity triggers Purkinje neuron degeneration in SCA1." Neuron. In Press.

We found differential alterations to neuronal response properties in distinct behavioural states. Strongly enhanced MLIN activity during epochs of QW was conserved in late stage mice (**Fig. 14A**). Similarly, MLINs again displayed large hyperresponsiveness in calcium signals to locomotion (**Fig. 14D**). We found a significant drop in Golgi cell activity during QW (**Fig. 14B**). Similarly, hypo-responsiveness of Golgi cell to locomotion was also conserved in P200 mice (**Fig. 14E**). We also identified decreased calcium fluctuations in PNs during QW, and a trend towards hyporesponsive properties to locomotion, however this was not significant (**Fig 14C, 14F**).

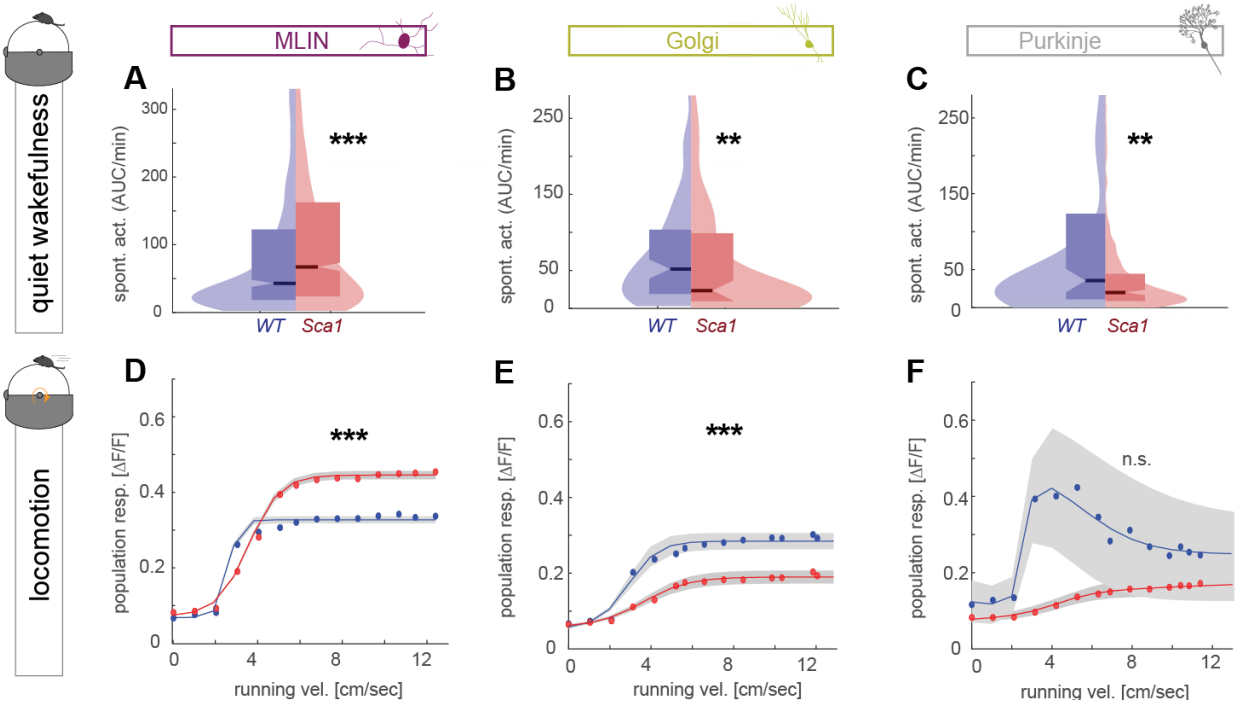

Figure 14: ***Altered neuronal function in late symptomatic Sca1 mice across distinct behavioural states. (A)*** *Significant changes in neuronal activity were observed during epochs of quiet wakefulness for MLIN ($p < 10^{-8}$, WT: 894 MLIN, Sca1: 1212 MLIN),* ***(B)*** *Golgi cells ($p = 0.0052$, WT: 105 Golgi, Sca1: 106 Golgi cells) and* ***(C)*** *Purkinje neurons ($p = 0.0054$, WT: 128 PN, Sca1: 231 PN, all KS tests).* ***(D)*** *Average population response as function of instantaneous running speed in MLIN superimposed by sigmoidal fit (genotype group effect: $F_{(1,2301)} = 37.69$, $p < 0.001$),* ***(E)*** *Golgi cells (genotype group effect: $F_{(1,229)} = 13.99$, $p < 0.001$) and* ***(F)*** *PN (genotype group effect: $F_{(1,367)} = 2.48$, $p = 0.12$, all 2-way repeated measures ANOVA). (**G**) Population response to air puff in MLIN normalised to the average activity within 1 second prior to air puff ($p < 0.0356$), Wilcoxon rank sum test of average 0 – 2 sec after air puff, gray area).* ***(H)*** *Same as in (G) with Golgi cells ($p = 0.5$).* ***(I)*** *same as in (G) with Purkinje neurons ($p = 0.0079$). Data in G, H, I are mean ± SEM. * $p < 0.05$, ** $p < 0.01$. Figure adapted from Pilotto, Douthwaite et al., "Early molecular layer interneuron hyperactivity triggers Purkinje neuron degeneration in SCA1." Neuron. In Press.*

To further explore alterations in calcium signals in the neuron groups at the late symptomatic stage, we again recorded from the same set of neurons under anesthesia. As in our recordings of early symptomatic mice, we found MLINs in late symptomatic displayed a slightly lower but significant baseline fluorescence (**Fig. 15A**), in combination with strong rise in spontaneous activity (**Fig. 15D**). Golgi cell baseline was here not altered (**Fig. 15B**), but

interestingly our recordings revealed a shift to enhanced Golgi activity under anesthesia (**Fig 15E**). PNs now revealed a substantial increase in baseline fluorescence (**Fig. 15C**) along with a decrease in calcium fluctuations (**Fig. 15F**). These findings were largely in line with the activity levels seen in awake mice during quiet wakefulness. Furthermore, these late symptomatic data clearly show that our initial observations of hyperexcitability in MLIN remain consistent over the disease course in *Sca1* mice and at the same time, PNs pathology worsens.

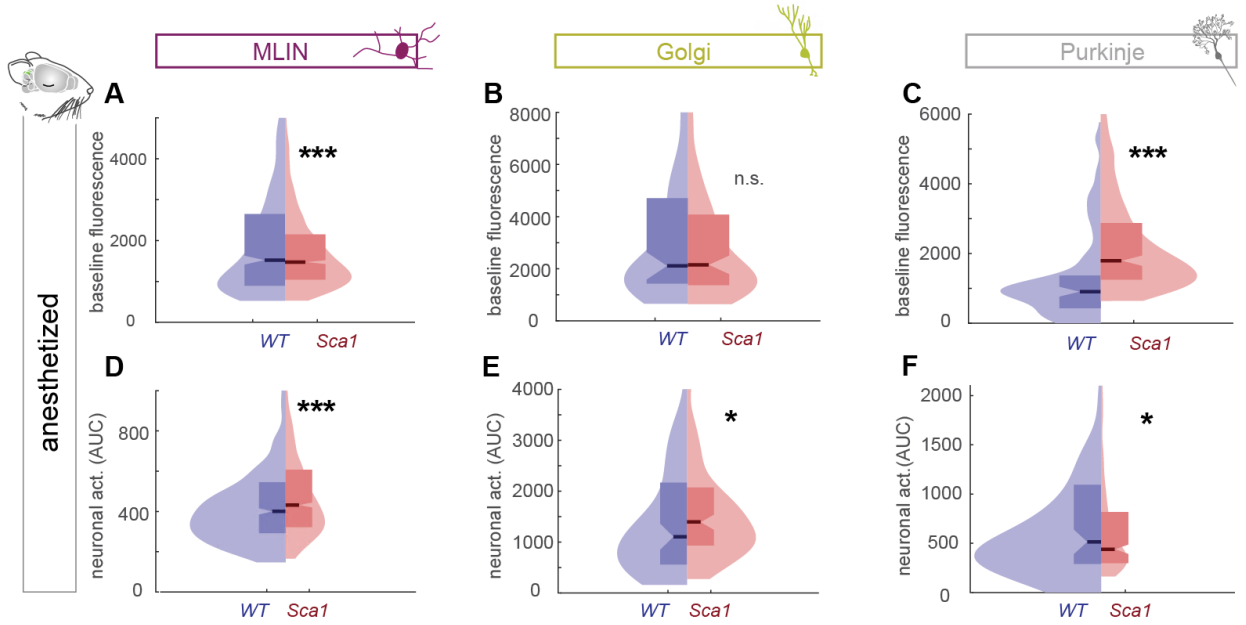

Figure 15: ***Alterations in calcium signals in late symptomatic Sca1 mice under anesthesia. (A)*** *Baseline fluorescence under light isoflurane anesthesia in MLIN ($p < 10^{-3}$),* ***(B)*** *Golgi cells (0.79) and* ***(C)*** *Purkinje neurons ($p < 10^{-14}$). Spontaneous neuronal activity (AUC across the entire recording) under light isoflurane anesthesia in* ***(D)*** *MLIN (p = 0.009, WT: 611 MLIN, Sca1: 1228 MLIN;* ***(E)*** *Golgi cells (p = 0.021, WT: 95 Golgi, Sca1: 138 Golgi, and in* ***(F)*** *Purkinje neurons (p = 0.032, WT: 103 PN, Sca1: 281 PN, all comparisons are based on data from WT: 9 FOV, 5 mice and Sca1: 18 FOV, 9 mice, all KS tests). * p < 0.05, *** p < 0.001. Figure adapted from Pilotto, Douthwaite et al., "Early molecular layer interneuron hyperactivity triggers Purkinje neuron degeneration in SCA1." Neuron. In Press.*

4.1.6. Purkinje Neuron Dendrites Display Aberrant Calcium Signals

Earlier work has identified excitability changes in PN dendrites as a critical contributor to PN degeneration and loss (Chopra et al., 2020). We thus, assessed calcium signals within PN dendrites (which previous work has shown to primarily reflect complex spiking activity (Wagner et al., 2021)), during both early and late disease stages in *Sca1* mice (**Fig. 16A-B**). In the early symptomatic P60 cohort we already detected an increase in dendritic excitability, as seen in a higher fraction of active dendrites (defined as a dendrite which display at least one clear calcium transient) (**Fig. 16C**). In addition, we identified elevated dendritic calcium signals, assessed as fluctuations in the fluorescence trace (in AUC/min) (**Fig. 16D**) and increased amplitudes of calcium transients (**Fig. 16E**). These alterations in calcium signals persisted until the late disease stage at P200, where we again found a higher proportion of

active dendrites (**Fig. 16F**), higher activity levels (**Fig. 16G**) and calcium transients with higher amplitudes (**Fig. 16H**). Overall whilst we could not detect clear changes in calcium signals in the PN somata at P60 in *Sca1* mice, there is a clear increase in dendritic calcium signals, indicating dendritic hyperexcitability of PNs at that disease stage.

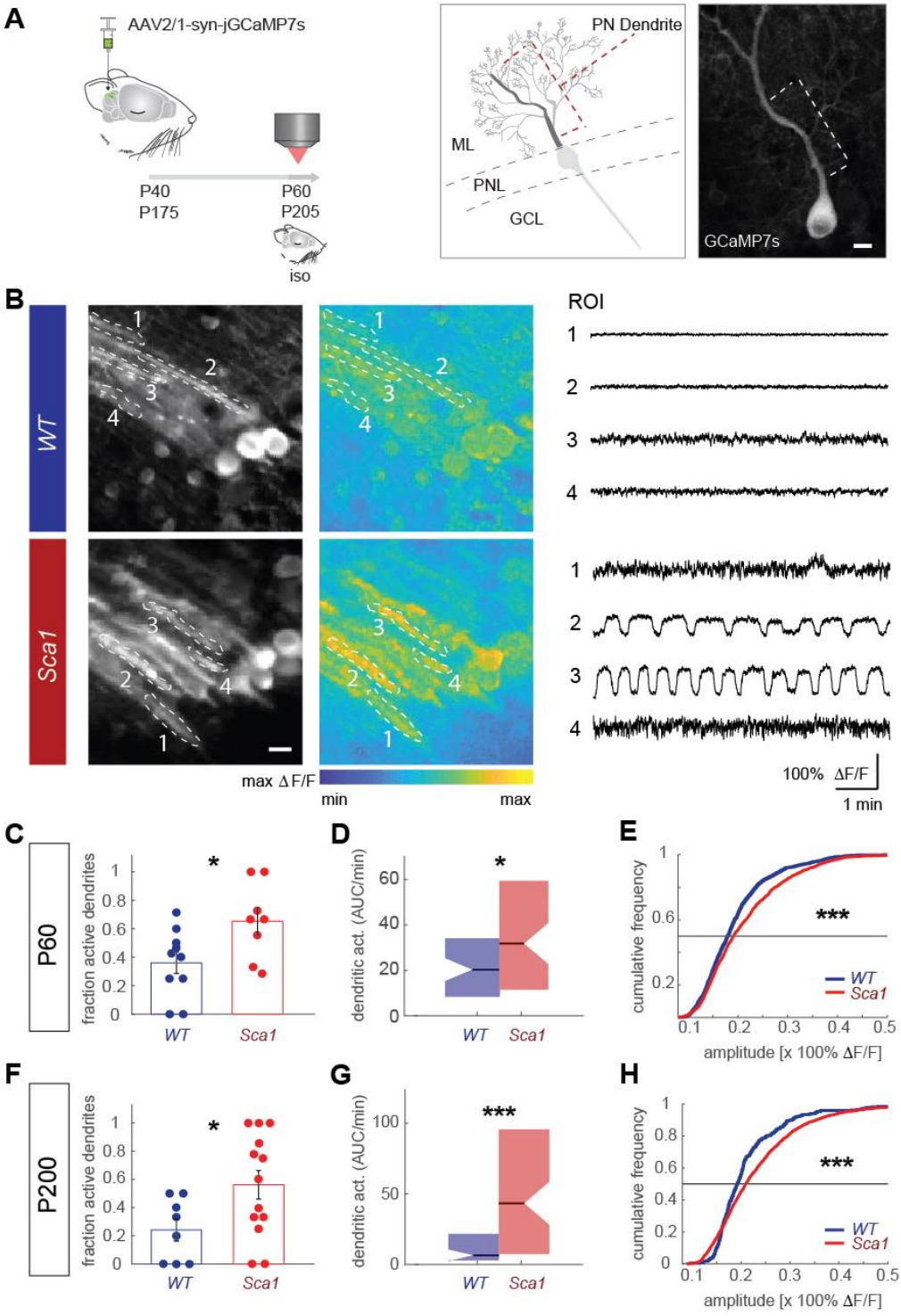

Figure 16: ***Purkinje cell dendrites display increased spontaneous calcium transients***

(A) *Left: Experimental design. Calcium signals in Purkinje neuron dendrites were assessed under light isoflurane anesthesia at the age of P60 and P200. Centre: Scheme depicting cerebellar cortical layers and orientation of Purkinje neurons and their dendrites extending across the molecular layer (ML – molecular layer, PNL – Purkinje neuron layer, GCL – granule cell layer). Right: Confocal image of a GCaMP7s - expressing Purkinje neuron. The apical dendrite is marked (right most image).* ***(B)*** *Example average projection of representative field of view of a WT (upper row) and Sca1 (lower row) mouse complemented by the maximum projection of the same FOV and calcium traces of the delineated regions of interest (ROIs) corresponding to PN dendrites.* ***(C)*** *Fraction of active PN dendrites at the age of P60 ($p = 0.025$, two-tailed Student's t-test).* ***(D)*** *Neuronal Dendritic activity (assessed as area under the curve (AUC)/min, $p = 0.03$, KS test).* ***(E)*** *Distribution of calcium transients amplitudes ($p < 10^{-10}$, KS test, data C-E is based on WT: 64 PN dendrites from 10 FOV, 6 mice and Sca1: 69 PN dendrites from 8 FOV, 5 mice).* ***(F)*** *Fraction of active PN dendrites at P200 ($p = 0.039$, two-tailed Student's t-test).* ***(G)*** *Activity of PN dendrites ($p < 10^{-5}$, KS test).* ***(H)*** *Distribution of calcium transient amplitudes ($p < 10^{-6}$, KS test, data F-H is based on WT: 49 PN dendrites from 8 FOV, 5 mice and Sca1: 82 PN dendrites from 14 FOV, 9 mice). Scale bars:* ***(A)*** *10 µm,* ***(B)*** *20 µm. * $p < 0.05$, *** $p < 0.001$. Figure adapted from Pilotto, Douthwaite et al., "Early molecular layer interneuron hyperactivity triggers Purkinje neuron degeneration in SCA1." Neuron. In Press.*

Overall, these data show strong evidence that neuronal function is disturbed early in *Sca1* mice, across multiple cell types and behavioural states. The primarily affected neuron type appears to be the MLIN population. With this is mind, we aimed to investigate the

functional relevance of these descriptive findings through manipulation of the MLIN, to unravel the extent by which changes in MLIN activity can directly influence the *Sca1* disease state.

4.2. Chemogenetic Modulation of MLIN Activity

4.2.1. Selective Manipulation of MLIN with Designer Receptors Exclusively Activated by Designer Drugs (DREADDs)

To determine the functional impact of MLIN hyperactivity on *Sca1* pathology and symptoms, we carried out chemogenetic experiments *in vivo*. To selectively target the MLIN population with this method, we therefore crossed our *Sca1* mouse line with homozygous PV-Cre mice to generate *Sca1::PV* or *WT::PV* animals. To validate that expression was only present in MLINs and not PNs we performed quantitative analysis to assess mCherry expression in these neurons across both *Sca1::PV* mice and *WT::PV* mice following injection of either AAV2/8-hSyn-DIO-mCherry or AAV2/8-hSyn-DIO-DREADDs(Gi)-mCherry **(Fig. 17)**. We found in the lobule of injection around ~70% of MLINs expressed mCherry. Whereas PN expression was 0% in the DREADDs and 0-5% with mCherry alone (N=3 mice, each data point is the mean of the 3-4 FOVs per mouse used for analysis) (**Fig. 17D**). We therefore concluded that this was suitable to selectively manipulate MLIN function in our designed paradigms.

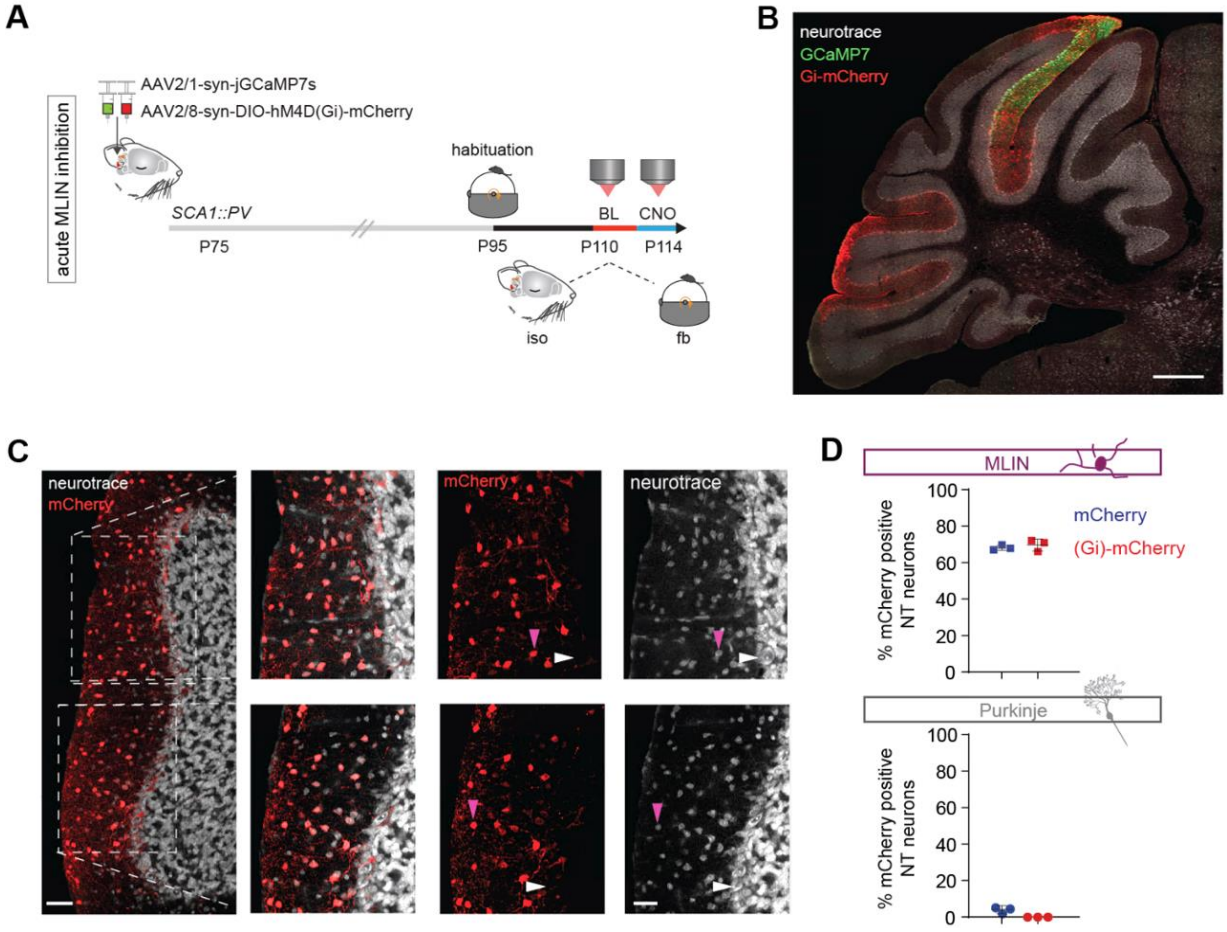

Figure 17:***Selective targeting of MLINs with DREADDs.*** *Figure legend continued on next page.*

(A) *Left: Outline of experimental procedures for acute treatment of clozapine-N-oxide (CNO), targeting specifically MLINs, with simultaneous two-photon imaging. DREADDs can be selectively expressed in MLINs of cerebellar cortex using AAV2/8-syn-DIO-DREADD(Gi)-mCherry or AAV2/8-syn-DIO-mCherry in Sca1::PV or WT::PV mice.* ***(B)*** *Representative confocal image of cerebellum from Sca1::PV mouse, following imaging cerebellar cortex circuit with acute MLIN inhibition. Mice are coinjected with AAV2/8-syn-DIO-DREADD(Gi)-mCherry in lobules VIII & VI and AAV2/1-syn-jGCaMP7s in lobule VI.* ***(C)*** *Representative confocal image of lobule VIII following AAV2/8-syn-DIO-DREADD(Gi)-mCherry and NeuroTrace (NT) staining. Expression of mCherry is localised to MLINs.* ***(D)*** *Quantification of mCherry expression in MLINs (above) and PNs (below) as a percentage of counted NT positive neurons in 350umx350um field of views. N = 3 mice, each data point is mean percentage of MLIN/PN from 3-4 FOVs per mouse. (C) Arrows indicate MLINs (magenta) and PNs (white). Scale bars: (A) 500 µm, (B) 50 µm, 50 µm. Figure adapted from Pilotto, Douthwaite et al., "Early molecular layer interneuron hyperactivity triggers Purkinje neuron degeneration in SCA1." Neuron. In Press.*

4.2.2. CNO Induced Inhibition of MLINs Modulates *Sca1* Circuit Dysfunction

We probed the impact of chemogenetic reduction of MLIN excitability on the activity levels of all three neuronal subtypes and the network encoding of sensorimotor behaviours, by means of *in vivo* calcium imaging. We co-injected AAV2/8-hSyn-DIO-hM4D(Gi)–mCherry (inhibitory DREADD) and AAV2/1-syn-jGCaMP7s into *Sca1::PV* and *WT::PV* control mice at the age of P75 to study the main inhibitory neuronal subtypes in ~P110 aged mice **(Fig. 17A).** DREADDs were activated following i.p. injection of exogenous ligand clozapine-N-oxide (CNO, 3mg/kg). This method resulted in ~50% of the identified MLINs in DREADD-injected mice displaying a decreased neuronal activity under light anesthesia (**Fig. 18A**). The overall distribution of absolute activity changes upon CNO shows a clear left shoulder, illustrating the reduction of activity levels in a substantial proportion of MLIN (**Fig. 18B**), exemplified in a representative activity map (maximum projection of the same FOV before and after CNO, **Fig. 18C**).

Upon quantifying neuronal activity levels under anesthesia in *WT::PV* and *Sca1::PV* mice, comparing the same set of neurons before and after CNO administration, revealed a strong reduction in calcium signals from the MLINs in the CNO recordings (**Fig. 18D**). In addition, we discovered a similar activity drop in Golgi cells exclusively in *WT::PV* mice (**Fig. 18E**), whilst calcium signals in PNs somata appeared unaffected by the CNO-triggered MLIN inhibition (**Fig. 18F**). However, we indeed uncovered a significant reduction in calcium signals within PN dendrites both in *WT::PV* and *Sca1::PV* mice (**Fig. 18G**).

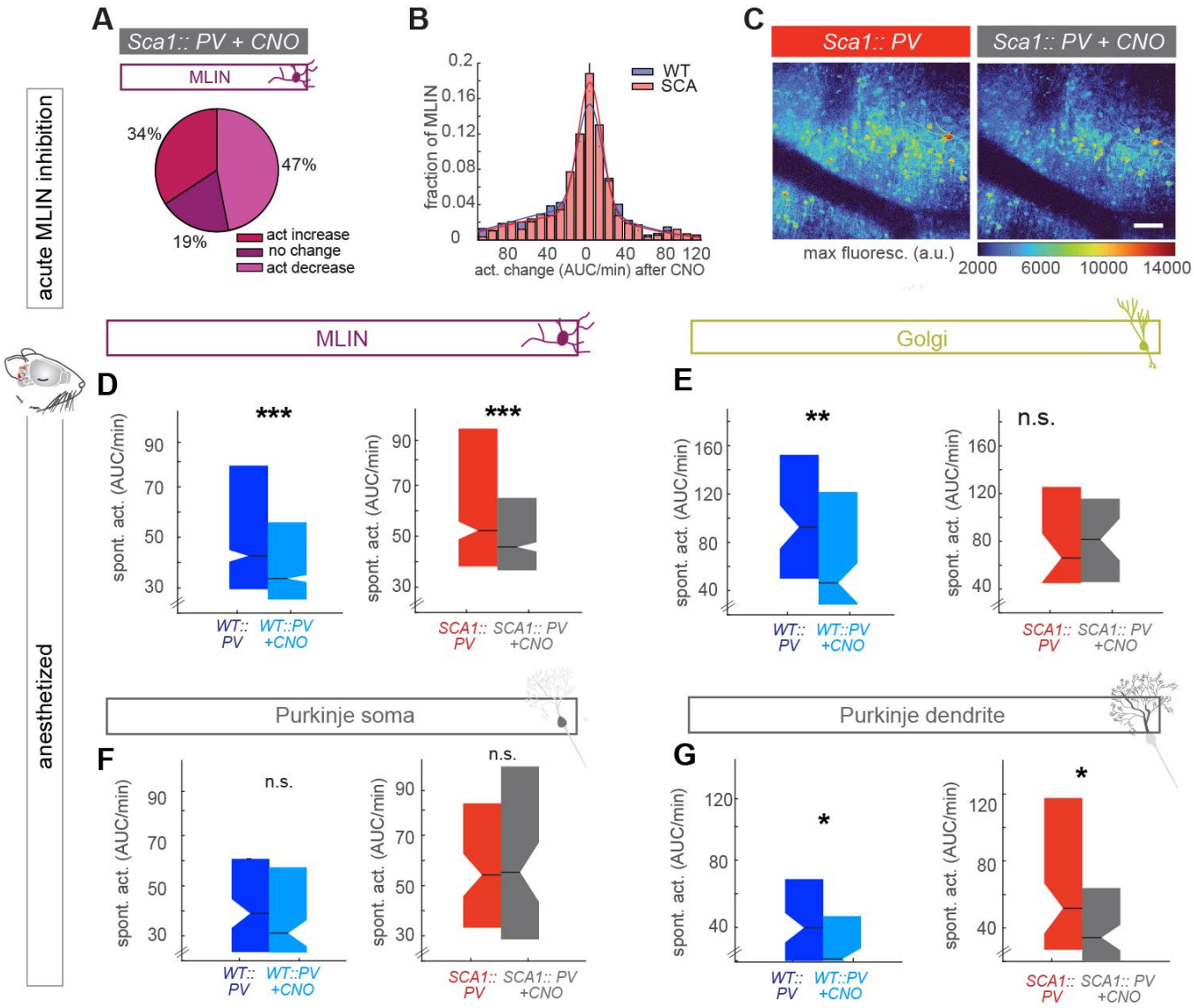

Figure 18: ***Acute inhibition of MLIN alters calcium signals across cerebellar cortex neurons in anesthetised mice.*** ***(A)*** *Change in neuronal activity of MLIN in Sca1::PV injected with AAV2/1-syn-GCaMP7s-WPRE, following CNO intraperitoneal (i.p.) application.* ***(B)*** *Absolute activity changes in MLIN upon CNO application.* ***(C)*** *Example of maximum intensity projection of an awake recording in a Sca1::PV mouse before and after CNO application.* ***(D)*** *MLIN activity under anesthesia before and after CNO in WT::PV (left, $p < 10^{-12}$, 1088 MLIN) and in Sca1::PV (right, $p < 10^{-5}$, 548 MLIN).* ***(E)*** *Golgi cell activity before and after CNO in WT::PV (p = 0.0017, 78 Golgi) and Sca1::PV (p = 0.87, 38 Golgi),* ***(F)*** *neuronal activity of PN upon CNO in WT::PV (p = 0.27, 102 PN) and Sca1::PV (p = 0.17, 83 PN) and* ***(G)*** *calcium signals in PN dendrites in WT::PV (p = 0.013, 83 PN dendrites) and Sca1::PV (p = 0.043, 88 PN dendrites, all KS tests, data in D-G is derived from WT::PV: 12 FOV, 5 mice and Sca1::PV: 8 FOV, 5 mice). Scale bar: (C) 50 µm. * p < 0.05, ** p < 0.01, *** p < 0.001. Figure adapted from Pilotto, Douthwaite et al., "Early molecular layer interneuron hyperactivity triggers Purkinje neuron degeneration in SCA1." Neuron. In Press.*

Recordings in awake mice overall upheld these findings, a clear activity reduction upon CNO mainly of the spontaneous activity of MLIN was observed during quiet wakefulness (**Fig. 19A**). In awake mice also Golgi cell activity decreased upon CNO in *WT::PV* and as a trend in *Sca1::PV* mice (**Fig. 19B**), as did the calcium signal fluctuations in PN somata (**Fig. 19C**), potentially reflecting a more stable pacemaker firing activity, which would cause less fluctuations in the fluorescence trace. Despite a trend in both groups matching our anesthetised data, PN dendrites were not significantly decreased upon CNO in awake mice (**Fig. 19D**). However, in the awake mice the PN dendrites displayed a lower baseline calcium signal, likely due to increased activity in particular of MLINs, driven by sensory and motor input (Haider et al., 2013). It was therefore more challenging to faithfully identify PN dendrites from recordings whilst mice were awake, leading to a considerably lower number of defined regions of interest (ROIs) corresponding to PN dendrites included in the analysis.

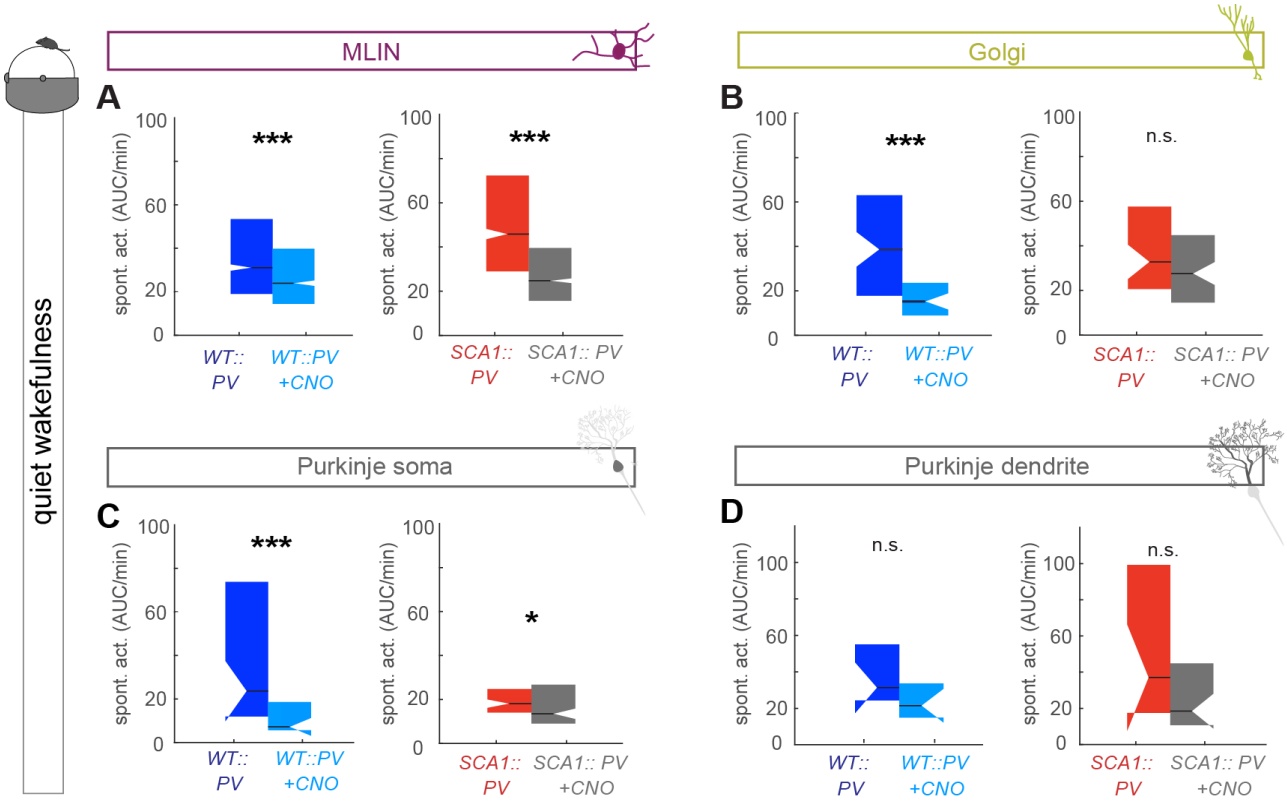

Figure 19: ***Acute inhibition of MLIN alters calcium signals across cerebellar cortex neurons in awake mice.*** ***(A)*** *Spontaneous activity during quiet wakefulness (QW) of MLIN before and after CNO in WT::PV ($p < 10$, 1316 MLIN) and Sca1::PV ($p < 10^{-52}$, 813 MLIN),* ***(B)*** *of Golgi cells in WT::PV ($p < 10^{-5}$, 82 Golgi) and Sca1::PV ($p = 0.094$, 56 Golgi),* ***(C)*** *of PN in WT::PV ($p < 10^{-3}$, 49 PN) and Sca1::PV ($p < 10^{-4}$, 76 PN) and* ***(D)*** *calcium signals in PN dendrites in WT::PV ($p = 0.19$, 12 PN dendrites) and Sca1::PV ($p = 0.12$, 19 PN dendrites, all KS tests, data is derived from WT::PV: 17 FOV, 7 mice and Sca1::PV: 17 FOV, 7 mice. * $p < 0.05$, ** $p < 0.01$, *** $p < 0.001$. Figure adapted from Pilotto, Douthwaite et al., "Early molecular layer interneuron hyperactivity triggers Purkinje neuron degeneration in SCA1." Neuron. In Press.*

In a separate set of control experiments with *Sca1* mice coinjected with AAV2/8-hSyn-mCherry and AAV2/1-syn-jGCaMP7s (**Fig. 20A-B**), we confirmed that CNO application alone had no effect on neuronal activity levels (**Fig. 20C-F**).

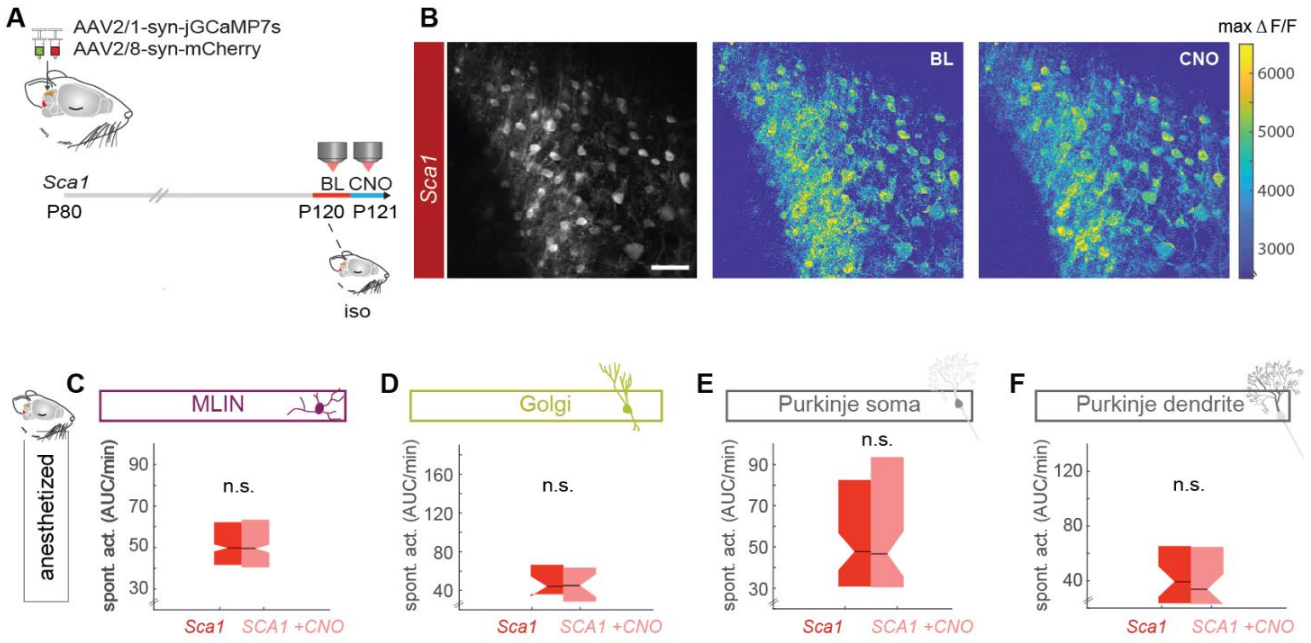

Figure 20: ***Acute CNO administration alone has no impact on neuronal activity in Sca1 mice. (A)*** *Experimental scheme. Sca1 mice received co-injections of AAV2/1-syn-jGCaMP7s and AAV2/8-syn-mCherry into the cerebellar cortex. Mice were imaged at the age of p120 (first a baseline (BL, prior to CNO) and subsequently the same neurons were imaged after CNO application).* ***(B)*** *From left to right images display average mean projection of a representative FOV, followed by the maximum projection of the same FOV in the baseline recording and the recording following CNO administration.* ***(C)*** *Neuronal activity levels under light anesthesia (isoflurane) were unaltered in MLIN (P = 0.31, 344 MLIN),* ***(D)*** *Golgi cells and (p = 0.53, 21 Golgi)* ***(E)*** *PN (p = 0.8, 80 PN, all KS tests, data from 6 FOV, 2 mice). Scale bar:* ***(B)*** *20 µm. Figure adapted from Pilotto, Douthwaite et al., "Early molecular layer interneuron hyperactivity triggers Purkinje neuron degeneration in SCA1." Neuron. In Press.*

With confirmation that the alterations in neuronal activity were due to CNO-DREADD interaction, we aimed to identify how the induced changes to neuronal activity alter the network coding properties. We therefore probed if the previously compromised coding capacity could be restored upon chemogenetic dampening of the overactive MLIN population. Once more computing the manifolds of all neurons in a given FOV again revealed 2 subspaces (**Fig. 21A**).

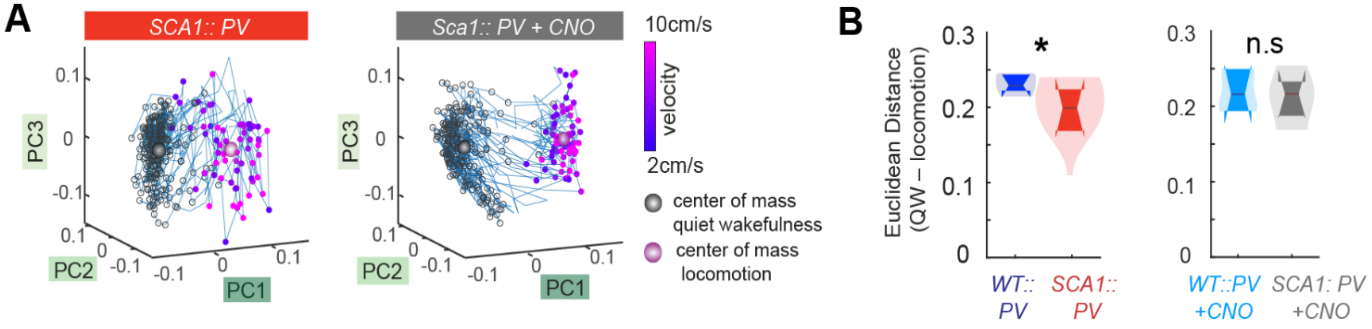

Figure 21: ***Network behavioural state representation is restored in behaving Sca1 mice following acute MLIN inhibition.*** *(A) Example manifold of all neurons in a FOV in a Sca1::PV mouse, depicting the less discrete segregation of quiet wakefulness and active states (color-coded for running speed), which is improved after CNO application (PC space on the right). (B) Euclidean distance in PC space between the centre of mass of quiet wakefulness and locomotion before CNO: p = 0.027, WT::PV: 10 FOV, 5 mice, Sca1::PV: 12 FOV, 5 mice and after CNO p = 0.97, WT::PV: 9 FOV, 5 mice, Sca1::PV 11 FOV, 6 mice, Wilcoxon rank sum test). * p < 0.05. Figure adapted from Pilotto, Douthwaite et al., "Early molecular layer interneuron hyperactivity triggers Purkinje neuron degeneration in SCA1." Neuron. In Press.*

These were less discrete in *Sca1::PV* mice, which is quantifiable in the form of reduced Euclidean distance between the centre of mass for quiet wakefulness and locomotion. Intriguingly, after CNO application, the subspaces became more distinguished, the Euclidean distance between both states was no longer significantly different between *WT::PV* and *Sca1::PV* mice (**Fig. 21B**). Together these data demonstrate that inhibition of MLINs can drive restoration of not only activity levels in distinct cell types but also the network's coding capacity

4.2.3. Acute MLIN Inhibition Can Alleviate Motor impairment and Molecular Pathology

To investigate the reduction in MLIN excitability further, we stereotaxically injected AAV2/8-hSyn-DIO-hM4D(Gi)–mCherry, bilaterally into the posterior cerebellum of P70 *Sca1::PV* and *WT::PV* animals, as outlined in the experimental timeline (**Fig 22A**). We tested whether the improved network encoding of behavioural state coincides with improvement of motor symptoms, by means of the classical coordination test, the rotarod. To confirm the surgical procedure did not affect motor control, mice were tested prior to after following the stereotaxic injection (**Fig. 22A-B**). At P85, mice injected with the inhibitory DREADD were tested for 3 consecutive days on the rotarod, where a single i.p. injection of CNO (3mg/kg) or saline was administrated 45 minutes before the test. Intriguingly, reducing MLIN excitability did not hinder *WT::PV* animals, but did indeed lead to a substantial improvement of motor performance in the *Sca1::PV* animals that received the CNO injections compared with the saline group (**Fig. 22B)**. After the CNO wash out period of 24h, *Sca1::PV* mice previously injected with CNO still displayed improved rotarod performance compared to the saline group, suggesting some form of lasting implications resulting from the three day treatment (**Fig. 22B**). Importantly this CNO concentration did not cause any adverse effects in relation to rotarod performance in mice not injected with DREADDs (**Fig. 22C**).

To further understand the impact of the reduction on excitability on MLINs, we evaluated the expression levels of the calcium binding protein parvalbumin (PV), a well-established marker for MLINs in adult mice (Collin et al., 2005). PV expression levels in inhibitory interneurons correlate with their neuronal activity levels (Donato et al., 2013), and can modulate calcium signals and paired-pulse facilitation in the cerebellar cortex (Caillard et al., 2000; Schwaller, 2020). Our earlier experiments had revealed that by P30, the proportion of MLIN expressing high levels of PV was already significantly elevated in *Sca1* mice when compared to their *WT* littermates (**Fig. 22D**). The fraction of mutant MLIN expressing high levels of PV increased over disease progression with 49% at P90 and 60% at P200 (**Fig. 22D**). Intriguingly, CNO treatment in *Sca1::PV* injected with inhibitory DREAD(Gi) (*Sca1::PV-DREADD(Gi))* but not saline application, led to reduced PV expression within MLIN. The

reduction following acute reduction of excitability suggests that higher PV expression in *Sca1* MLIN is a dynamic process, which can be reversed by reducing MLIN excitation (**Fig. 22D**).

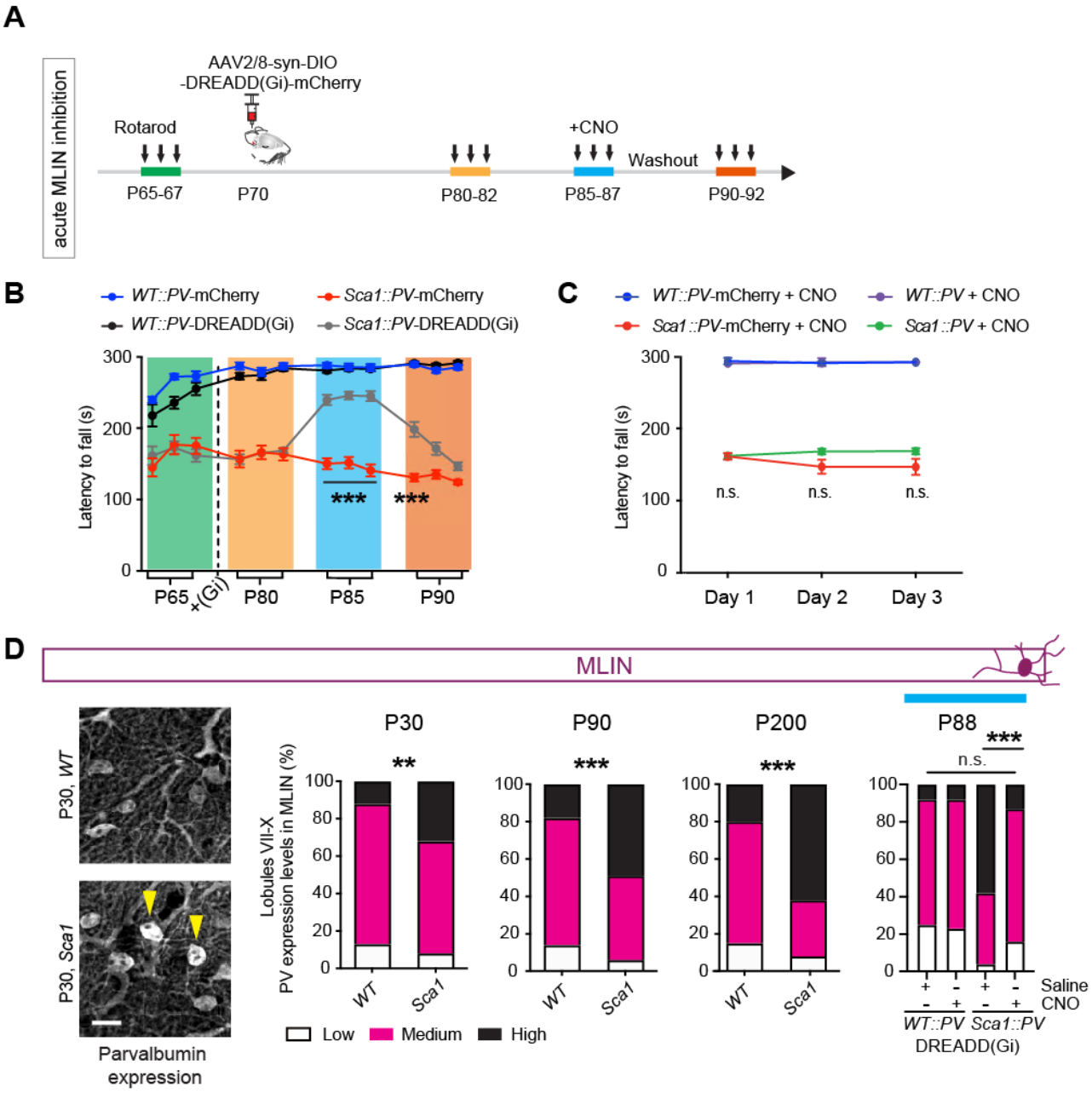

Figure 22: ***Acute MLIN inhibition alleviates motor symptoms and MLIN Sca1 molecular pathology. (A)*** *Timeline of the experimental design for acute cerebellar MLIN inhibition in WT::PV and SCA1::PV mice via AAV2/8-syn-DIO-DREADD(Gi)-mCherry with behavioural experiments. (**B**) Rotarod experiment following CNO administration (two-way ANOVA time points $F_{(11,192)}$= 9.76, p<0.0001, treatment $F_{(1,192)}$= 97.34, p<0.0001, interaction $F_{(11,192)}$= 12.35, p<0.0001; P85-87 Sca1::PV + saline vs Sca1::PV + CNO; P90 Sca1::PV + saline vs Sca1::PV + CNO. WT::PV + saline n=9 mice; WT::PV + CNO n=8 mice; Sca1::PV + saline n=8 mice; Sca1::PV + CNO n=10 mice). Figure legend continued on next page. **(C)** Rotarod test indicating latency to fall of naïve WT::PV, Sca1::PV and WT::PV-mCherry and Sca1::PV-mCherry animals after CNO injection. n= 5 animals per condition. **(D)** Representative confocal images of MLIN PV immunostaining from WT and Sca1 cerebellum at P30. Percentage of neuronal fractions expressing low, medium, and high levels of PV at P30 (presymptomatic), P90 (symptomatic), and P200 (end stage), (Chi-square P30: P=0.0025; Chi-square P90: P<0.0001, P200: P<0.0001. PV expression at P88 following i.p. injection of CNO or saline (Chi-square WT::PV + saline vs Sca1::PV + CNO: P = 0.19 n.s.; Sca1::PV + saline vs Sca1::PV + CNO: P<0.0001). ** p < 0.01, *** p < 0.001. Scale bar: (C) 20 µm. Yellow arrowheads in (C) indicate MLIN. Data courtesy of Federico Pilotto & Smita Saxena, Inselspital University Hospital, Bern, Switzerland. Figure adapted from Pilotto, Douthwaite et al., "Early molecular layer interneuron hyperactivity triggers Purkinje neuron degeneration in SCA1." Neuron. In Press.*

4.2.4. Chronic inhibition of MLINs Induces Lasting Alleviation of *Sca1* Motor and Molecular Features

Following the distinct positive impact of acute MLIN inhibition in *Sca1* mice, we investigated whether prolonged reduction in MLIN activity could further alleviate molecular pathology and motor symptoms. Accordingly, we selectively expressed the inhibitory hM4D(Gi)–mCherry or mCherry using AAV2/8, in *WT::PV* and *Sca1::PV* MLIN at P40, then exposed the groups to chronic administration of CNO in drinking water (40 µg/ml) for 30 days (from P60 to P90). Following the treatment, mice were behaviourally assessed and monitored until the end stage of the disease (**Fig. 23A**). A subgroup of late-stage symptomatic mice were sacrificed for analysis of molecular *Sca1* pathological features. The chronic reduction of MLIN activity, led to a sustained reduction of PV expression, specifically within the mutant MLIN population, a striking 90 days following the completion of the CNO treatment (**Fig. 23B**).

MLIN inhibition primarily targets PNs, therefore hyperactivity of MLINs could be driving alterations in PNs, we thus investigated if the well documented PN pathology in *Sca1* mice was altered following a reduction in MLIN activity. Studies have consistently found dysfunction in *Sca1* mice at the site of PN dendrites, a feature of which is the downregulation of proteins regulating calcium homeostasis, such as the scaffold protein Homer-3 (Ruegsegger et al., 2016; Serra et al., 2004). Furthermore, decreased expression of phosphorylated calcium-calmodulin kinases II (CAMKII) in the PN soma has been reported in this model, reflecting altered PN calcium handling, and is restored following increased Homer-3 expression (Ruegsegger et al., 2016). We therefore measured the expression of dendritic Homer-3 and somatic P-CAMKII to gain insight into PN molecular state following MLIN inhibition. A striking 90 days following the end of the chronic treatment, the calcium buffer precursor P-CAMKII was increased to a similar level in *WT* mice (**Fig. 23C**). Importantly, given the degeneration of PNs that occurs in late stage *Sca1* mice (Watase, et al., 2002), the total number of PNs was also raised (**Fig. 23D**). Finally, within PN dendritic spines, there was an increase in Homer-3 immunoreactive puncta at P180 (**Fig. 23E)**. These findings suggest that a chemogenetic-mediated reduction in MLIN hyperactivity alleviates PN molecular *Sca1* features, and promotes PN survival, sustained long after the CNO treatment ends. Through recording rotarod performance throughout CNO application and the following months, we observed an improvement in motor coordination deficits in *Sca1::PV-DREADD(Gi)* mice, in comparison to the mCherry control group (**Fig. 23F**). Notably, following the end of CNO application at P90, although both symptomatic Sca1 groups showed a gradual decline in rotarod performance, the *Sca1::PV-DREADD(Gi)* mice maintained a significantly improved latency to fall over their control counterparts, for two further months. In addition, there were no visible deficits in motor

coordination in either of the *WT::PV* groups (**Fig. 23F**). A classical phenotype and measurement of disease severity in *Sca1* mice is a clasping of the hindlimbs when suspended from the tail (Watase et al., 2002). Chronic suppression of MLIN activity deferred the onset of full clasped together hindlimbs with interlocked rear claws upon tail suspension (**Fig. 23G**). The humane termination criteria for our *Sca1* mice was a 10% decrease from the maximum weight of each individual mouse. We found the chronic MLIN inhibition delayed the drop of weight to reach this criteria in *Sca1::PV-DREADD(Gi)* animals, with an increase in survival (based on weight loss criteria) of 22 days later than the control group (**Fig. 23H**). These findings show that 4 months after the CNO application was discontinued, late stage symptomatic *Sca1::PV-DREADD(Gi)* mice still display improvements in condition. Further underlining our earlier data to show that acute reductions in MLIN activity can have beneficial impact on various *Sca1*-like features in the cerebellar cortex, and brings to light that early, chronic, MLIN modulation can drive improvements remaining for the entire *Sca1* disease course.

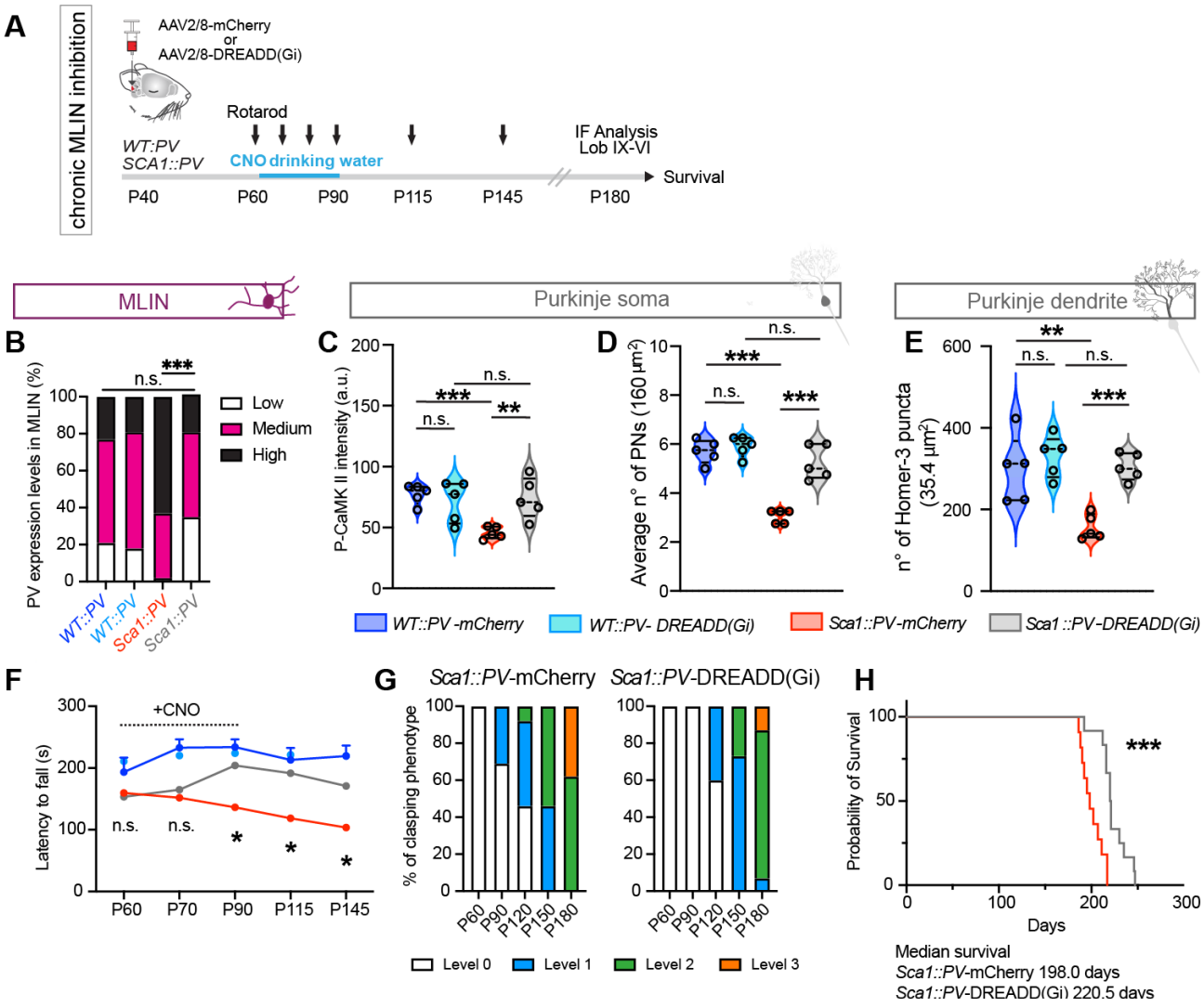

Figure 23: ***Suppression of MLINs delays appearance of hallmark Sca1 features. (A)*** *The experimental design for chronic cerebellar MLIN inhibition. Bold arrows mark longitudinal rotarod measurement.* ***(B)*** *PV expression levels in MLIN following chronic inhibition (Chi-square WT::PV-mCherry vs Sca1::PV-DREADD(Gi), P=0.56, Sca1::PV-mCherry vs Sca1::PV-DREADD(Gi) P<0.0001). Figure legend continued on next page.*

*(**C**) P-CAMKII expression levels in PN soma (unpaired t-test WT::PV-mCherry vs WT::PV-DREADD(Gi): P=0.48, Sca1::PV-mCherry vs Sca1::PV-DREADD(Gi): P=0.0066). (**D**) P180 PN numbers across the four groups labelled via calbindin immunostaining (unpaired t-test WT::PV-mCherry vs WT::PV-DREADD(Gi): P=0.50, n.s.; Sca1::PV-mCherry vs Sca1::PV-DREADD(Gi): P=0.0002). (**E**) Homer-3 expression within the molecular layer (unpaired t-test WT::PV-mCherry vs WT::PV-DREADD(Gi): P=0.49; Sca1::PV-mCherry vs Sca1::PV-DREADD(Gi): P<0.0001). (**F**) Rotarod performance plotted as latency to fall (two-way ANOVA time points $F_{(4,215)}$=1.030, P=0.3929, treatment $F_{(3,215)}$= 28,59, P<0.0001, interaction $F_{(12,215)}$= 1.039, P=0.4146 ; Tukey's multiple comparison: Sca1::PV-mCherry vs Sca1::PV-DREADD(Gi) P90-P115-P145; WT::PV-mCherry n=13; WT::PV-DREADD(Gi) n=11; Sca1::PV-mCherry n=13; Sca1::PV-DREADD(Gi) n=10). (**G**) Clasping phenotype scores at distinct time points in Sca1::PV-mCherry and Sca1::PV-DREADD(Gi). (**H**) Survival curve of Sca1::PV-DREADD(Gi) compared to Sca1::PV-mCherry (Sca1::PV-mCherry (n=5 female/6 male) median survival: 198 days, Sca1::PV-DREADD(Gi) (n=6 female/6 male) median survival: 220.5 days; Log- rank test: Chi square: 14.15, P=0.0002). n=3-5 for immunofluorescence analysis. Graphs (B-E) depict mean values per animal, * p < 0.05, ** p < 0.01, *** p < 0.001. Data in (B)-(E) courtesy of Federico Pilotto & Smita Saxena, Inselspital University Hospital, Bern, Switzerland. Data in (F)-(H) from combined experiments from ourselves and Federico Pilotto & Smita Saxena, analysed & arranged by Federico Pilotto, Inselspital University Hospital, Bern, Switzerland. Figure adapted from Pilotto, Douthwaite et al., "Early molecular layer interneuron hyperactivity triggers Purkinje neuron degeneration in SCA1." Neuron. In Press.*

4.2.5. Enhancing MLIN Activity is Sufficient to Induce *Sca1*-like Motor and Molecular Alterations in *WT* Mice

To investigate the notion that MLIN hyperactivity can drive *Sca1* pathology, rather than a bystander among many dysfunctional elements, we injected *WT::PV* with an excitatory DREADD (AAV2/8-hSyn-DIO-hM3D(Gq)–mCherry) to selectively enhance MLIN activity. Upon acute CNO application there is an increased excitability of MLIN, and as a result raised inhibition of PN, mimicking our findings in *Sca1* mice (**Fig. 24A).** Using the same experimental paradigm as described previously, we found that increasing inhibition on to the PNs can affect motor behaviour in *WT* mice, as rotarod performance of *WT::PV* that received CNO injections dropped (**Fig. 24B**). Furthermore, we found expression of PV within MLINs in *WT::PV* PNs, was similar to those in *Sca1::PV* MLIN, after CNO administration (**Fig. 24C**).

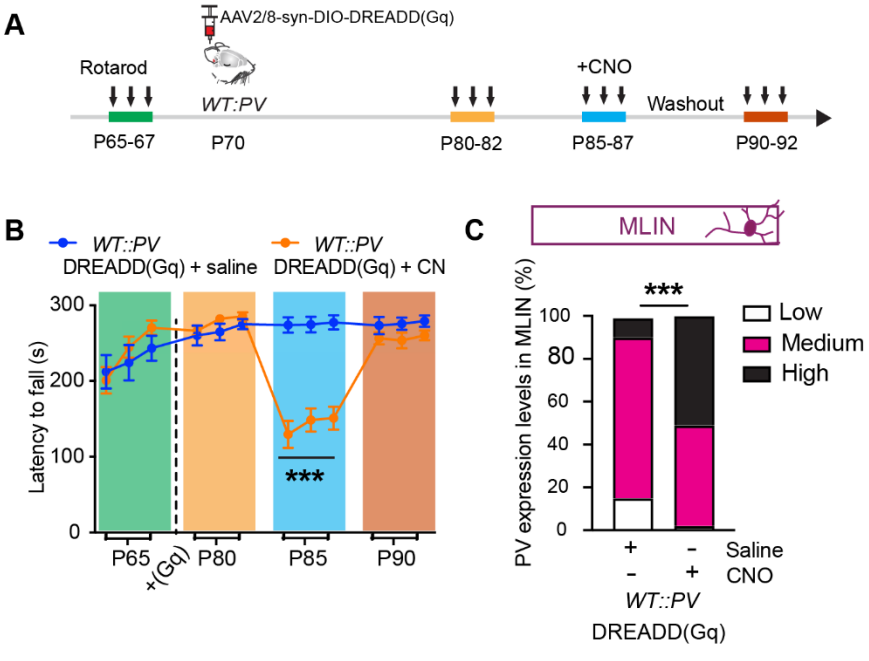

Figure 24: ***Acute stimulation of MLINs induces motor deficits and Sca1 like molecular pathology.***(***A***) *Timeline of experimental design for acute cerebellar MLIN activation in WT::PV animals.*(***B***) *Rotarod experiments indicating latency to fall in both groups; prior to and following surgery, then following administration of either CNO or saline, then washout (two-way ANOVA timepoints $F_{(11,180)}$= 10.55, P<0.0001, treatment $F_{(1,180)}$= 37.88, P<0.0001, interaction $F_{(11,180)}$= 12.09, P<0.0001; Multiple comparison P85-87 WT::PV + saline vs WT::PV + CNO; n=7 WT::PV + saline, n=10 WT::PV + CNO).* (***C***) *Percentage of low, medium and high parvalbumin expressing MLINs, following treatment with either CNO or saline (Chi-square WT::PV + saline vs WT::PV + CNO: P<0.0001). Data courtesy of Federico Pilotto & Smita Saxena, Inselspital University Hospital, Bern, Switzerland. Figure adapted from Pilotto, Douthwaite et al., "Early molecular layer interneuron hyperactivity triggers Purkinje neuron degeneration in SCA1." Neuron. In Press.*

4.2.6. Chronic Stimulation of MLINs Induces Lasting *Sca1*-like Pathological Alterations

Given that acutely increasing the excitability of MLINs induced motor deficits and influenced MLIN parvalbumin levels, we investigated the impact of chronic enhanced excitability of MLINs to explore the functional implications of our findings in a healthy network. We used a 30-day CNO treatment paradigm (**Fig. 25A**). We performed regular rotarod tests, beginning at 10 days into receiving CNO via drinking water. The tests revealed a consistent decline in the latency to fall in *WT::PV-DREADD(Gq)* mice, as opposed to an initial increase in latency on the rod, and then maintenance of performance from the *WT::PC-mCherry group* (**Fig. 25B**). Motor coordination deficits remained for 20 days following the end of the CNO treatment. The lack of improvement in rotarod performance indicates that hyperexcitable MLINs can not only provokes *Sca1*-like phenotypes, but prolonging this state in MLINs induces lasting deficits, even in the absence of CNO stimulation (**Fig. 25B**). Importantly, we found decreased PN dendritic expression of Homer-3 in *WT::PV-DREADD(Gq)* (**Fig. 25C**), while in the PN soma there was no difference in P-CAMKII or CAMKII levels in comparison to *WT::PV* mice (**Fig. 25C**). Taken together, these results provide evidence that MLIN-mediated, elevated inhibition of PNs, non-cell autonomously, promotes cellular pathology within PNs, and triggers manifestations of ataxia-like symptoms in *WT::PV* mice, lacking disease causing mutations. In addition, manipulating MLIN activation is capable of having a long-term effect on PN spines, which are considered as highly vulnerable in the context of *Sca1* pathology.

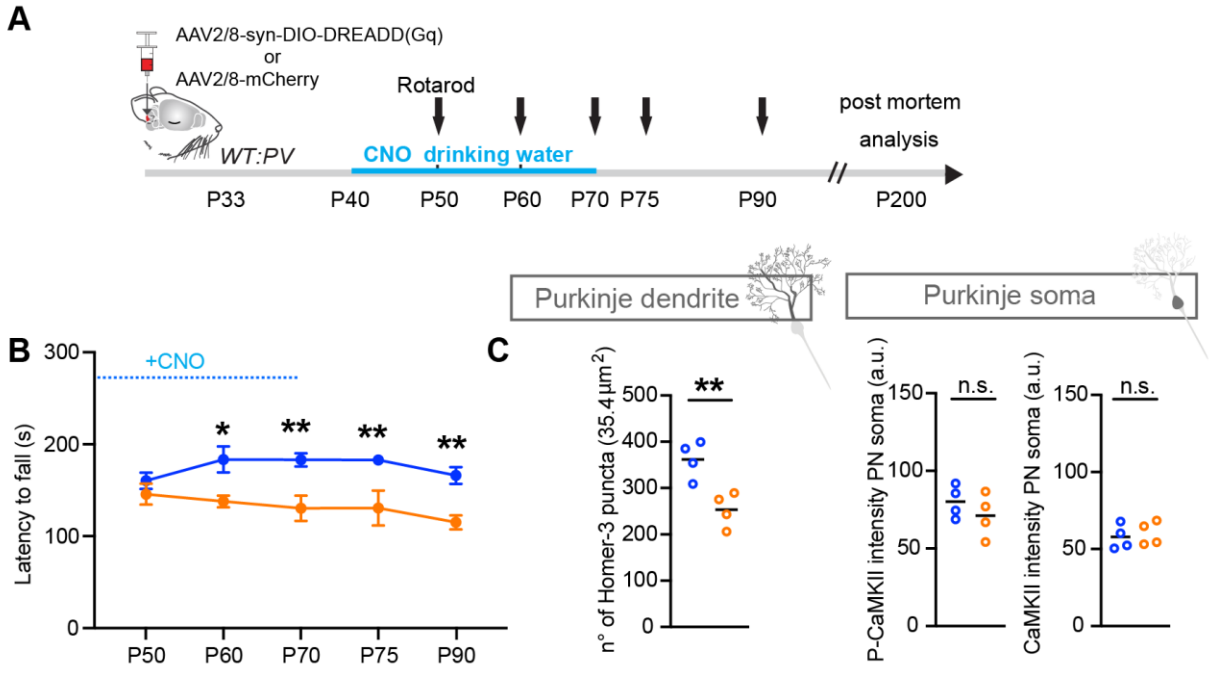

Figure 25: ***Chronic Stimulation of MLINs in WT mice Induces Prolonged Sca1 Motor Deficits and Sca1-like Molecular Alterations. (A)*** *Experimental timeline for chronic 30 day MLIN activation (treatment from P40-P70) in WT::PV animals, culminating in sacrifice of the animals at P200 for analysis. Bold arrows mark longitudinal rotarod measurements. Figure legend continued on next page.*

*(**B**) Rotarod performance plotted as latency to fall. Chronic CNO administration significantly affects motor performance in WT::PV-DREADD(Gq) mice (Two-way ANOVA time points $F_{(4,70)}$= 0.9894, P=0.42, treatment $F_{(1,70)}$= 38.49, P<0.0001, interaction $F_{(4,70)}$= 1.095, P=0.37; Sidak's multiple comparison: WT::PV-mCherry vs WT::PV-DREADD(Gq), n=8 animals/group). **(C)** Homer-3 expression in WT::PV-DREADD(Gq) compared to WT::PV-mCherry control (P=0.0074). P-CAMKII (P=0.34) and CAMKII (P=0.67), after chronic activation of MLIN in WT::PV animals at P200, all unpaired t-test. n=3-5 for immunofluorescence analysis. Graphs in (C) depict mean values per animal. * p < 0.05, ** p < 0.01, *** p < 0.001. (B) Surgery and following CNO treatment with behavioural experiments was entirely completed at Ludwig-Maximilian University Munich, following sacrifice of animals, brains were sent for analysis in (C) by Federico Pilotto & Smita Saxena, Inselspital University Hospital, Bern, Switzerland. Figure adapted from Pilotto, Douthwaite et al., "Early molecular layer interneuron hyperactivity triggers Purkinje neuron degeneration in SCA1." Neuron. In Press.*

5. DISCUSSION

Our results reveal three key findings; (1) MLINs are hyperactive, and hyperresponsive to sensorimotor input, in the early symptomatic phase of *Sca1* mice. (2) Encoding of behavioural state across cerebellar cortex circuit is disrupted. (3) Reducing excessive MLIN activity can restore network functionality, alleviate motor deficits, reduce molecular pathology and delay disease progression (**Fig. 26**). For the first time, we identify circuit deficits in *Sca1* related to MLINs and show they can be targeted therapeutically. The finding of early circuit dysfunction is also in line with emerging work across a number of neurodegenerative disorders.

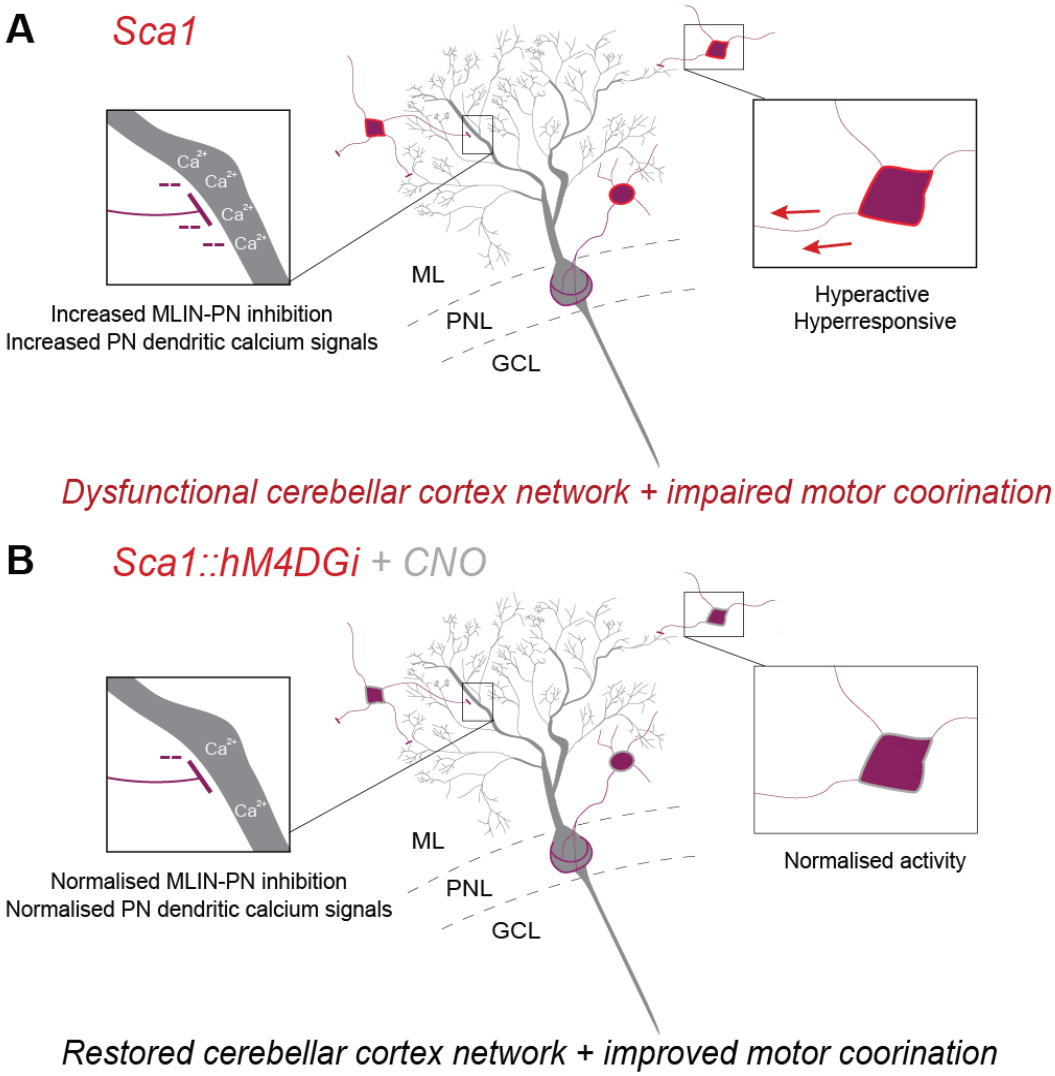

Figure 26: ***Summary of Key Findings. (A)*** *MLINs are hyperactive and hyperresponsive to sensorimotor input in Sca1 mice, PN dendrites display enhanced calcium signals. Network encoding of behavioural state is disrupted.* ***(B)*** *CNO mediated inhibition of MLIN activity in Sca1::hM4DGi mice drives normlised dendritic calcium signals, restores cerebellar network enconding of behavioural state, and improves motor coordination. Arrows in (A) indicate increased MLIN activity. - - indicates inhibition of PN dendrite from MLIN, high in (A), normailsed in (B).* Ca^{2+} *indicates calcium signals, elevated in (A), normalised in (B).*

5.1. Cerebellar Cortex Circuit Dysfunction in *Sca1*

5.1.1. Aberrant MLIN Activity is Implicated in Early Cerebellar Cortex Circuit Dysfunction

The three major inhibitory interneurons of the cerebellar cortex each play essential roles in the processing of sensory information, motor skills, balance, posture and higher cognitive function (Apps and Garwicz, 2005; Hull and Regehr, 2022). Disruption to these behaviours encompass a number of the wide range of symptoms that *Sca1* patients can endure. A hallmark feature of *Sca1* is PN degeneration, which has previously been the major focus of research in the field. It is however, neither the first nor only cell type to degenerate (Deelchand et al., 2019; Guerrini, et al., 2004; Koscik et al., 2020; Seidel et al., 2012). Loss of brainstem grey matter is one of the earliest features of *Sca1* patients (Jacobi et al., 2013), and in *Sca1* mice, alterations to both CFs and inhibitory connectivity onto PNs has been reported in the early and presymptomatic stages respectively (Edamakanti et al., 2018). Such evidence led us to study the primary inhibitory neurons of the cerebellar cortex in the early stages of *Sca1* mice, calcium imaging has revealed the hyperactive and sensorimotor hyperresponsive, properties of MLINs, as the clearest pathophysiological features of these neuron groups.

MLINs are the sole inhibitors of PNs, therefore provide essential modulation to the output cell of the cerebellar cortex. They modulate PN firing in local clusters with direct inhibitory connections providing distinct modulation of PN dendrites and somata. MLIN circuits can produce feedforward inhibition with the same parallel fibres (PFs) innervating both MLINs and PNs, sagittal projecting MLIN axons also facilitate lateral inhibition of PNs that do not share a PF input with, and finally PNs themselves have direct inputs onto MLINs shaping a feedback inhibition (Kim and Augustine, 2021). Although less studied in relation to *Sca1* symptoms, they are functionally implicated in several relevant motor roles to this disease, including orofacial movements (Astorga et al., 2017; Gaffield and Christie, 2017; Heinley et al., 2014; Wulff et al., 2009). Deficits in orofacial control closely align with the established *Sca1* symptoms dysarthria, dysphagia and ophthalmoplegia (Seidel et al., 2012). Here, we identified a hyperresponsiveness of MLIN calcium signals to locomotion and air puff stimulation, along with hyperactivity during quiet wakefulness and under anesthesia, in the early symptomatic phase of *Sca1* development.

Yet what causes such aberrant MLIN function? We detected severely reduced cytoplasmic calcium levels in MLIN, importantly, this finding was confirmed by using the FRET-based GECI, Twitch2B (Thestrup et al., 2014). Ratiometric imaging is able to give a more accurate insight into intracellular calcium levels, as the highly heterogeneous expression levels of the indicator do not influence the readout of fluorescence ratio (Thestrup et al., 2014).

Additionally, these data are in line with the finding of higher levels of the calcium buffer parvalbumin in these cells, which likely reduces cytosolic calcium. It has been reported that there is a decrease in parvalbumin immunoreactivity in surviving PNs of *Sca1* patient brains post-mortem (Vig et al.,1996), along with insight from mouse models showing decreased PN parvalbumin and calbindin D28k (calbindin) immunoreactivity (Vig et al., 1998), and reduced calbindin gene expression (Serra et al., 2004). Perhaps mutant ataxin-1 can drive increases in PV in MLINs, however, further work would need to explore if such cell autonomous mechanisms could be driving MLIN dysfunction. Altered MLIN firing properties and molecular composition may also be due to compensatory mechanisms driven by aberrant upstream inputs to the cerebellar cortex circuit. Certainly, CF synapses onto PNs are reduced in *Sca1*, actually in the early weeks of development (Ebner et al., 2013; Edamakanti et al., 2018). In addition, PNs also provide inhibition onto MLINs (Prestori et al., 2019a), as reduction in PN firing has been reported in *Sca1* early in the disorder (Dell'Orco et al., 2015; Hourez et al., 2011), there may be a role for reduced PN-MLIN feedback inhibition. Furthermore, the pons and other brainstem areas are also affected early in *Sca1* patients (Seidel et al., 2012). Dysfunction within the brainstem could alter both CF (inferior olive nuclei) and a proportion of the MF inputs to the cerebellar cortex circuit. Additionally, MLINs are partially through "glutamate spillover", from CF excitation of PNs. The EAAT4 transporter on PN dendrites are important for glutamate clearance and given that these transporters are downregulated as early as pP0 in *Sca1* mice (Serra et al., 2004), reduced glutamate uptake could potentially lead to increased spillover and co-excitation of MLINs.

Further research into the brainstem nuclei and CF/MF inputs, in the early phases of *Sca1*, could provide vital insight into the connectivity upstream of the cerebellar cortex. With this in mind, it is important to understand the cerebellar cortex circuit as a whole, not simply individual neuron groups, we therefore also investigated both PN and Golgi cells.

5.1.2. Altered Calcium Signals in Distinct Cerebellar Cortex Neuronal Populations

Golgi cells represent the primary inhibitory neurons within the granule cell (GC) layer – the input layer of the cerebellar cortex. Afferent MFs from oculomotor areas, the brainstem and spinal cord, among others, enter here, exciting the GCs, which then provide the glutamatergic drive to the cerebellar cortex, exciting both MLINs and PNs (Barmack and Yakhnitsa, 2011). Golgi cells are crucial components to regulate the granular layer dynamics. As summarized by D'Angelo, Golgi cell regulation of the granule layer can be categorised into key distinct forms; feed-forward inhibition creating a "time-windowing effect", lateral inhibition underlying "centre-surround organisation", "inhibition controlled plasticity" of local GCs, and finally feedback

inhibition from PF-Golgi cell activation that facilitates the “synchronous oscillations over large granular layer fields” (D’Angelo, 2008). Electrically coupled gap junctions can supports the loosely synchronous oscillations between Golgi cells but also allows rapid desynchronization and resultant independent activity following local MF stimulation (D’Angelo et al., 2013). Additionally, recent *in vivo* calcium imaging has indeed revealed multidimensional activity, underlying the encoding of sensorimotor behaviour (Gurnani and Silver, 2021). These findings makes it clear that Golgi cells are integral to the complex multifaceted processing of information conducted by the cerebellar cortex (Prestori et al., 2019a).

Here we found Golgi cells to be hyporesponsive to sensorimotor actions, early in symptomatic development. How might reduced Golgi activity alter circuit function and behaviour? Ablation of Golgi cells can induce ataxia (Watanabe et al., 1998), and in stargazer mutant mice, which present ataxic stance and oculomotor deficits, Golgi cells have reduced GABAergic immunoreactivity and decreased inhibitory synapses onto GCs (Richardson and Leitch, 2002). Interestingly, in a Sca8 mouse model, emerging from CTG CAG expansions, there is a reported upregulation of the gene for *GABA-A transporter 4* (Gabt4), at both the RNA and protein level, which is central to facilitating GABA clearance in the granular cell layer. The authors then show that upregulated Gabt4 can underlie a reduced inhibition of MF - GC synapse following whisker sensory stimulation (Daugthers et al., 2009). These studies reveal a comparable reduction in Golgi cell inhibition and symptoms similar to those seen in *Sca1* mice. It could therefore be of interest to explore underlying mechanisms of this *Sca1* Golgi hypo-responsiveness in further detail to understand the functional impact of our findings. It is reasonable that reduced regulation of MF input can contribute to a disrupted cerebellar cortex network, contributing to MLINs hyperresponsiveness.

Studies have indicated a direct inhibitory connection from MLINs to Golgi cells (Dumoulin et al., 2001; Eccles et al., 1967), although there is also counter evidence indicating Golgi cell inhibition is independent of MLINs (Hull and Regehr, 2012). If MLINs do play a role in modulating Golgi cell activity, the excessive MLIN inhibitory drive we uncover here, could reduce Golgi cell firing, in turn enhancing GC activity, which would then excite MLINs further, and once more inhibit Golgi cells. Which could lead to a cyclic incrementing of glutamatergic drive and MLIN stimulation, due to the loss of gain control, as well as disrupting other forms granular layer network dynamics. Further work would be required to explore the plausibility of this hypothesis. Firstly, to understand the discrepancies in the literature regarding the relationship between MLINs and Golgi cells in the healthy cerebellar circuit. Then secondly, to unravel how the connectivity between these cells might be altered and contribute to *Sca1* circuit dysfunction.

PNs are by far the most extensively studied neuronal population in *Sca1*. The timeline of PN pathology is well outlined, beginning with altered gene/protein expression as early as p10 (Serra et al., 2006), then over 2-5 weeks follows decreases in pacemaker firing properties (Barnes et al., 2011; Dell'Orco et al., 2015; Hourez et al., 2011) and altered connectivity with CFs and basket cells (Edamakanti et al., 2018). Later at around 15 weeks, there is a shrinkage of the dendritic tree (Dell'Orco et al., 2015), followed by severe PN atrophy and loss in both patients and animal models (Burright et al., 1995; Seidel et al., 2012; Watase et al., 2002). Cell autonomous (Pérez Ortiz and Orr, 2018; Serra et al., 2006) and non-cell autonomous mechanisms (Edamakanti et al., 2018) have been explored to unravel the pathogenesis of PNs in *Sca1*. As the sole output of the cerebellar cortex, modulating the signals from the deep cerebellar nuclei (DCN) to the rest of the brain, PN firing properties are essential to the coordination of movements and other cerebellar functions. Here we identify disrupted calcium signals in the early symptomatic phase of the disorder, particularly in PN dendrites, which showed both more frequent and greater strength of calcium signals.

Aberrant calcium handling in PNs is frequently reported in *Sca1* mouse models and across other SCAs (Prestori et al., 2019b). Here we saw fewer clear alterations to calcium signals at the level of PN somata, than in Golgi cells or MLINs, in early symptomatic *Sca1* cohort. However, it is highly likely that this is due to methodological limitations, given that the fast firing properties of PNs results in AP trains of 20-70Hz (Arancillo et al., 2015). The kinetics of GCaMP7s (time to rise for a single AP 50% ΔF/F is ~70ms, half decay time ~1,690 ms), do not allow us to record individual action potentials in PNs. Despite this limitation, ΔF/F scales with neuronal AP firing (~320% ΔF/F at 10 Hz to 620 ΔF/F at 160 Hz (Dana et al., 2019)). Therefore, we detect larger changes in firing frequency such as simple spike pauses (Ramirez and Stell, 2016), but more subtle changes could be lost. Indeed, the previous studies showing drops in PN firing in young *Sca1* mice, only show decreases to 15-20 Hz, from ~50 Hz (Dell'Orco et al., 2015; Hourez et al., 2011), which we may not be able to resolve using GCaMP7s.

Despite these limitations, there are varying reports of using genetically encoded calcium indicators to image Purkinje activity. Imaging of somatic calcium signals in PNs, utilising GCaMP6f in anesthetised mice, in combination with extracellular electrode recordings, showed a close correlation with continuous simple spike trains and rise in calcium transients, but not with complex spikes (Ramirez and Stell, 2016). Upon simple spike pauses, the calcium signal would decrease (Ramirez and Stell, 2016), which indicates that calcium imaging can reflect longer trains and pauses in PN pacemaker activity. We did pick up several clear alterations in somatic PN calcium signals. There was an enhanced response upon air puff application, a disproportional calcium signal associated with the air puff stimulation may reflect

dysfunctional processing of sensory information by PNs. Such alterations in sensory encoding in the cerebellar cortex are reported in several types of SCAs (Chandran et al., 2014). In addition, there was a significant shift to an increased overall PN activity, while mice were running in darkness to when running with visual feedback. The raised activity in darkness, was something we observed for each distinct cell type in the younger cohort. The cerebellum does indeed have a role in processing visual information, with visual evoked potentials recorded in lobule VI of the vermis in animals (Snider, and Stowell, 1944, Stein and Glickstein, 1992), alongside clinical reports and imaging studies indicating cerebellar neuronal circuits facilitate eye movement and visual attention (Striemer et al., 2015; Thier and Markanday, 2019). Intriguingly, electrophysiological recordings from the monkey lobule VI, revealed saccade-related PNs, that have elevated saccade-related peak burst activity in light when compared to saccade-related burst activity of the same amplitude in darkness (Helmchen and Büttner, 1995). Thus showing, in the healthy cerebellum, there is differential PN activity associated with eye movement, depending on light or dark environments. Therefore, our findings that each *Sca1* neuronal population displays a shift towards more activity in darkness when compared to *WT*, potentially underlies a breakdown in circuit differentiation between light and dark environments, or perhaps an inability of *Sca1* mice to focus on the VR screen. Eye movements, including visually guided saccades, have been shown to be altered in *Sca1* patients, underlying hypermetria (Rivaud-Pechoux et al., 1998), our findings may reflect neuron dysfunction related to these symptoms.

Interestingly, in contradiction with our GCaMP7s recordings, the ratiometric imaging found an elevated activity in Purkinje neuron somata of early symptomatic *Sca1* mice. Such an increase may be reflective of the reported longer trains of complex spikes reported in early slice recordings of a *Sca1* mouse model (Hourez et al., 2011). Previous studies could not reliably detect complex spike generation (Ramirez and Stell, 2016), however, it is plausible that elongated complex spike trains sufficiently increase intracellular calcium levels to be picked up by using the FRET based indicator, emerging as a prolonged increase in ΔF/F activity and therefore, increased area under the curve.

A previous study performing calcium imaging in the PN somata in *Sca1*, similarly found little deficits in comparison to *WT* mice (Inoue et al., 2001). These data appear contradictory to alterations in several genes that encode proteins regulating calcium homeostasis in PNs, and may be due to similar limitations in GECIs we have discussed here. However, it was speculated by Serra and colleagues, that alterations in calcium signals may be occurring in localised compartments, for example within the PN dendrites (Serra et al., 2004). Simultaneous electrophysiological recordings from PN dendrites and somata have revealed distinct excitatory postsynaptic currents occurring in both locations (Ohtsuki, 2020). With more

proximal dendritic recordings displaying a more similar profile to somatic activity, although there is only mild passive back-propagation, occurring from axon initial segment to dendrites in PNs (Bower, 2015; Stuart and Häusser, 1994; Ohtsuki, 2020). It is suggested that calcium currents in dendrites of healthy rodents are largely drive by CF innervation (Bower, 2015). Interestingly, calcium imaging studies indeed support that notion, combined electrophysiological recordings and calcium imaging *in vivo* of PN dendrites loaded with the calcium indicator Oregon Green BAPTA-1/AM (Mukamel et al., 2009; Ozden et al., 2009; Schultz et al., 2009) or labelled with GCaMP6f (Wagner et al., 2021) consistently correlate complex spiking with calcium imaging transients from PN dendrites. Thus analysis of PN dendritic calcium signals may provide an alternate insight into PN dysfunction in *Sca1*.

As a site of PN interaction with PFs, MLINs and CFs, PN dendrites have also been a major focus of research. In *Sca1* patients and mouse models, there is a distinctive shrinkage of the dendritic branch preceding PN loss (Seidel et al., 2012; Watase et al., 1998). Studies have shown that genes whose products are involved in PN dendritic function, such as Homer-3, EAAT4 or IP3R1, are reduced in the *Sca1* B05 mouse model (Serra et al., 2004). More precisely, these genes all implicate a role in glutamatergic signalling and calcium homeostasis, further research has indeed shown PN dendrite glutamate receptor related synaptic dysfunction, aberrant calcium handling and dendritic hyperexcitability in *Sca1* mice (Bushart et al., 2018; Lin et al., 2000; Ruegsegger et al., 2016; Serra et al., 2004). In line with these findings, and the notion that PN dendritic calcium signals may be altered differentially to signals from PN somata, our data show a higher resting calcium concentration, increased spontaneous activity and higher amplitude of calcium transients in early symptomatic mice, under anesthesia. Patch-clamp recordings from dendrites in *ATXN1*[82Q] mice also showed hyperexcitability, through increased back-propagation and raised susceptibility to calcium spiking, attributed to lower expression of calcium gated potassium channels (Chopra et al., 2018). Another cell-autonomous mechanisms may be that raised cytoplasmic calcium levels in PN dendrites is a result of reduced expression of calcium buffers calbindin and parvalbumin (Chopra et al., 2018). Such alterations in calcium handling, may lead to calcium signals that mask CF elicited responses, which have previously been shown to drive calcium transients in the wild type PN dendrite (Wagner et al., 2021). Investigation into CFs actually show reduced excitation of PN in the same *Sca1* model used in our experiments and at a similar age to the early symptomatic cohort (Edamakanti et al., 2018). These alterations in CFs suggest non-cell-autonomous mechanisms may also contribute to hyperexcitability in PN dendrites. Crucially, our identification of highly increased inhibition onto PNs from MLINs may also facilitate altered dendritic excitability. MLIN activation can present a CF driven rise in dendritic calcium, this mechanism has been shown to simultaneously facilitate LTP at the PF-PN dendrite (Rowan et al., 2018). These findings reveal that MLIN inhibition can modulate various

forms of plasticity in the PN dendrite, which includes support of potentiation. Sustained inhibition onto PN dendrites may also drive internal PN adaptions, studies have shown that neurons receiving increased and prolonged inhibition or excitation, can undergo adaptive changes to compensate and restore intrinsic firing rates (Nelson et al., 2003). Indeed, in rodent slices, PN excitability is increased following induction of LTD at the PF-PN synapse, occurring through downregulation of the hyperpolarization-activated cyclic nucleotide-gated (HCN)-mediated h current (Yang and Santamaria, 2016). The authors propose that this raised excitability is linked to biochemical pathways intertwined with LTD at the PN dendrite (Yang and Santamaria, 2016). It is therefore likely that a sustained increased inhibition onto PNs, can lead to internal adaptions to increase PN excitability, which then becomes maladaptive. An example of such maladaptive changes in PN dendrites has been shown in a *Sca1* mouse model (Dell'Orco et al., 2015). After recording a reduced PN simple spike firing, the authors observed that activity was partially restored following the PN dendritic branch shrinkage that classically occurs in *Sca1* (Dell'Orco et al., 2015). They suggest that this shrinkage is therefore an adaption to restore pacemaker activity.

Abnormal calcium regulation is a common feature across SCAs and models of ataxia disorders (Prestori et al., 2019b). Two polyglutamine SCAs, types 2 (Sca2) and 7 (Sca7), show downregulation of genes encoding voltage-dependent calcium channels and calcium activated potassium channels in mice models (Niewiadomska-Cimicka et al., 2021). Furthermore, the expansion of the ataxin-2 protein in PNs in a Sca2 mouse model associated with IP3R1 and calcium imaging in PN cultures derived from the Sca2 mice showed enhanced calcium discharge from endoplasmic reticulum stores (Liu et al., 2009). The excessive calcium discharge occurred via mGluR-IP3R1 pathway, and suppression of IP3R1 related calcium restored PN firing properties, reduced PN atrophy and alleviated motor symptoms (Kasumu et al., 2012). A mouse model of SCA type 3 (Sca3) also shows hypersensitive IP3R1 calcium release, stabilising intracellular calcium levels similarly reduced brainstem neuron loss and improved motor deficits (Chen et al., 2008). In line with these findings, in a Sca7 model, restoration of calcium handling following the increase of Sirtuin-1 expression, a protein facilitating the transcriptional activation of downregulated genes, to boost calcium channel expression, prevented neurodegeneration (Stoyas et al., 2020). Additionally in *Sca1*, boosting the PN expression of calcium gated potassium channels BK channels in re-establishes PN simple spiking rhythm, rescues dendritic hyperexcitability, prevents dendritic branch shrinkage and restores motor symptoms (Bushart et al., 2018; Chopra et al., 2018; Dell'Orco et al., 2015).

These are examples from a number of papers that have presented calcium related therapeutic options for a number of SCA types (Prestori et al., 2019b). Our work also supports the notion that aberrant calcium regulation is involved in *Sca1* pathophysiology. To understand

how the observed alterations in calcium signals develop later in the disease course, we also examined *Sca1* mice at the late symptomatic stage.

5.1.3. Age Dependent Changes in Calcium Signals in *Sca1* mice

Sca1 is classified as neurodegenerative disorder, nevertheless, the mutation in the *ATXN1* gene is of course always present throughout pre- and post-natal development. Recent findings argue that neurodegenerative disorders based on genetic mutations, such as HD, may well be classified as neurodevelopmental disorders (Barnat et al., 2020). Research in animal models has clearly shown that the pathogenesis of *Sca1* can be detected in the early weeks after birth, both in the form of protein expression changes (Lin et al., 2000; Serra et al., 2006; Serra et al., 2004) and firing properties of PNs (Edamakanti et al., 2018; Hourez et al., 2011). However, there is also evidence that shows physiological and molecular alterations are occurring throughout the disease course (Dell'Ocro et al., 2015). With this in mind, we also studied late symptomatic *Sca1* mice, to observe if the deficits we identified in early symptomatic mice are maintained across a lifespan, thus giving a more detailed insight into how these alterations match with increasing symptom severity.

We found that hyperresponsive MLIN detected in the early symptomatic phase indeed remained until the late symptomatic phase (P200), along with spontaneous hyperactivity both in quiet wakefulness and under anesthesia, compared to age matched healthy littermates. These findings demonstrate that these deficits do not adjust throughout disease stage. Similarly, decreased quiet wakefulness activity and reduced locomotion responses of Golgi cells were also maintained until the late stage. Conversely, under anesthesia, spontaneous Golgi activity appeared to be increased compared to P200 wild type mice, a finding not previously apparent. Although these data may initially appear opposing, there are of course significant differences between spontaneous activity under anesthesia and during quiet wakefulness. Awake "spontaneous" firing may be driven by behaviour not recorded in our setup. Indeed these mice are awake on a treadmill, the behaviour that we can measure is limited to forwards and backwards movements, along with whisking and changes in pupil width and position. It could be that later stage *Sca1* mice exhibit different muscle contractions to balance when they are static or different sensory processing not picked up in our recordings. We thus cannot exclude that aberrant spontaneous activity in fact actually reflects changes in balance or behaviour not recorded.

Golgi cells also display pacemaker activity (D'Angelo et al., 2013). The shift from hypo-activity under anesthesia early in the disorder hyperactive at later disease stage, could be an adaptive process to return to usual pacemaker frequency, which overcorrects later in the disease. Further study is required to identify the nature of such a shift. Recordings from PN

dendrites showed the same higher fraction of active dendrites, accompanied with even a stronger rise in hyperactivity and again larger increase in amplitude of calcium transients. In regards to PN somata, a notable finding is that there was a dramatically increased baseline calcium level. Raised cytoplasmic calcium supports earlier work, indicating a disruption in the expression of calcium buffering proteins (Serra et al., 2004) and is likely a reflection of the augmented PN pathology throughout ageing leading to PN atrophy (Prestori et al., 2019b). Recording from PN somata now also showed significantly reduced activity under anesthesia and during quiet wakefulness. This supports the understanding in the field that throughout ageing PNs in *Sca1* become gradually dysfunctional and display disrupted calcium handling.

Overall, we present evidence that the GABAergic network in *Sca1* is disrupted across the cerebellar cortex circuit, affecting the neural network representations of behavioural state. Given that loss of sensorimotor control underlies classical behavioural deficits in *Sca1* mice and indeed patients, we hypothesised that the network dysfunction we identified may underlie such symptoms. Therefore, correcting such circuit alterations could alleviate impaired behaviour and present a novel therapeutic target. To investigate this, we utilized chemogenetic tools to selectively modulate the neuronal population that we found displaying clearest deficits in the early symptomatic stage of *Sca1* mice, the molecular layer interneurons.

5.2. MLINs as a Novel Therapeutic Target in *Sca1*

5.2.1. Selective Expression of DREADDs in MLINs

Chemogenetic manipulation of neuronal activity using Designer Receptors Exclusively Activated by Designer Drugs (DREADDs) - based chemogenetic techniques are now well-established tools to unravel the direct functional roles of neural circuits. Use of adeno associated virus (AAV) delivery allows specific targeting of selected cell populations through combinations of serotype, promoter and also cre/loxP systems (Haery et al., 2019). Cre/loxP recombination is a common method in neuroscience that we took advantage of here, with PV-Cre knock-in mice, that express the protein Cre recombinase in parvalbumin positive interneurons (Hippenmeyer et al., 2005). Injection of AAVs that contain the gene of interest flanked by LoxP-variant recombination sites (referred to as “floxed”), requires interaction with Cre recombinase to allow expression of the gene in cells the virus enters. Therefore, in PV-Cre mice, despite the virus entering many cells around the injection site, the gene of interest is only expressed in parvalbumin positive interneurons (PV INs). These PV-Cre mice can be used in combination with DREADDs, with injection of AAVs containing floxed G - protein coupled receptors (GPCR), namely hM3Dq or hM4Di, allowing specific expression of these GPCRs in the PV INs. Thus, specific manipulation of PV INs with administration of so-called designer drugs, specifically targeting these receptors. The GPCRs are activated by the

designer drug clozapine-N-oxide (CNO), a metabolite of clozapine (Baldessarini et al., 1993; Bærentzen et al., 2019), which is inert when used within standard does of typically 0.1-3 mg/kg in mice (Roth, 2016). The G-protein coupled receptor hM3Dq increases excitability of the neuron following ligand binding, through mobilisation of intracellular calcium (Armbruster et al., 2007). The G-protein coupled hM4Di receptor on the other hand decreases neuronal activity via two pathways (Roth, 2016). Firstly, it induces modest hyperpolarisation, dependent upon Gi β/γ subunit mediated activation of Gi-coupled inwardly rectifying potassium channels (GIRKs). The second mechanism is inhibition of presynaptic release (Roth, 2016; Stachniak et al., 2014).

This system has been previously utilised for the selective targeting MLINs in the cerebellar cortex (Ma et al., 2020). Previous studies have shown that viral delivery of DREADDs into PV-Cre mice, specifically with AAV serotype 2/8, into the adult mouse cerebellum results in the receptor expression specifically in MLINs, as opposed to other PV IN in the cerebellum cortex (Astorga et al., 2015; Ma et al., 2020). We indeed confirmed this finding in our own mice, with quantification of viral expression in the injection lobule revealing selective MLIN labelling. In order to explore the impact of aberrant MLIN activity on behaviour and the cerebellar cortex network in *Sca1* mice, we utilized this technique both in acute and chronic settings.

5.2.2. Acute and Chronic Inhibition of MLINs Influences Cerebellar Network Activity and Alleviates Motor Deficits

We identified that reducing the activity of MLINs acutely (1) alleviates motor symptoms, (2) reduces PN dendritic hyperactivity and (3) corrects network encoding sensorimotor behaviour. Chronic MLIN inhibition over 30 days induces similar benefits to behavioural symptoms over a prolonged period, sustained long after the treatment end, and delays late stage disease severity.

Our quantification of DREADD expression around the injection site revealed that approximately 70% of MLINs expressed the receptor. When we compared MLIN activity in our baseline recordings to the same group of neurons under CNO, there was a reduction in activity of approximately 47% of MLINs following CNO administration. Inhibition of around half the target neurons is likely in part due to reciprocal MLIN-MLIN inhibition (Prestori et al., 2019a). It is well documented that MLIN are connected to surrounding MLINs via several chemical, electrical and synaptic connections, therefore silencing of some, likely causes disinhibition and resultant increased activity in others (Kim and Augustine, 2021). Furthermore, it is important to consider that Gi-coupled DREADDs, as detailed above, do not drive an absolute

hyperpolarisation, they are primarily blocking presynaptic release from MLINs (Roth, 2016; Stachniak et al., 2014). Thereby, it would still be possible to observe somatic calcium transients in these MLINs, but there may still not be downstream inhibition of their target neurons. Additionally, as these recordings are made over several hours, it is possible that there is some decrease in CNO-receptor interaction over this time. Early reports of CNO-DREADD interaction in mice, using similar dose concentration, showed that neurons peak modulation is at 1-2 hours, gradually reducing over the following 5 hours (Alexander et al., 2009). However, a recent reports show that CNO levels in the mouse brain tissue following a comparable i.p. injection are significantly reduced over one hour (Jendryka et al., 2019). Longer lasting inhibition possibly comes from clozapine, which CNO is converted to, via back-transformation (Manvich et al., 2018). The concentration of clozapine does not decrease in brain tissue over the first hour after CNO administration and has a high affinity for the receptors HM4Di/HM3Dq (Jendryka et al., 2019). Alternative designer drugs are available, however, off target binding is a common limitation. Compound-21 effectively penetrates the brain and has high affinity to hM4Di, but also binds to endogenous dopaminergic, serotonergic and muscarinic GPCRs, amongst others (Jendryka et al., 2019). The off target effects of CNO/clozapine and compound-21 do not limit their utility per se, as the behavioural impact, when used in appropriate doses, is limited (Jendryka et al., 2019). Nevertheless, it is essential to provide appropriate controls, such as administering CNO to mice lacking DREADDs as we have utilized here.

This reduction in activity across subsets of MLINs, did reduce activity across the MLIN population, both in anesthetised recordings and periods of quiet wakefulness, towards activity levels observed in wild type mice. As detailed above, hM4Di stimulation induces partial suppression of neuronal activity, rather than absolute silencing; this may support the intervention in being corrective rather than dysfunctional. Similarly, we do not observe behavioural deficits in wild type mice under the same treatment, the healthy cerebellar cortex network is likely able to compensate for decreased firing of MLIN. Strikingly, the reduced MLIN activity in *Sca1* mice led to an improvement motor and balance related symptoms, identified via an improved performance in the rotarod task. Additionally, CNO administration alleviated the *Sca1*-related molecular pathology in the MLIN population, reducing the percentage of high parvalbumin expressing MLINs. These data indicate that modifying neuronal activity can drive beneficial symptomatic improvements and intracellular molecular alterations.

Chemogenetic inhibition of MLINs also altered calcium signals of the downstream PNs. During quiet wakefulness, we observed a reduction in spontaneous activity in both the soma and dendrites of PN, however only activity in the somata was significantly altered. This may be due to limitations in imaging calcium signals from PN dendrites in awake mice. The general

expression of GCaMP7 across the cerebellar cortex results in diverse fluorescence signal from many cell types. During wakefulness the broad increase in fluorescence signal, due to sensory and motor input, and in particular from inhibitory neurons such as MLINs (Haider et al., 2013), made it challenging to isolate signal from PN dendrites also lying in the molecular layer. In the anesthetised recordings, the PN dendrites became clearly visible with a higher baseline calcium signal. Hence why we primarily used this condition for our initial analysis of PN dendrites. To further investigate calcium signals in PN dendrites of awake mice, selective expression of the GECI under a PN promoter would likely prove advantageous. In anesthetised mice, there was indeed a strong significant reduction in dendritic calcium activity whilst the soma remained largely unchanged. The reduction of aberrant calcium signals in PN dendrites through chemogenetic modulation of MLINs, could contribute to the clear behavioural improvements in *Sca1* mice. This is a crucial finding as it shows non-cell autonomous alleviation of a *Sca1* PN feature, supporting our earlier hypothesis (see **5.1.3.**) that altered inputs onto PNs can drive maladaptive intrinsic changes to dendrite excitability.

Naturally, alterations to the MLIN population drives changes in PN action potential firing, for example, in healthy mice PN pacemaker activity has been shown to be increased following the selective depletion of MLIN input (Brown et al., 2019). Future work could utilize electrophysiological recordings from PNs to reveal the precise nature of how the *Sca1* mediated increase in MLIN inhibition alters PN simple and complex spiking. A study investigating a model of chronic ethanol exposure found that, amplified spontaneous MLIN activity disrupted the PN pacemaker simple spike rhythm (Dong et al., 2022). The authors then revealed that reducing the MLIN input restored PN simple spike activity in the disease model, and the same MLIN inhibition did not disrupt the healthy control PN pacemaker activity (Dong, et al., 2022). Although these findings are in relation to a different disease model, and in *ex vivo* sections rather than *in vivo*, they present intriguing similarities. The data supports the principle that impact of aberrant MLIN firing disrupts PN activity, that reducing MLIN input can restore PN function, and that inhibition of MLINs in a healthy circuit is not sufficient to disrupt PN firing properties.

Intriguingly, overall encoding of behavioural state across the circuit was improved following acute MLIN inhibition. This insight gives an overall reflection of the ability of this network to encode sensorimotor behaviour; improvement here may underlie the stark behavioural improvement in the rotarod task. This supports the notion that the intervention provides a restoration to the balance of circuit excitation/inhibition.

With such clear alterations to *Sca1* features in the acute setting, we addressed whether chronic inhibition of MLINs would drive lasting changes to *Sca1* mice. A 30-day CNO treatment in early symptomatic *Sca1* mice, produced a prolonged improvement of motor symptoms and

molecular pathology. The latter was quantifiable 90 days after treatment ended via reduction in high parvalbumin expressing interneurons. Notably, the chronic treatment also resulted in a reduction in severe weight loss in the latest stage of disease progression. Furthermore, the reduction of MLIN activity also induced a sustained chronic restoration of molecular pathology in *Sca1* PNs. *Sca1::PV-DREADD(Gi)* mice displayed increased somatic p-CAMKII and synaptic Homer-3 expression, towards *WT* level, against *Sca1::PV-mCherry* mice also treated with CNO. Given that these proteins are highly linked to calcium homeostasis, this is important further evidence to support the notion that our observations of improved calcium signals in PN dendrites are underlined by intracellular adaptions in PNs that improve calcium handling, which is supported by the reduced inhibition from MLIN. Homer-3 is involved in PN dendritic spines mGluR1 signalling and plasticity (Ruegsegger et al., 2016), showing that the *Sca1* glutamatergic system associated deficits, also benefit from the decrease in GABAergic activity.

That inhibition of MLINs can restore their firing properties in distinct populations but also induce lasting molecular and behavioural symptom improvement is an important finding. Previous research had focussed on glutamatergic disruption in *Sca1*, showing a progressive dysfunction to mGluR1 signalling at the PN dendrite, which encompassed reduced synaptic response and impaired mGluR-plasticity (Shuvaev et al., 2017). By showing the GABAergic network is also disrupted presents an improved overall understanding of *Sca1* pathophysiology and opens up novel therapeutic avenues. To further understand the extent of how hyperactive MLIN may cause circuit alterations and symptoms, we aimed to recreate our observations from *Sca1* mice, in healthy *WT* mice.

5.2.3. Acute and Chronic Excitation of MLINs in Healthy Mice Drives *Sca1*-like Motor Symptoms and Molecular Pathology

We have shown that modulating hyperactive MLIN can have a beneficial effect on the cerebellar cortex circuit in *Sca1*. However, this poses the question whether hyperactive MLIN alone would be sufficient to trigger *Sca1*-like disease in healthy mice?

To this end, we selectively targeted MLINs with the HM4Dq excitatory DREADD (Alexander et al., 2009), allowing both acute and chronic stimulation of MLINs. Acute administration of CNO to raise excitability of MLINs and thus, mimic the conditions of our initial findings, indeed triggered motor coordination deficits. Not only this, but the treatment induced a higher percentage of high parvalbumin expressing MLINs, similar to our observations in *Sca1* mice. This experiment indicated that excessive MLIN activity alone, could indeed induce *Sca1* like behavioural symptoms in the form of reduced motor control, alongside intracellular MLIN molecular alterations that we also detected in our *Sca1* mice.

Furthermore, chronic MLIN stimulation in *WT* mice induced prolonged motor deficits. Earliest reports of motor deficits in *Sca1* mice are around 5 weeks old (P35). We aimed to induce the chronic MLIN stimulation as near as possible to this age, in order to closely match the disease timeline in *Sca1* mice. Allowing time for viral expression we therefore began the 30 day treatment at P40, ending at P70, around the same age as our early symptomatic cohorts used during imaging experiments. We found reduced performance in the rotarod task in the *WT::PV-DREADD(Gq)* mice in comparison to *WT::PV-mCherry* controls over the course of the CNO treatment. The performance of the *WT::PV-DREADD(Gq)* mice very gradually decreased, however the control group increased performance significantly following the first time point. This may suggest a prevention of motor learning, alongside balance deficits in the treated mice. Furthermore, the *WT::PV-DREADD(Gq)* mice showed no recovery in this task over the next three weeks following treatment ending. Mice were then observed until P200, and did not display any further *Sca1*-like features. However, upon analysis of the brain tissue we indeed found a reduced number Homer-3 puncta in the PN dendrites of the injected lobule VIII, a striking 130 days following the treatment end.

That a 30-day excitation of MLIN can induce chronic *Sca1* PN dendrite molecular pathology in healthy mice, is a critical insight, as it is direct evidence that *Sca1* PN alterations can be driven by non-cell autonomous mechanisms. Whilst there are certainly cell autonomous elements to *Sca1* PN pathology (Chopra et al 2020; Serra et al 2006), we reveal for the first time that PNs are indeed susceptible to upstream MLIN pathophysiological activity in *Sca1*. This non-cell autonomous drive of PN dysfunction not only implicates involvement of MLINs, as we have shown here, but could also apply to other cell types within the circuit and the input fiber tracts. For example CF inputs have been shown to be dysfunctional in presymptomatic *Sca1* mice (Edamakanti et al., 2018). Additionally this supports evidence that suggests PNs are a highly vulnerable cell population, which has been proposed as a reason as to why these show such dramatic atrophy in SCAs and several other disorders (Huang and Verbeek, 2019; Welsh et al., 2002).

Our findings also present a curious similarity in pathophysiology to episodic ataxia type 1 (EA1). EA1 is similar to *Sca1* in that it is also autosomal dominant and patients have some overlapping ataxia symptoms (Graves et al., 2014). However, EA1 patients only display short intense episodes of symptoms, which include spastic contractions along with the classical motor and balance dysfunction (Graves et al., 2014). Furthermore, EA1 is a potassium channelopathy, with point mutations on the voltage-dependent potassium channel gene *KCNA1* (Kv1.1) (Hasan et al., 2017). Kv1.1 channels in terminals of MLINs regulate GABA release, and the mutations have been shown to enhance amplitude and frequency of inhibitory post-synaptic currents recorded at the MLIN-PN synapse (D'Adamo et al., 2015). Such

increased inhibitory tone from MLINs, is akin to our findings here. Notably, EA1 does not lead to degeneration of PNs or other atrophy (D'Adamo et al., 2015), which may be due to the intermittent nature of the disease, similarly, in our experiments stimulating MLINs, we observed motor deficits, without PN degeneration. It may be that our chronic stimulation protocol lacks the longevity to induce severe PN deficits and atrophy.

Overall, our findings here provide functional evidence that strongly supports our initial descriptive data. Highlighting the relevance of the aberrant MLIN activity, and intriguingly opens up the potential for targeting MLINs in the in the SCA patients as a therapeutic strategy.

5.2.4. Modulation of Neuronal Circuit Dysfunction as a Therapeutic Strategy

How might modulation of neuronal populations be performed in a clinical setting? AAV mediated gene transfer has fascinating potential for the treatment of a variety of complex diseases (Hudry and Vandenberghe, 2019). Clinical trials have been performed with positive safety results in a number of neurological disorders including Alzheimer's disease (AD), Parkin's disease (PD) and spinal muscular atrophy (Hudry and Vandenberghe, 2019). An example of this was a trial with PD patients displaying moderately advanced symptoms, who were treated with bilateral infusions of the gene aromatic l-amino acid decarboxylase (AADC) via AAV2 (AAV2-CMV-hAADC) (Christine et al., 2009). The AADC enzyme that allows the conversation of levodopa into dopamine, is progressively lost with PD degeneration of nigrostriatal neurons, and the treatment resulted in an improvement of dyskinesia symptoms over 12 months (Christine et al., 2009). There have also been phase I, and are ongoing sham-controlled phase II, clinical trials using AAV mediated expression of nerve growth factor (NGF) to treat AD patients (Rafii et al., 2018; Rafii et al., 2014). The proposed mechanism was to reduce alterations in basal cholinergic neurons, which are susceptible to dysfunction in AD (Hudry and Vandenberghe, 2019). There were no clear efficacious results from the treatment as of yet, however this is partially due to low sample sizes. Importantly they were able to confirm chronic, localised expression of NGF and that the treatment was well tolerated and logistically possible in elderly patients (Rafii et al., 2018; Rafii et al., 2014). Despite these trials, and several others, showing promising results in terms of feasibility and safety, there is still evidence in animal studies that raises questions around adverse effects. A study using non-human primates and piglets showed an intravenous infusion of an AAV variant to induce toxicity, including degeneration of the dorsal root ganglia and ataxia (Hinderer et al., 2018; Hudry and Vandenberghe, 2019). Such finding implies caution show be taken especially considering the lack of chronic data and the lack of clear efficacy in neurodegenerative patients thus far (Hudry and Vandenberghe, 2019).

If a safe delivery was established, chemogenetic modulation of neurons could be applied to humans via AAV mediated delivery. Whilst this has to date not been trialled, inhibitory DREADDs are a major focus in treatment of epilepsy (Drew, 2018; Lieb et al., 2019). Localised suppression of hyperexcitable neurons generating seizures is highly desirable. Given that CNO is a metabolite of clozapine, an already clinically approved drug, it is favourable against lesser used compounds, and receptors such as hM4DGi are mutated from a human receptor which reduces immunogenicity (Lieb et al., 2019). Indeed, chemogenetic modulation has been shown to effectively suppress widespread seizures in non-human primates (Miyakawa et al., 2023).

Other methods of neuronal modulation have also shown potential in human patients. Repeated transmagnetic stimulation (rTMS) is a non-invasive approach that has been shown to have some benefit in SCA patients (Wang et al., 2023). An example of this was shown in Sca3 patients. Although small scale, this double blind and sham controlled trial improved Standard Ataxia Rating Assessment (SARA), up to one month following treatment end (Manor et al., 2019). The treatment encompassed 20 sessions over a month, with each session made up of 10 pulses per cerebellar region, reaching 30 pulses per session. Interestingly the benefits were largely due to differences in the “stance” sub category of SARA assessment, which was supported with improved measures of postural sway (Manor et al., 2019). The exact mechanisms of rTMS remain elusive, hence, one cannot actually draw specific conclusions to how this alters physiology. However, the authors speculate that targeting the cerebellum in this way drives PN output to the DCN (Manor et al., 2019). Similarities to our techniques cannot be certain given how little is understood about the physiology of rTMS, although it is of note that it has been suggested that rTMS stimulates excitatory tone and reduces inhibition (Lenz and Vlachos, 2016). A number of similar small-scale TMS studies across a variety of SCAs have been completed. A recent systematic review of eight studies comprising 272 SCA patients recently concluded that there are significant improvements seen in patient symptoms, via alteration excitability of the cerebellar-thalamus-cortical pathways (Wang et al., 2023). The authors suggest that a large-scale trial is now required to build upon this valuable research. Developments in technology that allow more specific and localised modulation will likely also provide novel therapeutic options here. What is clear is that understanding dysfunction of neural circuits across neurodegenerative diseases is becoming a crucial area to develop novel therapeutics.

5.2.5. Circuit Mechanisms of Neurodegenerative Diseases

In the mammalian brain, coordination of neural networks, both within regional circuits and on the macro scale, is essential to facilitate behaviour. In neurodegenerative disorders,

neuronal function is altered, leading to synaptic dysfunction and disturbed action potential firing, which has downstream consequences for connecting neurons, and creates large-scale disruption of circuits. Detection of aberrant neuronal activity in the form of alterations to individual neuronal firing, neuronal populations within and across brain regions, has been identified in animal models for a number of neurodegenerative disorders (Saxena and Liebscher, 2020). Emphasising the relevance of these findings to disease progression, such dysfunction is often reported independent of atrophy and occurring prior to symptom onset. This has been identified in models of AD (Frere and Slutsky, 2018; Mufson et al., 2015; Palop and Mucke, 2016), PD (McGregor and Nelson, 2019; Meles et al., 2021) and HD (Braz et al., 2022; Capizzi et al., 2022; Schippling et al., 2009). These findings of altered circuit activity in animal models are supported by work with patient populations in the clinic, which are gradually mapping aberrant neuronal activity patterns within and between brain regions (de Tommaso et al., 2003; Houmani et al., 2018; Seeley et al., 2009; Teipel et al., 2016). There is a notion that correcting neuronal firing early in the disease course, may delay further pathophysiology, symptom onset and have a higher success rate than trying to recover the brain from a later stage in the disease. Likewise, despite the onset of symptoms occurring late in life, it is likely that for genetic disorders such as HD and the autosomal dominant SCAs, the pathogenesis could begin during development (Barnat et al 2020; Braz et al., 2022). Therefore, it is plausible that earlier treatment options may be more fruitful.

Our data here shows neuronal dysfunction, manifesting as altered firing properties across distinct cell populations, along with disrupted encoding of behaviours across the network, in early stages of *Sca1*. Crucially, we show a direct causal link to motor incoordination, a central feature of SCAs, with a correction of aberrant neuronal activity, leading to simultaneous improvement of network behavioural encoding and motor coordination. Furthermore, motor coordination impairment can be induced in the healthy mouse, by mimicking hyperactive MLINs we initially identified in *Sca1* mice.

This is highly relevant to similar findings in other neurodegenerative diseases outlined above, neuronal dysfunction leads to altered firing of action potentials, which has downstream consequences for network function, which in turn can drive symptoms, as opposed to simply being a passive consequence of other pathology. Similarly, recent work from Braz and colleagues showed in a HD mouse model, excitatory transmission was reduced already just one week after birth in somatosensory neurons, in time with delayed dendritic development (Braz et al., 2022). Importantly, over the following weeks there appeared to be compensatory adaptions in HD mice that resulted in normalised amplitude and frequency of neuronal firing and dendritic development. Indistinguishable from their wild type littermates by P21-26. The authors suggest that these early developmental alterations during the establishment of

neuronal structure and function, although they appear to have normalised, set the disease course, therefore are in fact maladaptive. Indeed, when HD pups were treated with an ampakine, enhancing AMPA receptor signalling, the model mice did not develop the otherwise HD typical sensory, motor or cognitive symptoms and prevented altered brain morphology (Braz et al., 2022). In agreement with our own findings, that early manipulation of neuronal activity can have long-term effects on the disease course.

To effectively modulate neuronal activity for therapeutic benefit, it is important to understand the regions and neuron types that are affected in these disorders. Deficits in inhibitory interneuron (IN) function can drive network disruption, creating an imbalance of excitation and inhibition and represents an interesting overlap between several neurological disorders, in particular neurodegenerative diseases (Ferguson and Gao, 2018; Ruden et al 2021). A common feature in neurological disorders is reduced activity of parvalbumin expressing interneurons (PV INs) (Liu et al., 2021; Ruden et al., 2021). Amyotrophic lateral sclerosis (ALS) and Fragile X syndrome both display hypo-excitable cortical PV INs, suggested to add to hyperexcitable circuits (Khademullah et al., 2020; Liu et al., 2021). In AD, numerous studies have shown a decrease in PV IN numbers in the hippocampus, entorhinal cortex and cortical regions, both in patients and mice models, which is suggested to drive cognitive symptoms and epileptoform activity (Verret et al., 2012; Xu et al., 2020). However, a recent study from Hijaz and colleagues focussed on early stage of AD in mice at 16 weeks old found hyperactive PV INs in the CA1 region of the hippocampus (Hijazi et al., 2020). Preventing these neurons becoming hyperexcitable, via chemogenetic inhibition of PN INs, maintained hippocampal circuit balance, reduced protein aggregation, and improved memory (Hijazi et al., 2020). Indeed, at already 1-3 weeks old in the *Sca1*$^{154Q/2Q}$ model, there is an increased number of inhibitory connections from MLINs (which are also PV INs) onto PNs (Edamakanti et al., 2018). In line with these findings, we also outline early circuit PV IN pathophysiology in *Sca1*. We identified hyperexcitable MLINs, and further unravelled how modulating aberrant MLIN activity, can have a positive impact on network balance and behavioural symptoms.

Alongside chemogenetic modulation of hippocampal PV INs as described by Hijazi and colleagues, optogenetic modulation of hippocampal neurons has also been explored to alleviate early breakdown of long-term memory (Roy et al., 2016). A symptom that is reminiscent of early the mild cognitive dysfunction that emerges first AD in patients. In a transgenic mouse model of early AD, optogenetic stimulation of performant path synapses onto engram cells in the dentate gyrus, targeted to facilitate LTP, supported the restoration of long-term memory deficits (Roy et al., 2016). Furthermore, the stimulation protocol also induced an increase in spine density on engram cells, which had been shown to decrease in correlation with development of long-term memory symptoms (Roy et al., 2016). Thus

providing further evidence to support the notion that early modulation of neuronal activity is valuable in neurodegenerative disorders. Modulation of neuronal activity in the later stages of such diseases is also important to explore, as early interventions as performed in some of the studies above is unrealistic in many patients.

Several studies have investigated such treatments alleviate symptoms in later disease stages, in AD mouse models the classical pathological feature of amyloid-beta (Aβ) accumulation can be reduced by chemogenetic inhibition of hippocampal neurons (Yuan and Grutzendler, 2016). In 16 months old AD mice, a 6-week chemogenetic attenuation of entorhinal cortex activity reduced not only amyloid-beta (Aβ) aggregation but also the spread of pathological tau across the hippocampus (Rodriguez et al., 2020). Similarly, in PD mouse models chemogenetic excitation of direct striatal projecting neurons can improve forelimb impairment (Alcacer et al., 2017), whilst similar stimulation of external globus pallidus also improves motor function (Assaf and Schiller, 2019). Furthermore, stimulation of cortical inputs to the subthalamic nucleus via optogenetic tools also alleviates bradykinesia (Sanders and Jaeger, 2016).

Optogenetic tools are not yet useable in patients, however, are valuable to research deep brain stimulation (DBS), a current form of neuromodulation that whilst invasive, proves highly successful in reducing motor symptoms of PD patients (Gittis and Yttri, 2018). DBS involves a generation of electrical pulses in a specific brain region, whilst the exact mechanisms are unclear, it is suggested that this can normalise neuronal firing patterns (Chiken and Nambu, 2016). This is comparable to a selective manipulation of neuronal populations via techniques applied to the mouse models. DBS can be highly effective in easing PD symptoms, and is suggested to alleviate abnormal burst firing and beta frequency activity in the substantia nigra (Ashkan et al., 2017). The success of DBS in some PD patients, emphasises how valuable a strong understanding of aberrant neuronal activity can be, when combined with techniques to specifically correct such alterations. As improvements to our technology broadens the available tools in neuromodulation, identifying and correcting circuit dysfunction in neurodegenerative disorders could prove to be an invaluable element of therapeutic options.

5.3. Concluding Remarks & Outlook

The findings shown over this thesis reveal direct functional evidence as to how hyperactivity of MLINs drive dysfunction across the cerebellar cortex circuit in *Sca1*, and that mimicking these circuit alterations can induce *Sca1*-like pathology and symptoms in *WT* mice. These findings underline the importance of understanding how the ubiquitously expressed mutant ataxin-1 protein may affect different cell populations, and how these alterations may

contribute to *Sca1* pathogenesis. We indeed showed some alterations to the intracellular calcium handling of MLINs, however, future work should focus on understanding cell-autonomous mechanisms that may drive this hyperexcitability. Whilst this is worthy of exploration, we also revealed the significance of non-cell autonomous mechanisms in driving changes in excitability. It is therefore interesting also to look at the inputs to the cerebellar cortex. Reduced CF connectivity to PNs has been reported in *Sca1* already by 5 weeks old (Edamakanti et al., 2018) and volumetric alterations in regions from which MFs occur early and are predicative of *Sca1* severity in patients (Deelchand, et al., 2019; Koscik et al., 2020). Further investigation into these excitatory sources during presymptomatic *Sca1*, would provide valuable insight into dysfunction outside of the cerebellar cortex circuit, which could exacerbate the alterations we observe in our own findings.

Together, our results have provided a novel insight into how cerebellar cortex circuit dysfunction manifests in *Sca1*. For the first time we directly show early aberrant MLIN activity, which can directly induce non-cell autonomous pathological changes in PNs, and that this pathway can be targeted for long - term therapeutic benefit. Knowing that PNs are vulnerable to upstream pathophysiology, it is therefore essential moving forward to further unravel in detail distinct circuit elements and how they interact with one another, within the cerebellar cortex and beyond, during the pathogenesis of *Sca1*.

6. REFERENCES

Alcacer, C., Andreoli, L., Sebastianutto, I., Jakobsson, J., Fieblinger, T. and Cenci, M. A. (2017) 'Chemogenetic stimulation of striatal projection neurons modulates responses to Parkinson's disease therapy', *J Clin Invest,* 127(2), pp. 720-734.

Alexander, G. M., Rogan, S. C., Abbas, A. I., Armbruster, B. N., Pei, Y., Allen, J. A., Nonneman, R. J., Hartmann, J., Moy, S. S., Nicolelis, M. A., McNamara, J. O. and Roth, B. L. (2009) 'Remote control of neuronal activity in transgenic mice expressing evolved G protein-coupled receptors', *Neuron,* 63(1), pp. 27-39.

Apps, R. and Garwicz, M. (2005) 'Anatomical and physiological foundations of cerebellar information processing', *Nat Rev Neurosci,* 6(4), pp. 297-311.

Apps, R. and Lidierth, M. (1989) 'Simple spike discharge patterns of Purkinje cells in the paramedian lobule of the cerebellum during locomotion in the awake cat', *Neurosci Lett,* 102(2-3), pp. 205-10.

Apsley, E. J. and Becker, E. B. E. (2022) 'Purkinje Cell Patterning-Insights from Single-Cell Sequencing', *Cells,* 11(18).

Arancillo, M., White, J. J., Lin, T., Stay, T. L. and Sillitoe, R. V. (2015) 'In vivo analysis of Purkinje cell firing properties during postnatal mouse development', *J Neurophysiol,* 113(2), pp. 578-91.

Armbruster, B. N., Li, X., Pausch, M. H., Herlitze, S. and Roth, B. L. (2007) 'Evolving the lock to fit the key to create a family of G protein-coupled receptors potently activated by an inert ligand', *Proc Natl Acad Sci U S A,* 104(12), pp. 5163-8.

Armstrong, D. M. and Edgley, S. A. (1984) 'Discharges of Purkinje cells in the paravermal part of the cerebellar anterior lobe during locomotion in the cat', *J Physiol,* 352, pp. 403-24.

Armstrong, D. M. and Edgley, S. A. (1988) 'Discharges of interpositus and Purkinje cells of the cat cerebellum during locomotion under different conditions', *J Physiol,* 400, pp. 425-45.

Arrasate, M., Mitra, S., Schweitzer, E. S., Segal, M. R. and Finkbeiner, S. (2004) 'Inclusion body formation reduces levels of mutant huntingtin and the risk of neuronal death', *Nature,* 431(7010), pp. 805-10.

Ashkan, K., Rogers, P., Bergman, H. and Ughratdar, I. (2017) 'Insights into the mechanisms of deep brain stimulation', *Nat Rev Neurol,* 13(9), pp. 548-554.

Assaf, F. and Schiller, Y. (2019) 'A chemogenetic approach for treating experimental Parkinson's disease', *Mov Disord,* 34(4), pp. 469-479.

Astorga, G., Li, D., Therreau, L., Kassa, M., Marty, A. and Llano, I. (2017) 'Concerted Interneuron Activity in the Cerebellar Molecular Layer During Rhythmic Oromotor Behaviors', *J Neurosci,* 37(47), pp. 11455-11468.

Attwell, D. and Mehta, A. R. (2021) 'Anatomy embroiders function in Purkinje cells', *Lancet Neurol,* 20(10), pp. 793.

Azevedo, F. A., Carvalho, L. R., Grinberg, L. T., Farfel, J. M., Ferretti, R. E., Leite, R. E., Jacob Filho, W., Lent, R. and Herculano-Houzel, S. (2009) 'Equal numbers of neuronal and nonneuronal cells make the human brain an isometrically scaled-up primate brain', *J Comp Neurol,* 513(5), pp. 532-41.

Badura, A., Verpeut, J. L., Metzger, J. W., Pereira, T. D., Pisano, T. J., Deverett, B., Bakshinskaya, D. E. and Wang, S. S. (2018) 'Normal cognitive and social development require posterior cerebellar activity', *Elife,* 7.

Baldessarini, R. J., Centorrino, F., Flood, J. G., Volpicelli, S. A., Huston-Lyons, D. and Cohen, B. M. (1993) 'Tissue concentrations of clozapine and its metabolites in the rat', *Neuropsychopharmacology,* 9(2), pp. 117-24.

Banfi, S., Servadio, A., Chung, M. Y., Kwiatkowski, T. J., McCall, A. E., Duvick, L. A., Shen, Y., Roth, E. J., Orr, H. T. and Zoghbi, H. Y. (1994) 'Identification and characterization of the gene causing type 1 spinocerebellar ataxia', *Nat Genet,* 7(4), pp. 513-20.

Bao, J., Reim, K. and Sakaba, T. (2010) 'Target-dependent feedforward inhibition mediated by short-term synaptic plasticity in the cerebellum', *J Neurosci,* 30(24), pp. 8171-9.

Barboi, A. C. (2000) 'Cerebellar ataxia', *Arch Neurol,* 57(10), pp. 1525-7.

Barmack, N. H. and Yakhnitsa, V. (2011a) 'Microlesions of the inferior olive reduce vestibular modulation of Purkinje cell complex and simple spikes in mouse cerebellum', *J Neurosci,* 31(27), pp. 9824-35.

Barmack, N. H. and Yakhnitsa, V. (2011b) 'Topsy turvy: functions of climbing and mossy fibers in the vestibulo-cerebellum', *Neuroscientist,* 17(2), pp. 221-36.

Barnat, M., Capizzi, M., Aparicio, E., Boluda, S., Wennagel, D., Kacher, R., Kassem, R., Lenoir, S., Agasse, F., Braz, B. Y., Liu, J. P., Ighil, J., Tessier, A., Zeitlin, S. O., Duyckaerts, C., Dommergues, M., Durr, A. and Humbert, S. (2020) 'Huntington's disease alters human neurodevelopment', *Science,* 369(6505), pp. 787-793.

Batchelor, A. M. and Garthwaite, J. (1997) 'Frequency detection and temporally dispersed synaptic signal association through a metabotropic glutamate receptor pathway', *Nature,* 385(6611), pp. 74-7.

Baumann, O., Borra, R. J., Bower, J. M., Cullen, K. E., Habas, C., Ivry, R. B., Leggio, M., Mattingley, J. B., Molinari, M., Moulton, E. A., Paulin, M. G., Pavlova, M. A., Schmahmann, J. D. and Sokolov, A. A. (2015) 'Consensus paper: the role of the cerebellum in perceptual processes', *Cerebellum,* 14(2), pp. 197-220.

Beauchamp, A., Yee, Y., Darwin, B. C., Raznahan, A., Mars, R. B. and Lerch, J. P. (2022) 'Whole-brain comparison of rodent and human brains using spatial transcriptomics', *Elife,* 11.

Beckinghausen, J. and Sillitoe, R. V. (2019) 'Insights into cerebellar development and connectivity', *Neurosci Lett,* 688, pp. 2-13.

Binda, F., Pernaci, C. and Saxena, S. (2020) 'Cerebellar Development and Circuit Maturation: A Common Framework for Spinocerebellar Ataxias', *Front Neurosci,* 14, pp. 293.

Blot, A. and Barbour, B. (2014) 'Ultra-rapid axon-axon ephaptic inhibition of cerebellar Purkinje cells by the pinceau', *Nat Neurosci,* 17(2), pp. 289-95.

Blumenstock, S. and Dudanova, I. (2022) 'Balancing neuronal circuits', *Science,* 377(6613), pp. 1383-1384.

Bouvier, G., Senzai, Y. and Scanziani, M. (2020) 'Head Movements Control the Activity of Primary Visual Cortex in a Luminance-Dependent Manner', *Neuron,* 108(3), pp. 500-511.e5.

Bower, J. M. (2015) 'The 40-year history of modeling active dendrites in cerebellar Purkinje cells: emergence of the first single cell "community model"', *Front Comput Neurosci,* 9, pp. 129.

Brasnjo, G. and Otis, T. S. (2001) 'Neuronal glutamate transporters control activation of postsynaptic metabotropic glutamate receptors and influence cerebellar long-term depression', *Neuron,* 31(4), pp. 607-16.

Braz, B. Y., Wennagel, D., Ratié, L., de Souza, D. A. R., Deloulme, J. C., Barbier, E. L., Buisson, A., Lanté, F. and Humbert, S. (2022) 'Treating early postnatal circuit defect delays Huntington's disease onset and pathology in mice', *Science,* 377(6613), pp. eabq5011.

Brown, A. M., Arancillo, M., Lin, T., Catt, D. R., Zhou, J., Lackey, E. P., Stay, T. L., Zuo, Z., White, J. J. and Sillitoe, R. V. (2019) 'Molecular layer interneurons shape the spike activity of cerebellar Purkinje cells', *Sci Rep,* 9(1), pp. 1742.

Brown, S. A. and Loew, L. M. (2014) 'Integration of modeling with experimental and clinical findings synthesizes and refines the central role of inositol 1,4,5-trisphosphate receptor 1 in spinocerebellar ataxia', *Front Neurosci,* 8, pp. 453.

Burman, R. J., Watson, L. M., Smith, D. C., Raimondo, J. V., Ballo, R., Scholefield, J., Cowley, S. A., Wood, M. J. A., Kidson, S. H. and Greenberg, L. J. (2021) 'Molecular and electrophysiological features of spinocerebellar ataxia type seven in induced pluripotent stem cells', *PLoS One,* 16(2), pp. e0247434.

Burright, E. N., Clark, H. B., Servadio, A., Matilla, T., Feddersen, R. M., Yunis, W. S., Duvick, L. A., Zoghbi, H. Y. and Orr, H. T. (1995) 'SCA1 transgenic mice: a model for neurodegeneration caused by an expanded CAG trinucleotide repeat', *Cell,* 82(6), pp. 937-48.

Burright, E. N., Davidson, J. D., Duvick, L. A., Koshy, B., Zoghbi, H. Y. and Orr, H. T. (1997) 'Identification of a self-association region within the SCA1 gene product, ataxin-1', *Hum Mol Genet,* 6(4), pp. 513-8.

Burroughs, A., Wise, A. K., Xiao, J., Houghton, C., Tang, T., Suh, C. Y., Lang, E. J., Apps, R. and Cerminara, N. L. (2017) 'The dynamic relationship between cerebellar Purkinje cell simple spikes and the spikelet number of complex spikes', *J Physiol,* 595(1), pp. 283-299.

Busche, M. A., Eichhoff, G., Adelsberger, H., Abramowski, D., Wiederhold, K. H., Haass, C., Staufenbiel, M., Konnerth, A. and Garaschuk, O. (2008) 'Clusters of hyperactive neurons near amyloid plaques in a mouse model of Alzheimer's disease', *Science,* 321(5896), pp. 1686-9.

Bushart, D. D., Chopra, R., Singh, V., Murphy, G. G., Wulff, H. and Shakkottai, V. G. (2018) 'Targeting potassium channels to treat cerebellar ataxia', *Ann Clin Transl Neurol,* 5(3), pp. 297-314.

Buzsáki, G. (1984) 'Feed-forward inhibition in the hippocampal formation', *Prog Neurobiol,* 22(2), pp. 131-53.

Bærentzen, S., Casado-Sainz, A., Lange, D., Shalgunov, V., Tejada, I. M., Xiong, M., L'Estrade, E. T., Edgar, F. G., Lee, H., Herth, M. M. and Palner, M. (2019) 'The Chemogenetic Receptor Ligand Clozapine N-Oxide Induces', *Front Neurosci,* 13, pp. 187.

Bürk, K., Abele, M., Fetter, M., Dichgans, J., Skalej, M., Laccone, F., Didierjean, O., Brice, A. and Klockgether, T. (1996) 'Autosomal dominant cerebellar ataxia type I clinical features and MRI in families with SCA1, SCA2 and SCA3', *Brain,* 119 (Pt 5), pp. 1497-505.

Caillard, O., Moreno, H., Schwaller, B., Llano, I., Celio, M. R. and Marty, A. (2000) 'Role of the calcium-binding protein parvalbumin in short-term synaptic plasticity', *Proc Natl Acad Sci U S A,* 97(24), pp. 13372-7.

Canepari, M. and Ogden, D. (2006) 'Kinetic, pharmacological and activity-dependent separation of two Ca2+ signalling pathways mediated by type 1 metabotropic glutamate receptors in rat Purkinje neurones', *J Physiol,* 573(Pt 1), pp. 65-82.

Capizzi, M., Carpentier, R., Denarier, E., Adrait, A., Kassem, R., Mapelli, M., Couté, Y. and Humbert, S. (2022) 'Developmental defects in Huntington's disease show that axonal growth and microtubule reorganization require NUMA1', *Neuron,* 110(1), pp. 36-50.e5.

Cayco-Gajic, N. A. and Silver, R. A. (2019) 'Re-evaluating Circuit Mechanisms Underlying Pattern Separation', *Neuron,* 101(4), pp. 584-602.

Chandran, V., Jhunjhunwala, K., Purushottam, M., Jain, S. and Pal, P. K. (2014) 'Multimodal evoked potentials in spinocerebellar ataxia types 1, 2, and 3', *Ann Indian Acad Neurol,* 17(3), pp. 321-4.

Chang, W., Pedroni, A., Hohendorf, V., Giacomello, S., Hibi, M., Köster, R. W. and Ampatzis, K. (2020) 'Functionally distinct Purkinje cell types show temporal precision in encoding locomotion', *Proc Natl Acad Sci U S A,* 117(29), pp. 17330-17337.

Chapman, P. F., White, G. L., Jones, M. W., Cooper-Blacketer, D., Marshall, V. J., Irizarry, M., Younkin, L., Good, M. A., Bliss, T. V., Hyman, B. T., Younkin, S. G. and Hsiao, K. K. (1999) 'Impaired synaptic plasticity and learning in aged amyloid precursor protein transgenic mice', *Nat Neurosci,* 2(3), pp. 271-6.

Chen, H. K., Fernandez-Funez, P., Acevedo, S. F., Lam, Y. C., Kaytor, M. D., Fernandez, M. H., Aitken, A., Skoulakis, E. M., Orr, H. T., Botas, J. and Zoghbi, H. Y. (2003) 'Interaction of Akt-phosphorylated ataxin-1 with 14-3-3 mediates neurodegeneration in spinocerebellar ataxia type 1', *Cell,* 113(4), pp. 457-68.

Chen, J. M., Chen, S. K., Jin, P. P. and Sun, S. C. (2022) 'Identification of the ataxin-1 interaction network and its impact on spinocerebellar ataxia type 1', *Hum Genomics,* 16(1), pp. 29.

Chen, S., Augustine, G. J. and Chadderton, P. (2016) 'The cerebellum linearly encodes whisker position during voluntary movement', *Elife,* 5, pp. e10509.

Chen, T. W., Wardill, T. J., Sun, Y., Pulver, S. R., Renninger, S. L., Baohan, A., Schreiter, E. R., Kerr, R. A., Orger, M. B., Jayaraman, V., Looger, L. L., Svoboda, K. and Kim, D. S. (2013) 'Ultrasensitive fluorescent proteins for imaging neuronal activity', *Nature,* 499(7458), pp. 295-300.

Chen, X., Tang, T. S., Tu, H., Nelson, O., Pook, M., Hammer, R., Nukina, N. and Bezprozvanny, I. (2008) 'Deranged calcium signaling and neurodegeneration in spinocerebellar ataxia type 3', *J Neurosci,* 28(48), pp. 12713-24.

Chiken, S. and Nambu, A. (2016) 'Mechanism of Deep Brain Stimulation: Inhibition, Excitation, or Disruption?', *Neuroscientist,* 22(3), pp. 313-22.

Chopra, R., Bushart, D. D., Cooper, J. P., Yellajoshyula, D., Morrison, L. M., Huang, H., Handler, H. P., Man, L. J., Dansithong, W., Scoles, D. R., Pulst, S. M., Orr, H. T. and Shakkottai, V. G. (2020) 'Altered Capicua expression drives regional Purkinje neuron vulnerability through ion channel gene dysregulation in spinocerebellar ataxia type 1', *Hum Mol Genet,* 29(19), pp. 3249-3265.

Chopra, R., Bushart, D. D. and Shakkottai, V. G. (2018) 'Dendritic potassium channel dysfunction may contribute to dendrite degeneration in spinocerebellar ataxia type 1', *PLoS One,* 13(5), pp. e0198040.

Chu, C. P., Bing, Y. H., Liu, H. and Qiu, D. L. (2012) 'Roles of molecular layer interneurons in sensory information processing in mouse cerebellar cortex Crus II in vivo', *PLoS One,* 7(5), pp. e37031.

Clausi, S., Lupo, M., Funghi, G., Mammone, A. and Leggio, M. (2022) 'Modulating mental state recognition by anodal tDCS over the cerebellum', *Sci Rep,* 12(1), pp. 22616.

Collin, T., Chat, M., Lucas, M. G., Moreno, H., Racay, P., Schwaller, B., Marty, A. and Llano, I. (2005) 'Developmental changes in parvalbumin regulate presynaptic Ca2+ signaling', *J Neurosci,* 25(1), pp. 96-107.

Cornell, B. and Toyo-Oka, K. (2017) '14-3-3 Proteins in Brain Development: Neurogenesis, Neuronal Migration and Neuromorphogenesis', *Front Mol Neurosci,* 10, pp. 318.

Crespo-Barreto, J., Fryer, J. D., Shaw, C. A., Orr, H. T. and Zoghbi, H. Y. (2010) 'Partial loss of ataxin-1 function contributes to transcriptional dysregulation in spinocerebellar ataxia type 1 pathogenesis', *PLoS Genet,* 6(7), pp. e1001021.

Cummings, C. J., Reinstein, E., Sun, Y., Antalffy, B., Jiang, Y., Ciechanover, A., Orr, H. T., Beaudet, A. L. and Zoghbi, H. Y. (1999) 'Mutation of the E6-AP ubiquitin ligase reduces nuclear inclusion frequency while accelerating polyglutamine-induced pathology in SCA1 mice', *Neuron,* 24(4), pp. 879-92.

D'Adamo, M. C., Hasan, S., Guglielmi, L., Servettini, I., Cenciarini, M., Catacuzzeno, L. and Franciolini, F. (2015) 'New insights into the pathogenesis and therapeutics of episodic ataxia type 1', *Front Cell Neurosci,* 9, pp. 317.

D'Angelo, E. (2008) 'The critical role of Golgi cells in regulating spatio-temporal integration and plasticity at the cerebellum input stage', *Front Neurosci,* 2(1), pp. 35-46.

D'Angelo, E. and De Zeeuw, C. I. (2009) 'Timing and plasticity in the cerebellum: focus on the granular layer', *Trends Neurosci,* 32(1), pp. 30-40.

D'Angelo, E., Solinas, S., Mapelli, J., Gandolfi, D., Mapelli, L. and Prestori, F. (2013) 'The cerebellar Golgi cell and spatiotemporal organization of granular layer activity', *Front Neural Circuits,* 7, pp. 93.

Dana, H., Sun, Y., Mohar, B., Hulse, B. K., Kerlin, A. M., Hasseman, J. P., Tsegaye, G., Tsang, A., Wong, A., Patel, R., Macklin, J. J., Chen, Y., Konnerth, A., Jayaraman, V., Looger, L. L., Schreiter, E. R., Svoboda, K. and Kim, D. S. (2019) 'High-performance calcium sensors for imaging activity in neuronal populations and microcompartments', *Nat Methods,* 16(7), pp. 649-657.

Daughters, R. S., Tuttle, D. L., Gao, W., Ikeda, Y., Moseley, M. L., Ebner, T. J., Swanson, M. S. and Ranum, L. P. (2009) 'RNA gain-of-function in spinocerebellar ataxia type 8', *PLoS Genet,* 5(8), pp. e1000600.

de Chiara, C., Menon, R. P., Strom, M., Gibson, T. J. and Pastore, A. (2009) 'Phosphorylation of S776 and 14-3-3 binding modulate ataxin-1 interaction with splicing factors', *PLoS One,* 4(12), pp. e8372.

de Solages, C., Szapiro, G., Brunel, N., Hakim, V., Isope, P., Buisseret, P., Rousseau, C., Barbour, B. and Léna, C. (2008) 'High-frequency organization and synchrony of activity in the purkinje cell layer of the cerebellum', *Neuron,* 58(5), pp. 775-88.

de Tommaso, M., De Carlo, F., Difruscolo, O., Massafra, R., Sciruicchio, V. and Bellotti, R. (2003) 'Detection of subclinical brain electrical activity changes in Huntington's disease using artificial neural networks', *Clin Neurophysiol,* 114(7), pp. 1237-45.

Deelchand, D. K., Joers, J. M., Ravishankar, A., Lyu, T., Emir, U. E., Hutter, D., Gomez, C. M., Bushara, K. O., Lenglet, C., Eberly, L. E. and Öz, G. (2019) 'Sensitivity of Volumetric Magnetic Resonance Imaging and Magnetic Resonance Spectroscopy to Progression of Spinocerebellar Ataxia Type 1', *Mov Disord Clin Pract,* 6(7), pp. 549-558.

Dell'Orco, J. M., Wasserman, A. H., Chopra, R., Ingram, M. A., Hu, Y. S., Singh, V., Wulff, H., Opal, P., Orr, H. T. and Shakkottai, V. G. (2015) 'Neuronal Atrophy Early in Degenerative Ataxia Is a Compensatory Mechanism to Regulate Membrane Excitability', *J Neurosci,* 35(32), pp. 11292-307.

Didonna, A., Canto Puig, E., Ma, Q., Matsunaga, A., Ho, B., Caillier, S. J., Shams, H., Lee, N., Hauser, S. L., Tan, Q., Zamvil, S. S. and Oksenberg, J. R. (2020) 'Ataxin-1 regulates B cell function and the severity of autoimmune experimental encephalomyelitis', *Proc Natl Acad Sci U S A,* 117(38), pp. 23742-23750.

Donato, F., Rompani, S. B. and Caroni, P. (2013) 'Parvalbumin-expressing basket-cell network plasticity induced by experience regulates adult learning', *Nature,* 504(7479), pp. 272-6.

Dong, G. H., Xu, Y. H., Liu, L. Y., Lu, D., Chu, C. P., Cui, S. B. and Qiu, D. L. (2022) 'Chronic ethanol exposure during adolescence impairs simple spike activity of cerebellar Purkinje cells in vivo in mice', *Neurosci Lett,* 771, pp. 136396.

Drew, L. (2018) 'Gene therapy targets epilepsy', *Nature,* 564(7735), pp. S10-S11.

Duarri, A., Lin, M. C., Fokkens, M. R., Meijer, M., Smeets, C. J., Nibbeling, E. A., Boddeke, E., Sinke, R. J., Kampinga, H. H., Papazian, D. M. and Verbeek, D. S. (2015) 'Spinocerebellar ataxia type 19/22 mutations alter heterocomplex Kv4.3 channel function and gating in a dominant manner', *Cell Mol Life Sci,* 72(17), pp. 3387-99.

Dueñas, A. M., Goold, R. and Giunti, P. (2006) 'Molecular pathogenesis of spinocerebellar ataxias', *Brain,* 129(Pt 6), pp. 1357-70.

Duguid, I., Branco, T., Chadderton, P., Arlt, C., Powell, K. and Häusser, M. (2015) 'Control of cerebellar granule cell output by sensory-evoked Golgi cell inhibition', *Proc Natl Acad Sci U S A,* 112(42), pp. 13099-104.

Dugué, G. P., Brunel, N., Hakim, V., Schwartz, E., Chat, M., Lévesque, M., Courtemanche, R., Léna, C. and Dieudonné, S. (2009) 'Electrical coupling mediates tunable low-frequency oscillations and resonance in the cerebellar Golgi cell network', *Neuron,* 61(1), pp. 126-39.

Dumoulin, A., Triller, A. and Dieudonné, S. (2001) 'IPSC kinetics at identified GABAergic and mixed GABAergic and glycinergic synapses onto cerebellar Golgi cells', *J Neurosci,* 21(16), pp. 6045-57.

Duyckaerts, C., Dürr, A., Cancel, G. and Brice, A. (1999) 'Nuclear inclusions in spinocerebellar ataxia type 1', *Acta Neuropathol,* 97(2), pp. 201-7.

Ebner, B. A., Ingram, M. A., Barnes, J. A., Duvick, L. A., Frisch, J. L., Clark, H. B., Zoghbi, H. Y., Ebner, T. J. and Orr, H. T. (2013) 'Purkinje cell ataxin-1 modulates climbing fiber synaptic input in developing and adult mouse cerebellum', *J Neurosci,* 33(13), pp. 5806-20.

Eccles, J. C., Sasaki, K. and Strata, P. (1967) 'A comparison of the inhibitory actions of Golgi cells and of basket cells', *Exp Brain Res,* 3(1), pp. 81-94.

Edamakanti, C. R., Do, J., Didonna, A., Martina, M. and Opal, P. (2018) 'Mutant ataxin1 disrupts cerebellar development in spinocerebellar ataxia type 1', *J Clin Invest,* 128(6), pp. 2252-2265.

Edgley, S. A. and Lidierth, M. (1987) 'The discharges of cerebellar Golgi cells during locomotion in the cat', *J Physiol,* 392, pp. 315-32.

Emamian, E. S., Kaytor, M. D., Duvick, L. A., Zu, T., Tousey, S. K., Zoghbi, H. Y., Clark, H. B. and Orr, H. T. (2003) 'Serine 776 of ataxin-1 is critical for polyglutamine-induced disease in SCA1 transgenic mice', *Neuron,* 38(3), pp. 375-87.

Ferguson, B. R. and Gao, W. J. (2018) 'PV Interneurons: Critical Regulators of E/I Balance for Prefrontal Cortex-Dependent Behavior and Psychiatric Disorders', *Front Neural Circuits,* 12, pp. 37.

Ferrer, I., Genís, D., Dávalos, A., Bernadó, L., Sant, F. and Serrano, T. (1994) 'The Purkinje cell in olivopontocerebellar atrophy. A Golgi and immunocytochemical study', *Neuropathol Appl Neurobiol,* 20(1), pp. 38-46.

Flace, P., Benagiano, V., Lorusso, L., Girolamo, F., Rizzi, A., Virgintino, D., Roncali, L. and Ambrosi, G. (2004) 'Glutamic acid decarboxylase immunoreactive large neuron types in the granular layer of the human cerebellar cortex', *Anat Embryol (Berl),* 208(1), pp. 55-64.

Frere, S. and Slutsky, I. (2018) 'Alzheimer's Disease: From Firing Instability to Homeostasis Network Collapse', *Neuron,* 97(1), pp. 32-58.

Fryer, J. D., Yu, P., Kang, H., Mandel-Brehm, C., Carter, A. N., Crespo-Barreto, J., Gao, Y., Flora, A., Shaw, C., Orr, H. T. and Zoghbi, H. Y. (2011) 'Exercise and genetic rescue of SCA1 via the transcriptional repressor Capicua', *Science,* 334(6056), pp. 690-3.

Gaffield, M. A. and Christie, J. M. (2017) 'Movement Rate Is Encoded and Influenced by Widespread, Coherent Activity of Cerebellar Molecular Layer Interneurons', *J Neurosci,* 37(18), pp. 4751-4765.

Galliano, E., Mazzarello, P. and D'Angelo, E. (2010) 'Discovery and rediscoveries of Golgi cells', *J Physiol,* 588(Pt 19), pp. 3639-55.

Garcia-Lopez, P., Garcia-Marin, V. and Freire, M. (2010) 'The histological slides and drawings of cajal', *Front Neuroanat,* 4, pp. 9.

Gittis, A. H. and Yttri, E. A. (2018) 'Translating Insights From Optogenetics To Therapies For Parkinson's Disease', *Curr Opin Biomed Eng,* 8, pp. 14-19.

Glickstein, M., Strata, P. and Voogd, J. (2009) 'Cerebellum: history', *Neuroscience,* 162(3), pp. 549-59.

Globas, C., du Montcel, S. T., Baliko, L., Boesch, S., Depondt, C., DiDonato, S., Durr, A., Filla, A., Klockgether, T., Mariotti, C., Melegh, B., Rakowicz, M., Ribai, P., Rola, R., Schmitz-Hubsch, T., Szymanski, S., Timmann, D., Van de Warrenburg, B. P., Bauer, P. and Schols, L. (2008) 'Early symptoms in spinocerebellar ataxia type 1, 2, 3, and 6', *Mov Disord,* 23(15), pp. 2232-8.

Gobbo, F., Mitchell-Heggs, R. and Tse, D. (2022) 'Changes in brain activity and connectivity as memories age', *Cogn Neurosci,* 13(3-4), pp. 141-143.

Golgi, C. (1883) ‘Sulla fina anatomia degli organi centrali del sistema nervoso. V. Sulla fina anatomia del grande piede d’Hippocampo’ Riv. Sper. Fren. Med. Legale, 9, pp. 161-192

Graves, T. D., Cha, Y. H., Hahn, A. F., Barohn, R., Salajegheh, M. K., Griggs, R. C., Bundy, B. N., Jen, J. C., Baloh, R. W., Hanna, M. G. and Investigators, C. (2014) 'Episodic ataxia type 1: clinical characterization, quality of life and genotype-phenotype correlation', *Brain,* 137(Pt 4), pp. 1009-18.

Greenberg, D. S., Houweling, A. R. and Kerr, J. N. (2008) 'Population imaging of ongoing neuronal activity in the visual cortex of awake rats', *Nat Neurosci,* 11(7), pp. 749-51.

Greenfield JG. (1954) ‘The spino-cerebellar degenerations.’ Charles C. Thomas; Springfield

Grienberger, C. and Konnerth, A. (2012) 'Imaging calcium in neurons', *Neuron,* 73(5), pp. 862-85.

Guerrini, L., Lolli, F., Ginestroni, A., Belli, G., Della Nave, R., Tessa, C., Foresti, S., Cosottini, M., Piacentini, S., Salvi, F., Plasmati, R., De Grandis, D., Siciliano, G., Filla, A. and Mascalchi, M. (2004) 'Brainstem neurodegeneration correlates with clinical dysfunction in SCA1 but not in SCA2. A quantitative volumetric, diffusion and proton spectroscopy MR study', *Brain,* 127(Pt 8), pp. 1785-95.

Gurnani, H. and Silver, R. A. (2021) 'Multidimensional population activity in an electrically coupled inhibitory circuit in the cerebellar cortex', *Neuron,* 109(10), pp. 1739-1753.e8.

Hackam, A. S., Singaraja, R., Wellington, C. L., Metzler, M., McCutcheon, K., Zhang, T., Kalchman, M. and Hayden, M. R. (1998) 'The influence of huntingtin protein size on nuclear localization and cellular toxicity', *J Cell Biol,* 141(5), pp. 1097-105.

Haery, L., Deverman, B. E., Matho, K. S., Cetin, A., Woodard, K., Cepko, C., Guerin, K. I., Rego, M. A., Ersing, I., Bachle, S. M., Kamens, J. and Fan, M. (2019) 'Adeno-Associated Virus Technologies and Methods for Targeted Neuronal Manipulation', *Front Neuroanat,* 13, pp. 93.

Haider, B., Häusser, M. and Carandini, M. (2013) 'Inhibition dominates sensory responses in the awake cortex', *Nature,* 493(7430), pp. 97-100.

Hartmann, J., Henning, H. A. and Konnerth, A. (2011) 'mGluR1/TRPC3-mediated Synaptic Transmission and Calcium Signaling in Mammalian Central Neurons', *Cold Spring Harb Perspect Biol,* 3(4).

Hasan, S., Bove, C., Silvestri, G., Mantuano, E., Modoni, A., Veneziano, L., Macchioni, L., Hunter, T., Hunter, G., Pessia, M. and D'Adamo, M. C. (2017) 'A channelopathy mutation in the voltage-sensor discloses contributions of a conserved phenylalanine to gating properties of Kv1.1 channels and ataxia', *Sci Rep,* 7(1), pp. 4583.

Heiney, S. A., Wohl, M. P., Chettih, S. N., Ruffolo, L. I. and Medina, J. F. (2014) 'Cerebellar-dependent expression of motor learning during eyeblink conditioning in head-fixed mice', *J Neurosci,* 34(45), pp. 14845-53.

Hekman, K. E. and Gomez, C. M. (2015) 'The autosomal dominant spinocerebellar ataxias: emerging mechanistic themes suggest pervasive Purkinje cell vulnerability', *J Neurol Neurosurg Psychiatry,* 86(5), pp. 554-61.

Helmchen, C. and Büttner, U. (1995) 'Saccade-related Purkinje cell activity in the oculomotor vermis during spontaneous eye movements in light and darkness', *Exp Brain Res,* 103(2), pp. 198-208.

Hewitt, A. L., Popa, L. S. and Ebner, T. J. (2015) 'Changes in Purkinje cell simple spike encoding of reach kinematics during adaption to a mechanical perturbation', *J Neurosci,* 35(3), pp. 1106-24.

Hijazi, S., Heistek, T. S., Scheltens, P., Neumann, U., Shimshek, D. R., Mansvelder, H. D., Smit, A. B. and van Kesteren, R. E. (2020) 'Early restoration of parvalbumin interneuron activity prevents memory loss and network hyperexcitability in a mouse model of Alzheimer's disease', *Mol Psychiatry,* 25(12), pp. 3380-3398.

Hippenmeyer, S., Vrieseling, E., Sigrist, M., Portmann, T., Laengle, C., Ladle, D. R. and Arber, S. (2005) 'A developmental switch in the response of DRG neurons to ETS transcription factor signaling', *PLoS Biol,* 3(5), pp. e159.

Hirano, T. (2018) 'Purkinje Neurons: Development, Morphology, and Function', *Cerebellum,* 17(6), pp. 699-700.

Hirono, M., Saitow, F., Kudo, M., Suzuki, H., Yanagawa, Y., Yamada, M., Nagao, S., Konishi, S. and Obata, K. (2012) 'Cerebellar globular cells receive monoaminergic excitation and monosynaptic inhibition from Purkinje cells', *PLoS One,* 7(1), pp. e29663.

Hisatsune, C., Miyamoto, H., Hirono, M., Yamaguchi, N., Sugawara, T., Ogawa, N., Ebisui, E., Ohshima, T., Yamada, M., Hensch, T. K., Hattori, M. and Mikoshiba, K. (2013) 'IP3R1 deficiency in the cerebellum/brainstem causes basal ganglia-independent dystonia by triggering tonic Purkinje cell firings in mice', *Front Neural Circuits,* 7, pp. 156.

Holtmaat, A., Bonhoeffer, T., Chow, D. K., Chuckowree, J., De Paola, V., Hofer, S. B., Hübener, M., Keck, T., Knott, G., Lee, W. C., Mostany, R., Mrsic-Flogel, T. D., Nedivi, E., Portera-Cailliau, C., Svoboda, K., Trachtenberg, J. T. and Wilbrecht, L. (2009) 'Long-term, high-resolution imaging in the mouse neocortex through a chronic cranial window', *Nat Protoc,* 4(8), pp. 1128-44.

Holtzman, T., Mostofi, A., Phuah, C. L. and Edgley, S. A. (2006) 'Cerebellar Golgi cells in the rat receive multimodal convergent peripheral inputs via the lateral funiculus of the spinal cord', *J Physiol,* 577(Pt 1), pp. 69-80.

Horn, K. M., Pong, M. and Gibson, A. R. (2010) 'Functional relations of cerebellar modules of the cat', *J Neurosci,* 30(28), pp. 9411-23.

Houmani, N., Vialatte, F., Gallego-Jutglà, E., Dreyfus, G., Nguyen-Michel, V. H., Mariani, J. and Kinugawa, K. (2018) 'Diagnosis of Alzheimer's disease with Electroencephalography in a differential framework', *PLoS One,* 13(3), pp. e0193607.

Hourez, R., Servais, L., Orduz, D., Gall, D., Millard, I., de Kerchove d'Exaerde, A., Cheron, G., Orr, H. T., Pandolfo, M. and Schiffmann, S. N. (2011) 'Aminopyridines correct early dysfunction and delay neurodegeneration in a mouse model of spinocerebellar ataxia type 1', *J Neurosci,* 31(33), pp. 11795-807.

Huang, M. and Verbeek, D. S. (2019) 'Why do so many genetic insults lead to Purkinje Cell degeneration and spinocerebellar ataxia?', *Neurosci Lett,* 688, pp. 49-57.

Hudry, E. and Vandenberghe, L. H. (2019) 'Therapeutic AAV Gene Transfer to the Nervous System: A Clinical Reality', *Neuron,* 102(1), pp. 263.

Hull, C. and Regehr, W. G. (2012) 'Identification of an inhibitory circuit that regulates cerebellar Golgi cell activity', *Neuron,* 73(1), pp. 149-58.

Hull, C. and Regehr, W. G. (2022) 'The Cerebellar Cortex', *Annu Rev Neurosci,* 45, pp. 151-175.

Häusser, M. and Clark, B. A. (1997) 'Tonic synaptic inhibition modulates neuronal output pattern and spatiotemporal synaptic integration', *Neuron,* 19(3), pp. 665-78.

Ingram, M., Wozniak, E. A. L., Duvick, L., Yang, R., Bergmann, P., Carson, R., O'Callaghan, B., Zoghbi, H. Y., Henzler, C. and Orr, H. T. (2016) 'Cerebellar Transcriptome Profiles of ATXN1 Transgenic Mice Reveal SCA1 Disease Progression and Protection Pathways', *Neuron,* 89(6), pp. 1194-1207.

Irwin, S., Vandelft, M., Pinchev, D., Howell, J. L., Graczyk, J., Orr, H. T. and Truant, R. (2005) 'RNA association and nucleocytoplasmic shuttling by ataxin-1', *J Cell Sci,* 118(Pt 1), pp. 233-42.

Ito, M. and Kano, M. (1982) 'Long-lasting depression of parallel fiber-Purkinje cell transmission induced by conjunctive stimulation of parallel fibers and climbing fibers in the cerebellar cortex', *Neurosci Lett,* 33(3), pp. 253-8.

Jackson, J. F., Currier, R. D., Terasaki, P. I. and Morton, N. E. (1977) 'Spinocerebellar ataxia and HLA linkage: risk prediction by HLA typing', *N Engl J Med,* 296(20), pp. 1138-41.

Jacobi, H., du Montcel, S. T., Bauer, P., Giunti, P., Cook, A., Labrum, R., Parkinson, M. H., Durr, A., Brice, A., Charles, P., Marelli, C., Mariotti, C., Nanetti, L., Panzeri, M., Rakowicz, M., Sulek, A., Sobanska, A., Schmitz-Hübsch, T., Schöls, L., Hengel, H., Baliko, L., Melegh, B., Filla, A., Antenora, A., Infante, J., Berciano, J., van de Warrenburg, B. P., Timmann, D., Szymanski, S., Boesch, S., Kang, J. S., Pandolfo, M., Schulz, J. B., Molho, S., Diallo, A. and Klockgether, T. (2015) 'Long-term disease progression in spinocerebellar ataxia types 1, 2, 3, and 6: a longitudinal cohort study', *Lancet Neurol,* 14(11), pp. 1101-8.

Jacobi, H., Faber, J., Timmann, D. and Klockgether, T. (2021) 'Update cerebellum and cognition', *J Neurol,* 268(10), pp. 3921-3925.

Jacobi, H., Reetz, K., du Montcel, S. T., Bauer, P., Mariotti, C., Nanetti, L., Rakowicz, M., Sulek, A., Durr, A., Charles, P., Filla, A., Antenora, A., Schöls, L., Schicks, J., Infante, J., Kang, J. S., Timmann, D., Di Fabio, R., Masciullo, M., Baliko, L., Melegh, B., Boesch, S., Bürk, K., Peltz, A., Schulz, J. B., Dufaure-Garé, I. and

Klockgether, T. (2013) 'Biological and clinical characteristics of individuals at risk for spinocerebellar ataxia types 1, 2, 3, and 6 in the longitudinal RISCA study: analysis of baseline data', *Lancet Neurol,* 12(7), pp. 650-8.

Jafar-Nejad, P., Ward, C. S., Richman, R., Orr, H. T. and Zoghbi, H. Y. (2011) 'Regional rescue of spinocerebellar ataxia type 1 phenotypes by 14-3-3epsilon haploinsufficiency in mice underscores complex pathogenicity in neurodegeneration', *Proc Natl Acad Sci U S A,* 108(5), pp. 2142-7.

Jelitai, M., Puggioni, P., Ishikawa, T., Rinaldi, A. and Duguid, I. (2016) 'Dendritic excitation-inhibition balance shapes cerebellar output during motor behaviour', *Nat Commun,* 7, pp. 13722.

Jendryka, M., Palchaudhuri, M., Ursu, D., van der Veen, B., Liss, B., Kätzel, D., Nissen, W. and Pekcec, A. (2019) 'Pharmacokinetic and pharmacodynamic actions of clozapine-N-oxide, clozapine, and compound 21 in DREADD-based chemogenetics in mice', *Sci Rep,* 9(1), pp. 4522.

Jirenhed, D. A., Bengtsson, F. and Hesslow, G. (2007) 'Acquisition, extinction, and reacquisition of a cerebellar cortical memory trace', *J Neurosci,* 27(10), pp. 2493-502.

Jörntell, H., Bengtsson, F., Schonewille, M. and De Zeeuw, C. I. (2010) 'Cerebellar molecular layer interneurons - computational properties and roles in learning', *Trends Neurosci,* 33(11), pp. 524-32.

Jörntell, H. and Ekerot, C. F. (2002) 'Reciprocal bidirectional plasticity of parallel fiber receptive fields in cerebellar Purkinje cells and their afferent interneurons', *Neuron,* 34(5), pp. 797-806.

Kalinichenko, S. G. and Okhotin, V. E. (2005) 'Unipolar brush cells--a new type of excitatory interneuron in the cerebellar cortex and cochlear nuclei of the brainstem', *Neurosci Behav Physiol,* 35(1), pp. 21-36.

Kang, S. and Hong, S. (2009) 'Molecular pathogenesis of spinocerebellar ataxia type 1 disease', *Mol Cells,* 27(6), pp. 621-7.

Kanichay, R. T. and Silver, R. A. (2008) 'Synaptic and cellular properties of the feedforward inhibitory circuit within the input layer of the cerebellar cortex', *J Neurosci,* 28(36), pp. 8955-67.

Kasumu, A. and Bezprozvanny, I. (2012) 'Deranged calcium signaling in Purkinje cells and pathogenesis in spinocerebellar ataxia 2 (SCA2) and other ataxias', *Cerebellum,* 11(3), pp. 630-9.

Kasumu, A. W., Liang, X., Egorova, P., Vorontsova, D. and Bezprozvanny, I. (2012) 'Chronic suppression of inositol 1,4,5-triphosphate receptor-mediated calcium signaling in cerebellar purkinje cells alleviates pathological phenotype in spinocerebellar ataxia 2 mice', *J Neurosci,* 32(37), pp. 12786-96.

Kato, S., Kaplan, H. S., Schrödel, T., Skora, S., Lindsay, T. H., Yemini, E., Lockery, S. and Zimmer, M. (2015) 'Global brain dynamics embed the motor command sequence of Caenorhabditis elegans', *Cell,* 163(3), pp. 656-69.

Khademullah, C. S., Aqrabawi, A. J., Place, K. M., Dargaei, Z., Liang, X., Pressey, J. C., Bedard, S., Yang, J. W., Garand, D., Keramidis, I., Gasecka, A., Côté, D., De Koninck, Y., Keith, J., Zinman, L., Robertson, J., Kim, J. C. and Woodin, M. A. (2020) 'Cortical interneuron-mediated inhibition delays the onset of amyotrophic lateral sclerosis', *Brain,* 143(3), pp. 800-810.

Kim, J. and Augustine, G. J. (2021) 'Molecular Layer Interneurons: Key Elements of Cerebellar Network Computation and Behavior', *Neuroscience,* 462, pp. 22-35.

Kim, J., Lee, S., Tsuda, S., Zhang, X., Asrican, B., Gloss, B., Feng, G. and Augustine, G. J. (2014) 'Optogenetic mapping of cerebellar inhibitory circuitry reveals spatially biased coordination of interneurons via electrical synapses', *Cell Rep,* 7(5), pp. 1601-1613.

Klement, I. A., Skinner, P. J., Kaytor, M. D., Yi, H., Hersch, S. M., Clark, H. B., Zoghbi, H. Y. and Orr, H. T. (1998) 'Ataxin-1 nuclear localization and aggregation: role in polyglutamine-induced disease in SCA1 transgenic mice', *Cell,* 95(1), pp. 41-53.

Koeppen, A. H. (2005) 'The pathogenesis of spinocerebellar ataxia', *Cerebellum,* 4(1), pp. 62-73.

Kohiyama, M. F. and Lagalwar, S. (2015) 'Stabilization and Degradation Mechanisms of Cytoplasmic Ataxin-1', *J Exp Neurosci,* 9(Suppl 2), pp. 123-9.

Koscik, T. R., Sloat, L., van der Plas, E., Joers, J. M., Deelchand, D. K., Lenglet, C., Öz, G. and Nopoulos, P. C. (2020) 'Brainstem and striatal volume changes are detectable in under 1 year and predict motor decline in spinocerebellar ataxia type 1', *Brain Commun,* 2(2), pp. fcaa184.

Lai, S., O'Callaghan, B., Zoghbi, H. Y. and Orr, H. T. (2011) '14-3-3 Binding to ataxin-1(ATXN1) regulates its dephosphorylation at Ser-776 and transport to the nucleus', *J Biol Chem,* 286(40), pp. 34606-16.

Laidou, S., Alanis-Lobato, G., Pribyl, J., Raskó, T., Tichy, B., Mikulasek, K., Tsagiopoulou, M., Oppelt, J., Kastrinaki, G., Lefaki, M., Singh, M., Zink, A., Chondrogianni, N., Psomopoulos, F., Prigione, A., Ivics, Z., Pospisilova, S., Skladal, P., Izsvák, Z., Andrade-Navarro, M. A. and Petrakis, S. (2020) 'Nuclear inclusions of pathogenic ataxin-1 induce oxidative stress and perturb the protein synthesis machinery', *Redox Biol,* 32, pp. 101458.

Larsell O. (1970) 'The Comparative Anatomy and Histology of the Cerebellum from Monotremes through Apes. Minneapolis': University of Minnesota Press.

Lanore, F., Cayco-Gajic, N. A., Gurnani, H., Coyle, D. and Silver, R. A. (2021) 'Cerebellar granule cell axons support high-dimensional representations', *Nat Neurosci,* 24(8), pp. 1142-1150.

Lenz, M. and Vlachos, A. (2016) 'Releasing the Cortical Brake by Non-Invasive Electromagnetic Stimulation? rTMS Induces LTD of GABAergic Neurotransmission', *Front Neural Circuits,* 10, pp. 96.

Lieb, A., Weston, M. and Kullmann, D. M. (2019) 'Designer receptor technology for the treatment of epilepsy', *EBioMedicine,* 43, pp. 641-649.

Liebscher, S. and Meyer-Luehmann, M. (2012) 'A Peephole into the Brain: Neuropathological Features of Alzheimer's Disease Revealed by in vivo Two-Photon Imaging', *Front Psychiatry,* 3, pp. 26.

Lin, X., Antalffy, B., Kang, D., Orr, H. T. and Zoghbi, H. Y. (2000) 'Polyglutamine expansion down-regulates specific neuronal genes before pathologic changes in SCA1', *Nat Neurosci,* 3(2), pp. 157-63.

Linnemann, C., Tezenas du Montcel, S., Rakowicz, M., Schmitz-Hübsch, T., Szymanski, S., Berciano, J., van de Warrenburg, B. P., Pedersen, K., Depondt, C., Rola, R., Klockgether, T., García, A., Mutlu, G. and Schöls, L. (2016) 'Peripheral Neuropathy in Spinocerebellar Ataxia Type 1, 2, 3, and 6', *Cerebellum,* 15(2), pp. 165-73.

Lisberger, S. G., Pavelko, T. A., Bronte-Stewart, H. M. and Stone, L. S. (1994) 'Neural basis for motor learning in the vestibuloocular reflex of primates. II. Changes in the responses of horizontal gaze velocity Purkinje cells in the cerebellar flocculus and ventral paraflocculus', *J Neurophysiol,* 72(2), pp. 954-73.

Lisman, J. (2003) 'Long-term potentiation: outstanding questions and attempted synthesis', *Philos Trans R Soc Lond B Biol Sci,* 358(1432), pp. 829-42.

Liu, J., Tang, T. S., Tu, H., Nelson, O., Herndon, E., Huynh, D. P., Pulst, S. M. and Bezprozvanny, I. (2009) 'Deranged calcium signaling and neurodegeneration in spinocerebellar ataxia type 2', *J Neurosci,* 29(29), pp. 9148-62.

Liu, X., Kumar, V., Tsai, N. P. and Auerbach, B. D. (2021) 'Hyperexcitability and Homeostasis in Fragile X Syndrome', *Front Mol Neurosci,* 14, pp. 805929.

Llinás, R. R. (2011) 'Cerebellar motor learning versus cerebellar motor timing: the climbing fibre story', *J Physiol,* 589(Pt 14), pp. 3423-32.

Lyu, J., Nagarajan, R., Kambali, M., Wang, M. and Rudolph, U. (2023) 'Selective inhibition of somatostatin-positive dentate hilar interneurons induces age-related cellular changes and cognitive dysfunction', *PNAS Nexus,* 2(5), pp. pgad134.

Ma, M., Futia, G. L., de Souza, F. M. S., Ozbay, B. N., Llano, I., Gibson, E. A. and Restrepo, D. (2020) 'Molecular layer interneurons in the cerebellum encode for valence in associative learning', *Nat Commun,* 11(1), pp. 4217.

Ma, Q., Pu, M., Li, M., Haihambo, N., Baetens, K., Heleven, E., Deroost, N., Baeken, C. and Van Overwalle, F. (2023) 'Can transcranial direct current stimulation (tDCS) of the cerebellum improve implicit social and cognitive sequence learning?', *Int J Clin Health Psychol,* 23(2), pp. 100355.

Mann-Metzer, P. and Yarom, Y. (2000) 'Electrotonic coupling synchronizes interneuron activity in the cerebellar cortex', *Prog Brain Res,* 124, pp. 115-22.

Manor, B., Greenstein, P. E., Davila-Perez, P., Wakefield, S., Zhou, J. and Pascual-Leone, A. (2019) 'Repetitive Transcranial Magnetic Stimulation in Spinocerebellar Ataxia: A Pilot Randomized Controlled Trial', *Front Neurol,* 10, pp. 73.

Manto, M., Bower, J. M., Conforto, A. B., Delgado-García, J. M., da Guarda, S. N., Gerwig, M., Habas, C., Hagura, N., Ivry, R. B., Mariën, P., Molinari, M., Naito, E., Nowak, D. A., Oulad Ben Taib, N., Pelisson, D., Tesche, C. D., Tilikete, C. and Timmann, D. (2012) 'Consensus paper: roles of the cerebellum in motor control--the diversity of ideas on cerebellar involvement in movement', *Cerebellum,* 11(2), pp. 457-87.

Manto, M. and Marmolino, D. (2009) 'Animal models of human cerebellar ataxias: a cornerstone for the therapies of the twenty-first century', *Cerebellum,* 8(3), pp. 137-54.

Manvich, D. F., Webster, K. A., Foster, S. L., Farrell, M. S., Ritchie, J. C., Porter, J. H. and Weinshenker, D. (2018) 'The DREADD agonist clozapine N-oxide (CNO) is reverse-metabolized to clozapine and produces clozapine-like interoceptive stimulus effects in rats and mice', *Sci Rep,* 8(1), pp. 3840.

Mapelli, J. and D'Angelo, E. (2007) 'The spatial organization of long-term synaptic plasticity at the input stage of cerebellum', *J Neurosci,* 27(6), pp. 1285-96.

Mapelli, L., Soda, T., D'Angelo, E. and Prestori, F. (2022) 'The Cerebellar Involvement in Autism Spectrum Disorders: From the Social Brain to Mouse Models', *Int J Mol Sci,* 23(7).

Matilla, A., Roberson, E. D., Banfi, S., Morales, J., Armstrong, D. L., Burright, E. N., Orr, H. T., Sweatt, J. D., Zoghbi, H. Y. and Matzuk, M. M. (1998) 'Mice lacking ataxin-1 display learning deficits and decreased hippocampal paired-pulse facilitation', *J Neurosci,* 18(14), pp. 5508-16.

Matilla-Dueñas, A., Goold, R. and Giunti, P. (2008) 'Clinical, genetic, molecular, and pathophysiological insights into spinocerebellar ataxia type 1', *Cerebellum,* 7(2), pp. 106-14.

McGregor, M. M. and Nelson, A. B. (2019) 'Circuit Mechanisms of Parkinson's Disease', *Neuron,* 101(6), pp. 1042-1056.

Meles, S. K., Oertel, W. H. and Leenders, K. L. (2021) 'Circuit imaging biomarkers in preclinical and prodromal Parkinson's disease', *Mol Med,* 27(1), pp. 111.

Meng, X., McGraw, C. M., Wang, W., Jing, J., Yeh, S. Y., Wang, L., Lopez, J., Brown, A. M., Lin, T., Chen, W., Xue, M., Sillitoe, R. V., Jiang, X. and Zoghbi, H. Y. (2019) 'Neurexophilin4 is a selectively expressed α-neurexin ligand that modulates specific cerebellar synapses and motor functions', *Elife,* 8.

Menon, R. P., Nethisinghe, S., Faggiano, S., Vannocci, T., Rezaei, H., Pemble, S., Sweeney, M. G., Wood, N. W., Davis, M. B., Pastore, A. and Giunti, P. (2013) 'The role of interruptions in polyQ in the pathology of SCA1', *PLoS Genet,* 9(7), pp. e1003648.

Menon, R. P., Soong, D., de Chiara, C., Holt, M. R., Anilkumar, N. and Pastore, A. (2012) 'The importance of serine 776 in Ataxin-1 partner selection: a FRET analysis', *Sci Rep,* 2, pp. 919.

Miles, F. A., Fuller, J. H., Braitman, D. J. and Dow, B. M. (1980) 'Long-term adaptive changes in primate vestibuloocular reflex. III. Electrophysiological observations in flocculus of normal monkeys', *J Neurophysiol,* 43(5), pp. 1437-76.

Miterko, L. N., Lackey, E. P., Heck, D. H. and Sillitoe, R. V. (2018) 'Shaping Diversity Into the Brain's Form and Function', *Front Neural Circuits,* 12, pp. 83.

Miyakawa, N., Nagai, Y., Hori, Y., Mimura, K., Orihara, A., Oyama, K., Matsuo, T., Inoue, K. I., Suzuki, T., Hirabayashi, T., Suhara, T., Takada, M., Higuchi, M., Kawasaki, K. and Minamimoto, T. (2023) 'Chemogenetic attenuation of cortical seizures in nonhuman primates', *Nat Commun,* 14(1), pp. 971.

Miyazaki, T., Yamasaki, M., Tanaka, K. F. and Watanabe, M. (2021) 'Compartmentalized Input-Output Organization of Lugaro Cells in the Cerebellar Cortex', *Neuroscience,* 462, pp. 89-105.

Mufson, E. J., Mahady, L., Waters, D., Counts, S. E., Perez, S. E., DeKosky, S. T., Ginsberg, S. D., Ikonomovic, M. D., Scheff, S. W. and Binder, L. I. (2015) 'Hippocampal plasticity during the progression of Alzheimer's disease', *Neuroscience,* 309, pp. 51-67.

Mukamel, E. A., Nimmerjahn, A. and Schnitzer, M. J. (2009) 'Automated analysis of cellular signals from large-scale calcium imaging data', *Neuron,* 63(6), pp. 747-60.

Muzzu, T., Mitolo, S., Gava, G. P. and Schultz, S. R. (2018) 'Encoding of locomotion kinematics in the mouse cerebellum', *PLoS One,* 13(9), pp. e0203900.

Nakai, J., Ohkura, M. and Imoto, K. (2001) 'A high signal-to-noise Ca(2+) probe composed of a single green fluorescent protein', *Nat Biotechnol,* 19(2), pp. 137-41.

Narayanan, S. and Thirumalai, V. (2019) 'Contributions of the Cerebellum for Predictive and Instructional Control of Movement', *Curr Opin Physiol,* 8, pp. 146-151.

Nelson, A. B., Krispel, C. M., Sekirnjak, C. and du Lac, S. (2003) 'Long-lasting increases in intrinsic excitability triggered by inhibition', *Neuron,* 40(3), pp. 609-20.

Nguyen-Vu, T. D., Kimpo, R. R., Rinaldi, J. M., Kohli, A., Zeng, H., Deisseroth, K. and Raymond, J. L. (2013) 'Cerebellar Purkinje cell activity drives motor learning', *Nat Neurosci,* 16(12), pp. 1734-6.

Nieus, T., Sola, E., Mapelli, J., Saftenku, E., Rossi, P. and D'Angelo, E. (2006) 'LTP regulates burst initiation and frequency at mossy fiber-granule cell synapses of rat cerebellum: experimental observations and theoretical predictions', *J Neurophysiol,* 95(2), pp. 686-99.

Niewiadomska-Cimicka, A., Doussau, F., Perot, J. B., Roux, M. J., Keime, C., Hache, A., Piguet, F., Novati, A., Weber, C., Yalcin, B., Meziane, H., Champy, M. F., Grandgirard, E., Karam, A., Messaddeq, N., Eisenmann, A., Brouillet, E., Nguyen, H. H. P., Flament, J., Isope, P. and Trottier, Y. (2021) 'SCA7 Mouse Cerebellar Pathology Reveals Preferential Downregulation of Key Purkinje Cell-Identity Genes and Shared Disease Signature with SCA1 and SCA2', *J Neurosci,* 41(22), pp. 4910-4936.

Nigri, A., Sarro, L., Mongelli, A., Castaldo, A., Porcu, L., Pinardi, C., Grisoli, M., Ferraro, S., Canafoglia, L., Visani, E., Bruzzone, M. G., Nanetti, L., Taroni, F. and Mariotti, C. (2022) 'Spinocerebellar Ataxia Type 1: One-Year Longitudinal Study to Identify Clinical and MRI Measures of Disease Progression in Patients and Presymptomatic Carriers', *Cerebellum,* 21(1), pp. 133-144.

Norris, S. A., Greger, B., Hathaway, E. N. and Thach, W. T. (2004) 'Purkinje cell spike firing in the posterolateral cerebellum: correlation with visual stimulus, oculomotor response, and error feedback', *J Neurophysiol,* 92(3), pp. 1867-79.

Notartomaso, S., Zappulla, C., Biagioni, F., Cannella, M., Bucci, D., Mascio, G., Scarselli, P., Fazio, F., Weisz, F., Lionetto, L., Simmaco, M., Gradini, R., Battaglia, G., Signore, M., Puliti, A. and Nicoletti, F. (2013) 'Pharmacological enhancement of mGlu1 metabotropic glutamate receptors causes a prolonged symptomatic benefit in a mouse model of spinocerebellar ataxia type 1', *Mol Brain,* 6, pp. 48.

Ohtsuki, G. (2020) 'Modification of Synaptic-Input Clustering by Intrinsic Excitability Plasticity on Cerebellar Purkinje Cell Dendrites', *J Neurosci,* 40(2), pp. 267-282.

Ojakangas, C. L. and Ebner, T. J. (1992) 'Purkinje cell complex and simple spike changes during a voluntary arm movement learning task in the monkey', *J Neurophysiol,* 68(6), pp. 2222-36.

Olmos, V., Gogia, N., Luttik, K., Haidery, F. and Lim, J. (2022) 'The extra-cerebellar effects of spinocerebellar ataxia type 1 (SCA1): looking beyond the cerebellum', *Cell Mol Life Sci,* 79(8), pp. 404.

Ophoff, R. A., Terwindt, G. M., Vergouwe, M. N., van Eijk, R., Oefner, P. J., Hoffman, S. M., Lamerdin, J. E., Mohrenweiser, H. W., Bulman, D. E., Ferrari, M., Haan, J., Lindhout, D., van Ommen, G. J., Hofker, M. H., Ferrari, M. D. and Frants, R. R. (1996) 'Familial hemiplegic migraine and episodic ataxia type-2 are caused by mutations in the Ca2+ channel gene CACNL1A4', *Cell,* 87(3), pp. 543-52.

Opitz, A., Falchier, A., Linn, G. S., Milham, M. P. and Schroeder, C. E. (2017) 'Limitations of ex vivo measurements for in vivo neuroscience', *Proc Natl Acad Sci U S A,* 114(20), pp. 5243-5246.

Orlovsky GN. (1972) 'Activity of the Purkinje cells during locomotion', *Biofizika.* 5:891–896.

Orr, H. T. (2001) 'Hereditary ataxia. An unfolded protein', *Lancet,* 358 Suppl, pp. S35.

Orr, H. T. (2012) 'SCA1-phosphorylation, a regulator of Ataxin-1 function and pathogenesis', *Prog Neurobiol,* 99(3), pp. 179-85.

Orr, H. T., Chung, M. Y., Banfi, S., Kwiatkowski, T. J., Servadio, A., Beaudet, A. L., McCall, A. E., Duvick, L. A., Ranum, L. P. and Zoghbi, H. Y. (1993) 'Expansion of an unstable trinucleotide CAG repeat in spinocerebellar ataxia type 1', *Nat Genet,* 4(3), pp. 221-6.

Orr, H. T. and Clark, H. B. (1995) 'Genetic approaches to pathogenesis of neurodegenerative diseases', *Lab Invest,* 73(2), pp. 161-71.

Orr, H. T. and Zoghbi, H. Y. (2001) 'SCA1 molecular genetics: a history of a 13 year collaboration against glutamines', *Hum Mol Genet,* 10(20), pp. 2307-11.

Osorno, T., Rudolph, S., Nguyen, T., Kozareva, V., Nadaf, N. M., Norton, A., Macosko, E. Z., Lee, W. A. and Regehr, W. G. (2022) 'Candelabrum cells are ubiquitous cerebellar cortex interneurons with specialized circuit properties', *Nat Neurosci,* 25(6), pp. 702-713.

Ozden, I., Dombeck, D. A., Hoogland, T. M., Tank, D. W. and Wang, S. S. (2012) 'Widespread state-dependent shifts in cerebellar activity in locomoting mice', *PLoS One,* 7(8), pp. e42650.

Ozden, I., Sullivan, M. R., Lee, H. M. and Wang, S. S. (2009) 'Reliable coding emerges from coactivation of climbing fibers in microbands of cerebellar Purkinje neurons', *J Neurosci,* 29(34), pp. 10463-73.

Palop, J. J., Chin, J. and Mucke, L. (2006) 'A network dysfunction perspective on neurodegenerative diseases', *Nature,* 443(7113), pp. 768-73.

Palop, J. J. and Mucke, L. (2016) 'Network abnormalities and interneuron dysfunction in Alzheimer disease', *Nat Rev Neurosci,* 17(12), pp. 777-792.

Paulson, H. L., Perez, M. K., Trottier, Y., Trojanowski, J. Q., Subramony, S. H., Das, S. S., Vig, P., Mandel, J. L., Fischbeck, K. H. and Pittman, R. N. (1997) 'Intranuclear inclusions of expanded polyglutamine protein in spinocerebellar ataxia type 3', *Neuron,* 19(2), pp. 333-44.

Paulson, H. L., Shakkottai, V. G., Clark, H. B. and Orr, H. T. (2017) 'Polyglutamine spinocerebellar ataxias - from genes to potential treatments', *Nat Rev Neurosci,* 18(10), pp. 613-626.

Pauly, M. G., Steinmeier, A., Bolte, C., Hamami, F., Tzvi, E., Münchau, A., Bäumer, T. and Weissbach, A. (2021) 'Cerebellar rTMS and PAS effectively induce cerebellar plasticity', *Sci Rep,* 11(1), pp. 3070.

Perkins, E. M., Clarkson, Y. L., Suminaite, D., Lyndon, A. R., Tanaka, K., Rothstein, J. D., Skehel, P. A., Wyllie, D. J. A. and Jackson, M. (2018) 'Loss of cerebellar glutamate transporters EAAT4 and GLAST differentially affects the spontaneous firing pattern and survival of Purkinje cells', *Hum Mol Genet,* 27(15), pp. 2614-2627.

Pilotto, F., Douthwaite, C., Diab, R., Ye, X., Al Qassab, Z., Tietje, C., Mounassir, M., Odriozola, A., Thapa, A., Buijsen, R. A. M., Lagache, S., Uldry, A. C., Heller, M., Müller, S., van Roon-Mom, W. M. C., Zuber, B., Liebscher, S. and Saxena, S. (2023) 'Early molecular layer interneuron hyperactivity triggers Purkinje neuron degeneration in SCA1', *Neuron*.

Powell, K., Mathy, A., Duguid, I. and Häusser, M. (2015) 'Synaptic representation of locomotion in single cerebellar granule cells', *Elife,* 4.

Power, E. M., Morales, A. and Empson, R. M. (2016) 'Prolonged Type 1 Metabotropic Glutamate Receptor Dependent Synaptic Signaling Contributes to Spino-Cerebellar Ataxia Type 1', *J Neurosci,* 36(18), pp. 4910-6.

Prestori, F., Mapelli, L. and D'Angelo, E. (2019a) 'Diverse Neuron Properties and Complex Network Dynamics in the Cerebellar Cortical Inhibitory Circuit', *Front Mol Neurosci,* 12, pp. 267.

Prestori, F., Moccia, F. and D'Angelo, E. (2019b) 'Disrupted Calcium Signaling in Animal Models of Human Spinocerebellar Ataxia (SCA)', *Int J Mol Sci,* 21(1).

Prsa, M., Dash, S., Catz, N., Dicke, P. W. and Thier, P. (2009) 'Characteristics of responses of Golgi cells and mossy fibers to eye saccades and saccadic adaptation recorded from the posterior vermis of the cerebellum', *J Neurosci,* 29(1), pp. 250-62.

Pérez Ortiz, J. M. and Orr, H. T. (2018) 'Spinocerebellar Ataxia Type 1: Molecular Mechanisms of Neurodegeneration and Preclinical Studies', *Adv Exp Med Biol,* 1049, pp. 135-145.

Rafii, M. S., Baumann, T. L., Bakay, R. A., Ostrove, J. M., Siffert, J., Fleisher, A. S., Herzog, C. D., Barba, D., Pay, M., Salmon, D. P., Chu, Y., Kordower, J. H., Bishop, K., Keator, D., Potkin, S. and Bartus, R. T. (2014) 'A phase1 study of stereotactic gene delivery of AAV2-NGF for Alzheimer's disease', *Alzheimers Dement,* 10(5), pp. 571-81.

Rafii, M. S., Tuszynski, M. H., Thomas, R. G., Barba, D., Brewer, J. B., Rissman, R. A., Siffert, J., Aisen, P. S. and Team, A.-N. S. (2018) 'Adeno-Associated Viral Vector (Serotype 2)-Nerve Growth Factor for Patients With Alzheimer Disease: A Randomized Clinical Trial', *JAMA Neurol,* 75(7), pp. 834-841.

Rakowicz, M., Rola, R., Sobanska, A., Antczak, J., Inglot, E., Sulek, A., (2019) 'O-06 Motor cortex excitability and conduction time of pyramidal tracts in preclinical SCA1 gene carriers', Clinical Neurophysiology, Volume 130, Issue 7.

Ramirez, J. E. and Stell, B. M. (2016) 'Calcium Imaging Reveals Coordinated Simple Spike Pauses in Populations of Cerebellar Purkinje Cells', *Cell Rep,* 17(12), pp. 3125-3132.

Resendez, S. L., Jennings, J. H., Ung, R. L., Namboodiri, V. M., Zhou, Z. C., Otis, J. M., Nomura, H., McHenry, J. A., Kosyk, O. and Stuber, G. D. (2016) 'Visualization of cortical, subcortical and deep brain neural circuit dynamics during naturalistic mammalian behavior with head-mounted microscopes and chronically implanted lenses', *Nat Protoc,* 11(3), pp. 566-97.

Richardson, C. A. and Leitch, B. (2002) 'Cerebellar Golgi, Purkinje, and basket cells have reduced gamma-aminobutyric acid immunoreactivity in stargazer mutant mice', *J Comp Neurol,* 453(1), pp. 85-99.

Rivaud-Pechoux, S., Dürr, A., Gaymard, B., Cancel, G., Ploner, C. J., Agid, Y., Brice, A. and Pierrot-Deseilligny, C. (1998) 'Eye movement abnormalities correlate with genotype in autosomal dominant cerebellar ataxia type I', *Ann Neurol,* 43(3), pp. 297-302.

Rizza, M. F., Locatelli, F., Masoli, S., Sánchez-Ponce, D., Muñoz, A., Prestori, F. and D'Angelo, E. (2021) 'Stellate cell computational modeling predicts signal filtering in the molecular layer circuit of cerebellum', *Sci Rep,* 11(1), pp. 3873.

Robitaille, Y., Schut, L. and Kish, S. J. (1995) 'Structural and immunocytochemical features of olivopontocerebellar atrophy caused by the spinocerebellar ataxia type 1 (SCA-1) mutation define a unique phenotype', *Acta Neuropathol,* 90(6), pp. 572-81.

Rodriguez, G. A., Barrett, G. M., Duff, K. E. and Hussaini, S. A. (2020) 'Chemogenetic attenuation of neuronal activity in the entorhinal cortex reduces Aβ and tau pathology in the hippocampus', *PLoS Biol,* 18(8), pp. e3000851.

Roizin, L., 1979. Neuronal nuclear-cytoplasmic changes in Huntington's chorea: electron microscope investigations in Advances in nueorlogy 23. *Huntingtons disease*, pp.95-122.

Rose, T., Goltstein, P. M., Portugues, R. and Griesbeck, O. (2014) 'Putting a finishing touch on GECIs', *Front Mol Neurosci,* 7, pp. 88.

Rosenbaum, R., Tchumatchenko, T. and Moreno-Bote, R. (2014) 'Correlated neuronal activity and its relationship to coding, dynamics and network architecture', *Front Comput Neurosci,* 8, pp. 102.

Rosenberg, R. N. and Grossman, A. (1989) 'Hereditary ataxia', *Neurol Clin,* 7(1), pp. 25-36.

Ross, C. A. and Poirier, M. A. (2004) 'Protein aggregation and neurodegenerative disease', *Nat Med,* 10 Suppl, pp. S10-7.

Roth, B. L. (2016) 'DREADDs for Neuroscientists', *Neuron,* 89(4), pp. 683-94.

Rousseaux, M. W. C., Tschumperlin, T., Lu, H. C., Lackey, E. P., Bondar, V. V., Wan, Y. W., Tan, Q., Adamski, C. J., Friedrich, J., Twaroski, K., Chen, W., Tolar, J., Henzler, C., Sharma, A., Bajić, A., Lin, T., Duvick, L., Liu, Z., Sillitoe, R. V., Zoghbi, H. Y. and Orr, H. T. (2018) 'ATXN1-CIC Complex Is the Primary Driver of Cerebellar Pathology in Spinocerebellar Ataxia Type 1 through a Gain-of-Function Mechanism', *Neuron,* 97(6), pp. 1235-1243.e5.

Rowan, M. J. M., Bonnan, A., Zhang, K., Amat, S. B., Kikuchi, C., Taniguchi, H., Augustine, G. J. and Christie, J. M. (2018) 'Graded Control of Climbing-Fiber-Mediated Plasticity and Learning by Inhibition in the Cerebellum', *Neuron,* 99(5), pp. 999-1015.e6.

Roy, D. S., Arons, A., Mitchell, T. I., Pignatelli, M., Ryan, T. J. and Tonegawa, S. (2016) 'Memory retrieval by activating engram cells in mouse models of early Alzheimer's disease', *Nature,* 531(7595), pp. 508-12.

Ruden, J. B., Dugan, L. L. and Konradi, C. (2021) 'Parvalbumin interneuron vulnerability and brain disorders', *Neuropsychopharmacology,* 46(2), pp. 279-287.

Ruegsegger, C., Stucki, D. M., Steiner, S., Angliker, N., Radecke, J., Keller, E., Zuber, B., Rüegg, M. A. and Saxena, S. (2016) 'Impaired mTORC1-Dependent Expression of Homer-3 Influences SCA1 Pathophysiology', *Neuron,* 89(1), pp. 129-46.

Russell, J. T. (2011) 'Imaging calcium signals in vivo: a powerful tool in physiology and pharmacology', *Br J Pharmacol,* 163(8), pp. 1605-25.

Rüb, U., Schöls, L., Paulson, H., Auburger, G., Kermer, P., Jen, J. C., Seidel, K., Korf, H. W. and Deller, T. (2013) 'Clinical features, neurogenetics and neuropathology of the polyglutamine spinocerebellar ataxias type 1, 2, 3, 6 and 7', *Prog Neurobiol,* 104, pp. 38-66.

Saegusa, H., Wakamori, M., Matsuda, Y., Wang, J., Mori, Y., Zong, S. and Tanabe, T. (2007) 'Properties of human Cav2.1 channel with a spinocerebellar ataxia type 6 mutation expressed in Purkinje cells', *Mol Cell Neurosci,* 34(2), pp. 261-70.

Sauerbrei, B. A., Lubenov, E. V. and Siapas, A. G. (2015) 'Structured Variability in Purkinje Cell Activity during Locomotion', *Neuron,* 87(4), pp. 840-52.

Saxena, S. and Liebscher, S. (2020) 'Editorial: Circuit Mechanisms of Neurodegenerative Diseases', *Front Neurosci,* 14, pp. 593329.

Scekic-Zahirovic, J., Sanjuan-Ruiz, I., Kan, V., Megat, S., De Rossi, P., Dieterlé, S., Cassel, R., Jamet, M., Kessler, P., Wiesner, D., Tzeplaeff, L., Demais, V., Sahadevan, S., Hembach, K. M., Muller, H. P., Picchiarelli, G., Mishra, N., Antonucci, S., Dirrig-Grosch, S., Kassubek, J., Rasche, V., Ludolph, A., Boutillier, A. L., Roselli, F., Polymenidou, M., Lagier-Tourenne, C., Liebscher, S. and Dupuis, L. (2021) 'Cytoplasmic FUS triggers early behavioral alterations linked to cortical neuronal hyperactivity and inhibitory synaptic defects', *Nat Commun,* 12(1), pp. 3028.

Schippling, S., Schneider, S. A., Bhatia, K. P., Münchau, A., Rothwell, J. C., Tabrizi, S. J. and Orth, M. (2009) 'Abnormal motor cortex excitability in preclinical and very early Huntington's disease', *Biol Psychiatry,* 65(11), pp. 959-65.

Schmolesky, M. T., Weber, J. T., De Zeeuw, C. I. and Hansel, C. (2002) 'The making of a complex spike: ionic composition and plasticity', *Ann N Y Acad Sci,* 978, pp. 359-90.

Schultz, S. R., Kitamura, K., Post-Uiterweer, A., Krupic, J. and Häusser, M. (2009) 'Spatial pattern coding of sensory information by climbing fiber-evoked calcium signals in networks of neighboring cerebellar Purkinje cells', *J Neurosci,* 29(25), pp. 8005-15.

Schwaller, B. (2020) 'Cytosolic Ca', *Cold Spring Harb Perspect Biol,* 12(1).

Schöls, L., Amoiridis, G., Büttner, T., Przuntek, H., Epplen, J. T. and Riess, O. (1997a) 'Autosomal dominant cerebellar ataxia: phenotypic differences in genetically defined subtypes?', *Ann Neurol,* 42(6), pp. 924-32.

Schöls, L., Amoiridis, G., Langkafel, M., Schöls, S. and Przuntek, H. (1997b) 'Motor evoked potentials in the spinocerebellar ataxias type 1 and type 3', *Muscle Nerve,* 20(2), pp. 226-8.

Schöls, L., Linnemann, C. and Globas, C. (2008) 'Electrophysiology in spinocerebellar ataxias: spread of disease and characteristic findings', *Cerebellum,* 7(2), pp. 198-203.

Schöls, L., Riess, O., Schöls, S., Zeck, S., Amoiridis, G., Langkafel, M., Epplen, J. T. and Przuntek, H. (1995) 'Spinocerebellar ataxia type 1: Clinical and neurophysiological characteristics in German kindreds', *Acta Neurol Scand,* 92(6), pp. 478-85.

Seeley, W. W., Crawford, R. K., Zhou, J., Miller, B. L. and Greicius, M. D. (2009) 'Neurodegenerative diseases target large-scale human brain networks', *Neuron,* 62(1), pp. 42-52.

Seidel, K., Siswanto, S., Brunt, E. R., den Dunnen, W., Korf, H. W. and Rüb, U. (2012) 'Brain pathology of spinocerebellar ataxias', *Acta Neuropathol,* 124(1), pp. 1-21.

Semple, B. D., Blomgren, K., Gimlin, K., Ferriero, D. M. and Noble-Haeusslein, L. J. (2013) 'Brain development in rodents and humans: Identifying benchmarks of maturation and vulnerability to injury across species', *Prog Neurobiol,* 106-107, pp. 1-16.

Sereno, M. I., Diedrichsen, J., Tachrount, M., Testa-Silva, G., d'Arceuil, H. and De Zeeuw, C. (2020) 'The human cerebellum has almost 80% of the surface area of the neocortex', *Proc Natl Acad Sci U S A,* 117(32), pp. 19538-19543.

Serra, H. G., Byam, C. E., Lande, J. D., Tousey, S. K., Zoghbi, H. Y. and Orr, H. T. (2004) 'Gene profiling links SCA1 pathophysiology to glutamate signaling in Purkinje cells of transgenic mice', *Hum Mol Genet,* 13(20), pp. 2535-43.

Serra, H. G., Duvick, L., Zu, T., Carlson, K., Stevens, S., Jorgensen, N., Lysholm, A., Burright, E., Zoghbi, H. Y., Clark, H. B., Andresen, J. M. and Orr, H. T. (2006) 'RORalpha-mediated Purkinje cell development determines disease severity in adult SCA1 mice', *Cell,* 127(4), pp. 697-708.

Servadio, A., Koshy, B., Armstrong, D., Antalffy, B., Orr, H. T. and Zoghbi, H. Y. (1995) 'Expression analysis of the ataxin-1 protein in tissues from normal and spinocerebellar ataxia type 1 individuals', *Nat Genet,* 10(1), pp. 94-8.

Sgritta, M., Locatelli, F., Soda, T., Prestori, F. and D'Angelo, E. U. (2017) 'Hebbian Spike-Timing Dependent Plasticity at the Cerebellar Input Stage', *J Neurosci,* 37(11), pp. 2809-2823.

Shiraishi, Y., Mizutani, A., Yuasa, S., Mikoshiba, K. and Furuichi, T. (2004) 'Differential expression of Homer family proteins in the developing mouse brain', *J Comp Neurol,* 473(4), pp. 582-99.

Shuvaev, A. N., Hosoi, N., Sato, Y., Yanagihara, D. and Hirai, H. (2017) 'Progressive impairment of cerebellar mGluR signalling and its therapeutic potential for cerebellar ataxia in spinocerebellar ataxia type 1 model mice', *J Physiol,* 595(1), pp. 141-164.

Skinner, P. J., Koshy, B. T., Cummings, C. J., Klement, I. A., Helin, K., Servadio, A., Zoghbi, H. Y. and Orr, H. T. (1997) 'Ataxin-1 with an expanded glutamine tract alters nuclear matrix-associated structures', *Nature,* 389(6654), pp. 971-4.

Snider, R.S. and Stowell, A., 1944. Receiving areas of the tactile, auditory, and visual systems in the cerebellum. *Journal of Neurophysiology*, *7*(6), pp.331-357.

Sotelo, C. (2008) 'Viewing the cerebellum through the eyes of Ramón Y Cajal', *Cerebellum,* 7(4), pp. 517-22.

Soto, C. and Pritzkow, S. (2018) 'Protein misfolding, aggregation, and conformational strains in neurodegenerative diseases', *Nat Neurosci,* 21(10), pp. 1332-1340.

Srinivasan, S. R., Huang, H., Chang, W. C., Nasburg, J. A., Nguyen, H. M., Strassmaier, T., Wulff, H. and Shakkottai, V. G. (2022) 'Discovery of Novel Activators of Large-Conductance Calcium-Activated Potassium Channels for the Treatment of Cerebellar Ataxia', *Mol Pharmacol,* 102(1), pp. 438-449.

Stachniak, T. J., Ghosh, A. and Sternson, S. M. (2014) 'Chemogenetic synaptic silencing of neural circuits localizes a hypothalamus→midbrain pathway for feeding behavior', *Neuron,* 82(4), pp. 797-808.

Stein, J. F. and Glickstein, M. (1992) 'Role of the cerebellum in visual guidance of movement', *Physiol Rev,* 72(4), pp. 967-1017.

Stoodley, C. J. (2016) 'The Cerebellum and Neurodevelopmental Disorders', *Cerebellum,* 15(1), pp. 34-37.

Stoyas, C. A., Bushart, D. D., Switonski, P. M., Ward, J. M., Alaghatta, A., Tang, M. B., Niu, C., Wadhwa, M., Huang, H., Savchenko, A., Gariani, K., Xie, F., Delaney, J. R., Gaasterland, T., Auwerx, J., Shakkottai, V. G. and La Spada, A. R. (2020) 'Nicotinamide Pathway-Dependent Sirt1 Activation Restores Calcium Homeostasis to Achieve Neuroprotection in Spinocerebellar Ataxia Type 7', *Neuron,* 105(4), pp. 630-644.e9.

Streng, M. L., Popa, L. S. and Ebner, T. J. (2018) 'Modulation of sensory prediction error in Purkinje cells during visual feedback manipulations', *Nat Commun,* 9(1), pp. 1099.

Striemer, C. L., Cantelmi, D., Cusimano, M. D., Danckert, J. A. and Schweizer, T. A. (2015) 'Deficits in reflexive covert attention following cerebellar injury', *Front Hum Neurosci,* 9, pp. 428.

Stuart, G. and Häusser, M. (1994) 'Initiation and spread of sodium action potentials in cerebellar Purkinje cells', *Neuron,* 13(3), pp. 703-12.

Sudhakar, S. K., Hong, S., Raikov, I., Publio, R., Lang, C., Close, T., Guo, D., Negrello, M. and De Schutter, E. (2017) 'Spatiotemporal network coding of physiological mossy fiber inputs by the cerebellar granular layer', *PLoS Comput Biol,* 13(9), pp. e1005754.

Sultan, F. and Bower, J. M. (1998) 'Quantitative Golgi study of the rat cerebellar molecular layer interneurons using principal component analysis', *J Comp Neurol,* 393(3), pp. 353-73.

Tabata, T. and Kano, M. (2006) 'GABA(B) receptor-mediated modulation of glutamate signaling in cerebellar Purkinje cells', *Cerebellum,* 5(2), pp. 127-33.

Takahashi, T., Kikuchi, S., Katada, S., Nagai, Y., Nishizawa, M. and Onodera, O. (2008) 'Soluble polyglutamine oligomers formed prior to inclusion body formation are cytotoxic', *Hum Mol Genet,* 17(3), pp. 345-56.

Takalo, M., Salminen, A., Soininen, H., Hiltunen, M. and Haapasalo, A. (2013) 'Protein aggregation and degradation mechanisms in neurodegenerative diseases', *Am J Neurodegener Dis,* 2(1), pp. 1-14.

Takeuchi, T. and Nagai, Y. (2017) 'Protein Misfolding and Aggregation as a Therapeutic Target for Polyglutamine Diseases', *Brain Sci,* 7(10).

Teipel, S., Grothe, M. J., Zhou, J., Sepulcre, J., Dyrba, M., Sorg, C. and Babiloni, C. (2016) 'Measuring Cortical Connectivity in Alzheimer's Disease as a Brain Neural Network Pathology: Toward Clinical Applications', *J Int Neuropsychol Soc,* 22(2), pp. 138-63.

Tejwani, L. and Lim, J. (2020) 'Pathogenic mechanisms underlying spinocerebellar ataxia type 1', *Cell Mol Life Sci,* 77(20), pp. 4015-4029.

Thach, W. T. (1967) 'Somatosensory receptive fields of single units in cat cerebellar cortex', *J Neurophysiol,* 30(4), pp. 675-96.

Thestrup, T., Litzlbauer, J., Bartholomäus, I., Mues, M., Russo, L., Dana, H., Kovalchuk, Y., Liang, Y., Kalamakis, G., Laukat, Y., Becker, S., Witte, G., Geiger, A., Allen, T., Rome, L. C., Chen, T. W., Kim, D. S., Garaschuk, O., Griesinger, C. and Griesbeck, O. (2014) 'Optimized ratiometric calcium sensors for functional in vivo imaging of neurons and T lymphocytes', *Nat Methods,* 11(2), pp. 175-82.

Thier, P. and Markanday, A. (2019) 'Role of the Vermal Cerebellum in Visually Guided Eye Movements and Visual Motion Perception', *Annu Rev Vis Sci,* 5, pp. 247-268.

Tian, L., Hires, S. A., Mao, T., Huber, D., Chiappe, M. E., Chalasani, S. H., Petreanu, L., Akerboom, J., McKinney, S. A., Schreiter, E. R., Bargmann, C. I., Jayaraman, V., Svoboda, K. and Looger, L. L. (2009) 'Imaging neural activity in worms, flies and mice with improved GCaMP calcium indicators', *Nat Methods,* 6(12), pp. 875-81.

Tobin, A. J. and Signer, E. R. (2000) 'Huntington's disease: the challenge for cell biologists', *Trends Cell Biol,* 10(12), pp. 531-6.

Todd, T. W. and Lim, J. (2013) 'Aggregation formation in the polyglutamine diseases: protection at a cost?', *Mol Cells,* 36(3), pp. 185-94.

Tong, X., Gui, H., Jin, F., Heck, B. W., Lin, P., Ma, J., Fondell, J. D. and Tsai, C. C. (2011) 'Ataxin-1 and Brother of ataxin-1 are components of the Notch signalling pathway', *EMBO Rep,* 12(5), pp. 428-35.

Trombetta-Lima, M., Krabbendam, I. E. and Dolga, A. M. (2020) 'Calcium-activated potassium channels: implications for aging and age-related neurodegeneration', *Int J Biochem Cell Biol,* 123, pp. 105748.

Tsutsumi, S., Chadney, O., Yiu, T. L., Bäumler, E., Faraggiana, L., Beau, M. and Häusser, M. (2020) 'Purkinje Cell Activity Determines the Timing of Sensory-Evoked Motor Initiation', *Cell Rep,* 33(12), pp. 108537.

Urban, D. J., Zhu, H., Marcinkiewcz, C. A., Michaelides, M., Oshibuchi, H., Rhea, D., Aryal, D. K., Farrell, M. S., Lowery-Gionta, E., Olsen, R. H., Wetsel, W. C., Kash, T. L., Hurd, Y. L., Tecott, L. H. and Roth, B. L. (2016) 'Elucidation of The Behavioral Program and Neuronal Network Encoded by Dorsal Raphe Serotonergic Neurons', *Neuropsychopharmacology,* 41(5), pp. 1404-15.

Velázquez-Pérez, L., Tünnerhoff, J., Rodríguez-Labrada, R., Torres-Vega, R., Ruiz-Gonzalez, Y., Belardinelli, P., Medrano-Montero, J., Canales-Ochoa, N., González-Zaldivar, Y., Vazquez-Mojena, Y., Auburger, G. and Ziemann, U. (2017) 'Early corticospinal tract damage in prodromal SCA2 revealed by EEG-EMG and EMG-EMG coherence', *Clin Neurophysiol,* 128(12), pp. 2493-2502.

Verret, L., Mann, E. O., Hang, G. B., Barth, A. M., Cobos, I., Ho, K., Devidze, N., Masliah, E., Kreitzer, A. C., Mody, I., Mucke, L. and Palop, J. J. (2012) 'Inhibitory interneuron deficit links altered network activity and cognitive dysfunction in Alzheimer model', *Cell,* 149(3), pp. 708-21.

Vervaeke, K., Lorincz, A., Gleeson, P., Farinella, M., Nusser, Z. and Silver, R. A. (2010) 'Rapid desynchronization of an electrically coupled interneuron network with sparse excitatory synaptic input', *Neuron,* 67(3), pp. 435-51.

Vig, P. J., Fratkin, J. D., Desaiah, D., Currier, R. D. and Subramony, S. H. (1996) 'Decreased parvalbumin immunoreactivity in surviving Purkinje cells of patients with spinocerebellar ataxia-1', *Neurology,* 47(1), pp. 249-53.

Vig, P. J., Subramony, S. H., Burright, E. N., Fratkin, J. D., McDaniel, D. O., Desaiah, D. and Qin, Z. (1998) 'Reduced immunoreactivity to calcium-binding proteins in Purkinje cells precedes onset of ataxia in spinocerebellar ataxia-1 transgenic mice', *Neurology,* 50(1), pp. 106-13.

Vos, B. P., Maex, R., Volny-Luraghi, A. and De Schutter, E. (1999) 'Parallel fibers synchronize spontaneous activity in cerebellar Golgi cells', *J Neurosci,* 19(11), pp. RC6.

Vos, B. P., Volny-Luraghi, A. and De Schutter, E. (1999) 'Cerebellar Golgi cells in the rat: receptive fields and timing of responses to facial stimulation', *Eur J Neurosci,* 11(8), pp. 2621-34.

Vyas, S., Golub, M. D., Sussillo, D. and Shenoy, K. V. (2020) 'Computation Through Neural Population Dynamics', *Annu Rev Neurosci,* 43, pp. 249-275.

Wagner, M. J., Savall, J., Hernandez, O., Mel, G., Inan, H., Rumyantsev, O., Lecoq, J., Kim, T. H., Li, J. Z., Ramakrishnan, C., Deisseroth, K., Luo, L., Ganguli, S. and Schnitzer, M. J. (2021) 'A neural circuit state change underlying skilled movements', *Cell,* 184(14), pp. 3731-3747.e21.

Wang, P. S., Liu, R. S., Yang, B. H. and Soong, B. W. (2007) 'Topographic brain mapping of the international cooperative ataxia rating scale. A positron emission tomography study', *J Neurol,* 254(6), pp. 722-8.

Wang, Y., Zhang, D., Wang, J., Ma, J., Lu, L. and Jin, S. (2023) 'Effects of transcranial magnetic stimulation on cerebellar ataxia: A systematic review and meta-analysis', *Front Neurol,* 14, pp. 1049813.

Watanabe, D., Inokawa, H., Hashimoto, K., Suzuki, N., Kano, M., Shigemoto, R., Hirano, T., Toyama, K., Kaneko, S., Yokoi, M., Moriyoshi, K., Suzuki, M., Kobayashi, K., Nagatsu, T., Kreitman, R. J., Pastan, I. and Nakanishi, S. (1998) 'Ablation of cerebellar Golgi cells disrupts synaptic integration involving GABA inhibition and NMDA receptor activation in motor coordination', *Cell,* 95(1), pp. 17-27.

Watase, K., Weeber, E. J., Xu, B., Antalffy, B., Yuva-Paylor, L., Hashimoto, K., Kano, M., Atkinson, R., Sun, Y., Armstrong, D. L., Sweatt, J. D., Orr, H. T., Paylor, R. and Zoghbi, H. Y. (2002) 'A long CAG repeat in the mouse Sca1 locus replicates SCA1 features and reveals the impact of protein solubility on selective neurodegeneration', *Neuron,* 34(6), pp. 905-19.

Waters, M. F., Minassian, N. A., Stevanin, G., Figueroa, K. P., Bannister, J. P., Nolte, D., Mock, A. F., Evidente, V. G., Fee, D. B., Müller, U., Dürr, A., Brice, A., Papazian, D. M. and Pulst, S. M. (2006) 'Mutations in voltage-gated potassium channel KCNC3 cause degenerative and developmental central nervous system phenotypes', *Nat Genet,* 38(4), pp. 447-51.

Welsh, J. P. (2002) 'Functional significance of climbing-fiber synchrony: a population coding and behavioral analysis', *Ann N Y Acad Sci,* 978, pp. 188-204.

White, J. J. and Sillitoe, R. V. (2013) 'Development of the cerebellum: from gene expression patterns to circuit maps', *Wiley Interdiscip Rev Dev Biol,* 2(1), pp. 149-64.

Wilms, C. D. and Häusser, M. (2014) 'Twitching towards the ideal calcium sensor', *Nat Methods,* 11(2), pp. 139-40.

Wu, J. W., Hussaini, S. A., Bastille, I. M., Rodriguez, G. A., Mrejeru, A., Rilett, K., Sanders, D. W., Cook, C., Fu, H., Boonen, R. A., Herman, M., Nahmani, E., Emrani, S., Figueroa, Y. H., Diamond, M. I., Clelland, C. L., Wray, S. and Duff, K. E. (2016) 'Neuronal activity enhances tau propagation and tau pathology in vivo', *Nat Neurosci,* 19(8), pp. 1085-92.

Wu, Q. W. and Kapfhammer, J. P. (2022) 'The Emerging Key Role of the mGluR1-PKCγ Signaling Pathway in the Pathogenesis of Spinocerebellar Ataxias: A Neurodevelopmental Viewpoint', *Int J Mol Sci,* 23(16).

Wulff, P., Schonewille, M., Renzi, M., Viltono, L., Sassoè-Pognetto, M., Badura, A., Gao, Z., Hoebeek, F. E., van Dorp, S., Wisden, W., Farrant, M. and De Zeeuw, C. I. (2009) 'Synaptic inhibition of Purkinje cells mediates consolidation of vestibulo-cerebellar motor learning', *Nat Neurosci,* 12(8), pp. 1042-9.

Yakura, H., Wakisaka, A., Fujimoto, S. and Itakura, K. (1974) 'Letter: Hereditary ataxia and HL-A genotypes', *N Engl J Med,* 291(3), pp. 154-5.

Yang, Z. and Santamaria, F. (2016) 'Purkinje cell intrinsic excitability increases after synaptic long term depression', *J Neurophysiol,* 116(3), pp. 1208-17.

Yuan, P. and Grutzendler, J. (2016) 'Attenuation of β-Amyloid Deposition and Neurotoxicity by Chemogenetic Modulation of Neural Activity', *J Neurosci,* 36(2), pp. 632-41.

Zhang, Y. and Kaczmarek, L. K. (2016) 'Kv3.3 potassium channels and spinocerebellar ataxia', *J Physiol,* 594(16), pp. 4677-84.

Zoghbi, H. Y. and Orr, H. T. (1995) 'Spinocerebellar ataxia type 1', *Semin Cell Biol,* 6(1), pp. 29-35.

Zoghbi, H. Y. and Orr, H. T. (2009) 'Pathogenic mechanisms of a polyglutamine-mediated neurodegenerative disease, spinocerebellar ataxia type 1', *J Biol Chem,* 284(12), pp. 7425-9.

Declaration of Dissertation Contributions

All results in this thesis including experimental design, experimental data acquisition and data analysis were performed by the author, excluding the following work:

Sabine Liebscher is hereby acknowledged for contributions to data analysis throughout two-photon imaging experiments.

XiaoQian Ye is hereby acknowledged for the manifold data analysis and contributing to associated text in methods and results sections (**Fig**. **9** & **Fig. 20**).

Meriem Mounassir is hereby acknowledged for acquiring part of the datasets and completing part of the image processing for the simultaneous calcium imaging with acute MLIN inhibition (**Fig. 18, Fig. 19** & **Fig. 20**).

Christoph Tietje is hereby acknowledged for acquiring part of the datasets, completing part of the image processing for the ratiometric imaging (**Fig. 12**), and performing parts of the behavioural experiments for the chronic CNO application experiments (**Fig. 23F-H** & **Fig. 25 A-B**).

Federico Pilotto is hereby acknowledged for acquiring the data and performing the analysis for UniBe immunohistochemistry and behavioural experiments, along with contributions to the associated text of this work (**Fig. 22**, **Fig. 23, Fig. 24 and Fig. 25**).

Acknowledgments

I am proud to look over this thesis as the culmination of 5 years of dedication and grit, putting in the long days that merged into long evenings, nights and weekends, to build this project from scratch. Such work would have been impossible without those around me, providing a family to enjoy my life in Munich and support in my scientific endeavor. I must first thank the relentless work of my supervisor Prof. Dr. Dr. Sabine Liebscher, for her tireless effort literally day and night to ensure the lab functions. Thank you for the opportunity to complete my PhD, providing insight into almost every area of science and medicine I ever asked about, alongside detailed and dedicated feedback on everything I do, helping me develop as a scientist. I doubt I will ever meet anyone with the same level of attention to detail and dedication. I want to also thank my Thesis Advisory Committee; Prof. Dr. Tobias Rose, Prof. Dr. Moritz Rossener and Prof. Dr. Simon Jacob, for always making the time to give detailed, honest and vital input into this project over the years. Whilst only once a year, these meetings gave me essential insight and perspective, the opportunity to have this over my PhD is something I will always appreciate.

Sincere thanks go to every member of the Liescher lab, who are genuinely always there for each other, especially the amazing PhD students (Dr.) Pavel, (Dr.) Vanessa, XiaoQian, Zeynep and Shenyi. I also want to mention the incredibly hard working medical students I have been fortunate to work with Christoph, Meriem and Cem. Your valuable contributions have improved my own research and have given me the gift of extra time, the most precious commodity to a PhD student. Special mention to Pavel, Vanessa and XiaoQian who were running the lab when I first joined, you have always been incredibly supportive, both in patiently teaching me a variety of skills, and simply providing friendship to make the lab an enjoyable place to work. I also want to thank everyone across the Clinical Neuroimmunology department for creating the friendly and fun environment between the groups. I want to extend my gratitude to the Graduate School of Systemic Neurosciences. The social events, courses, talks organized through the GSN are outstanding. Thank you to all the hard working people behind this organization, your dedication provides a wonderful community for neuroscience students across Munich. Those early GSN welcome events all the way back in 2018, introduced me to wonderful people, Clara (Gloria?), Almir, Katja and Ash, thank you for being such incredibly fun, kind and intelligent people. Clara and Almir thank you also for fun and help when needed in our department.

Outside of the neuroscience world, first and foremost, I want to thank my family and Ciara for putting up with me throughout this period, you have always been endlessly supportive despite my chaotic work life taking up far too much time. Ciara especially, I signed up for this madness, but you did not, so I will always appreciate you enduring everything yet still making sure we were laughing along the way. A further extension of thanks has to go to the silly people of T17 and the Rovers family, the importance of being able to switch off and escape the lab cannot be understated, you were all vital to my happiness over the years.

This research was supported by German Research Foundation under Germany's Excellence Strategy within the framework of the Munich Cluster for Systems Neurology -EXC 2145 SyNergy- ID 390857198, and the Emmy Noether Program.

List of Publications

Pilotto, F., Douthwaite, C*., Diab, R., Ye, X., Al Qassab, Z., Tietje, C., Mounassir, M., Odriozola, A., Thapa, A., Buijsen, R. A. M., Lagache, S., Uldry, A. C., Heller, M., Müller, S., van Roon-Mom, W. M. C., Zuber, B., Liebscher, S. and Saxena, S. (2023) 'Early molecular layer interneuron hyperactivity triggers Purkinje neuron degeneration in SCA1', ***Neuron***.

Declaration of Author Contributions

Publication 1: (Pilotto, Douthwaite, et al., 2023) ""*Early molecular layer interneuron hyperactivity triggers Purkinje neuron degeneration in SCA1." Neuron. In Press.*

Federica Pilotto, **Christopher Douthwaite**, Rim Diab, XiaoQian Ye, Zahraa Al qassab, Christoph Tietje, Meriem Mounassir, Adolfo Odriozola, Aishwarya Thapa, Ronald A.M. Buijsen, Sophie Lagache, Anne-Christine Uldry, Manfred Heller, Stefan Müller, Willeke M.C. van Roon-Mom, Benoît Zuber, Sabine Liebscher, Smita Saxena.

Author contributions

Conceptualization and writing, F.P., S.S., and S. Liebscher; investigation and analyses, F.P., C.D., R.D., X.Y., Z.A.Q., A.O., C.T., M.M., and A.T.; FACS, mass spectrometry, and analyses, S.M., S. Lagache, A.C.U., and M.H.; reagents, R.A.M.B., W.M.C.v.R.-M., and B.Z.; supervision, S.S. and S. Liebscher.

My contribution to this publication in detail:

For this publication I developed the cerebellum craniotomy protocol and performed all two-photon imaging experiments using GCaMP7s in P60 and P200 mice. I assisted in developing the protocol to, and performed a proportion of the experiments of, all other two-photon imaging data. I performed or assisted in all data processing, analysis and figure design for all two-photon imaging experiments. I assisted in developing the protocol for, and performed, all chronic behavioural treatments conducted at LMU, and analysed the data. Additionally I commented on the manuscript in full and contributed to writing parts of the methods, figure legends and discussion.

co-first author: Christopher Douthwatie **1st supervisor: Prof. Dr. Sabine Liebscher**

_____ _____